THE HONG KONG
POLYTECHNIC UNIVERSITY
香港理工大學

Pao Yue-kong Library
包玉剛圖書館

Copyright Undertaking

This thesis is protected by copyright, with all rights reserved.

By reading and using the thesis, the reader understands and agrees to the following terms:

1. The reader will abide by the rules and legal ordinances governing copyright regarding the use of the thesis.

2. The reader will use the thesis for the purpose of research or private study only and not for distribution or further reproduction or any other purpose.

3. The reader agrees to indemnify and hold the University harmless from and against any loss, damage, cost, liability or expenses arising from copyright infringement or unauthorized usage.

IMPORTANT

If you have reasons to believe that any materials in this thesis are deemed not suitable to be distributed in this form, or a copyright owner having difficulty with the material being included in our database, please contact lbsys@polyu.edu.hk providing details. The Library will look into your claim and consider taking remedial action upon receipt of the written requests.

The Hong Kong Polytechnic University

Department of Building Services Engineering

A Multi-functional Solar Assisted Ground Coupled Heat Pump System for Space Heating and Hot Water Supply

CHEN Xi

A thesis submitted in partial fulfillment of the requirements for the

Degree of Master of Philosophy

June 2011

CERTIFICATE OF ORIGINALITY

I hereby declare that this thesis is my own work and that, to the best of my knowledge and belief, it reproduces no material previously published or written, nor material that has been accepted for the award of any other degree or diploma, except where due acknowledgement has been made in the text.

I also declare that the intellectual content of this thesis is the product of my own work, even though I may have received assistance from others on style, presentation and language expression.

_____ (Signed)

_____CHEN Xi_____ (Name of student)

Department of Building Services Engineering

The Hong Kong Polytechnic University

Hong Kong, China

May 2011

ABSTRACT

Abstract of this thesis entitled: A Multi-functional Solar Assisted Ground Coupled Heat

Pump System for Space Heating and Hot water supply

Submitted by: CHEN Xi

For the degree of: MPhil

    Solar energy and geothermal energy are considered promising renewable sources for energy saving applications in buildings. Solar heat can be collected for space heating and domestic hot water (DHW) supply, while geothermal energy could be ideal heat source or sink for heat pump systems. Geothermal heat pump systems with vertical/horizontal heat exchangers, also called ground coupled heat pump (GCHP) systems, are considered relatively efficient for heating, cooling or hot water supply in cold areas. Because underground soil temperature is rather constant compared with ambient air temperature, the GCHP could achieve higher energy efficiency as well as more stable performance compared with traditional air source heat pumps. However, geothermal potential as heat source or sink could be impaired under short-time continuous operation or long-term imbalanced-load conditions, which has been observed and discussed by many researchers.

    As a result, the solar assisted ground coupled heat pump (SAGCHP), a technology to couple solar energy collecting system with the GCHP, could provide a possible solution to the abovementioned problems of a GCHP system and improve the stability and efficiency of the heat pump system for space heating. Furthermore, additional solar

energy could be utilized for DHW supply and soil recharging during non-heating seasons. This thesis intends to carry out optimization, numerical simulation and experimental studies on the energy performances of this combined system for space heating and hot water supply in cold areas of northern China.

First of all, a SAGCHP system with an energy storage tank is proposed and its mathematical models are constructed in the TRNSYS environment. The new system mainly consists of a ground heat exchanger (GHE) subsystem, a solar collecting subsystem with heat storage, a water to water heat pump and a DHW supply subsystem, which could achieve multi-mode space heating, water heating, heat storage as well as soil recharging based on heating requirements, weather conditions and control strategies.

The model optimization is then performed under the weather condition of Beijing. The typical meteorological year (TMY) weather data of Beijing has been generated from the Meteonorm. Five models in different system configurations are compared by simulation to explore the optimal coupling method of solar collectors and GHEs. The optimal mass flow rate in the solar collectors and the storage factors are determined by evaluating the heating performance and the solar fraction. The ratio of the collector size and GHE loop length is further investigated by parametric studies including the heat pump efficiency, energy savings and economic factors. In addition, effects of alternative control strategies are discussed by comparing the system performances to realize flexible change between diverse working modes and maximum utilization of solar heat.

After optimization procedures are finished, numerical simulations are performed for operation of 20 years under the meteorological conditions of Beijing. The simulating results show that the long term yearly average space heating efficiency is improved by

26.3% compared to a traditional GCHP system because the solar thermal collecting system is used to elevate the thermal energy in the soil and to provide direct space heating with heat storage. At the same time, the underground heat load imbalance problem for a heating load dominated GCHP is solved by soil recharging during non-heating periods, while extra solar energy is utilized to supply DHW. The operational characteristics of the system in one simulation year are also investigated with specific analysis on each working mode. Furthermore, the energy balance of the optimized design is confirmed with a minor difference of 0.75%, and the system is proved more efficient and economical for its application in Beijing area than in other cold weather regions like Harbin.

Finally, experiments are carried out under the weather conditions similar to Beijing to study the practical operation features and confirm the applicability of the SAGCHP system. The test rig was installed at the Hebei Academy of Sciences in Shijiazhuang (lat. N38°03', long. E114°26'), China. Solar collectors are in series connection with the borehole array through plate heat exchangers. Four operation modes of the system were investigated throughout the coldest period in winter (Dec 5th to Dec 27th). The heat pump performance, borehole temperature distributions and solar colleting characteristics of the SAGCHP system are analyzed and compared when the system worked in continuous or intermittent modes with or without solar assisted heating. The SAGCHP system is proved to perform space heating with high energy efficiency and satisfactory solar fraction, which is a promising substitute for conventional heating systems. It is also recommended to use the collected solar thermal energy as an alternative source for the heat pump

instead of recharging boreholes for heat storage because of the enormous heat capacity of the earth.

PUBILICATIONS DURING MPHIL STUDY

Chen Xi, Lu Lin and Yang Hongxing (2011), Long term operation of a solar assisted ground coupled heat pump system for space heating and domestic hot water, Energy & Buildings **43**(8): 1835-1844.

Chen Xi and Yang Hongxing (2011), Performance analysis of a proposed solar assisted ground coupled heat pump system, Proceedings of 3rd International Conference of Applied Energy.

Chen Xi, et al. (2011), Experimental studies on a ground coupled heat pump with solar thermal collectors for space heating, Energy 36: 5292-5300.

Chen Xi and Yang Hongxing (2010), Numerical simulation and optimization of a multi-functional solar assisted ground source heat pump system, Proceedings of 9th International Conference of Sustainable Energy Technologies.

ACKNOWLEDGEMENTS

I would like to express my most sincere gratitude to my chief supervisor, Prof. Yang Hongxing, Department of Building Services Engineering of The Hong Kong Polytechnic University for his professional guidance and help on my research studies as well as his great support in my personal living and career development. I am also grateful for valuable suggestions from my co-supervisor, Dr. Lu Lin.

I would like to thank all members of the Renewable Energy Research Group (RERG) for their help and assistance on my study during two years' life in The Hong Kong Polytechnic University, especially Mr. Sun Ke, Dr. Han Jun, Ms. Man Yi and Ms. Sun Liangliang.

Most importantly, I would like to deeply acknowledge infinite support from my family and friends. Without their encouragement and love the accomplishment of this thesis should never be possible.

TABLE OF CONTENTS

LIST OF FIGURES

LIST OF TABLES

NOMENCLATURE

A_C	collector area [m^2]
A_S	amplitude of ground surface temperature [K]
$SAGCHP$	solar assisted ground coupled heat pump
B	borehole spacing [m]
CAP	thermal capacitance
$C_{p,load}$	specific heat of load fluid [kJ/(kg K)]
C_p	specific heat of flow stream [kJ/(kg K)]
C_{pf}	specific heat of collector fluid [kJ/(kg K)]
$C_{p,source}$	specific heat of source fluid [kJ/(kg K)]
C_w	specific heat of water flow [kJ/(kg K)]
COP_{hp}	coefficient of performance of heat pump
COP_{sys}	coefficient of performance of the system
C_{min}	minimum capacitance rate of heat exchanging fluids
DHW	domestic hot water
f	solar fraction
F_R	overall collector heat removal efficiency factor
F'	collector efficiency factor
GHE	ground heat exchanger
$GCHP$	ground coupled heat pump
H	borehole depth [m]

HTF	heat transfer fluid
HEX	heat exchanger
I_T	global radiation incident on solar collectors [kJ/(hr m^2)]
L	upper limit of the measuring range
m	mass flow rate [kg/m^3]
m_f	collector mass flow rate [kg/m^3]
m_c	condenser water mass flow rate [kg/s]
m_e	evaporator water mass flow rate [kg/s]
m_{load}	load water mass flow rate [kg/s]
m_s	solar loop mass flow rate [kg/s]
m_{source}	source water mass flow rate [kg/s]
N	number of segments
N_b	number of boreholes
N_S	number of identical collectors in series
Q_{aux}	auxiliary energy to the room [kJ/hr]
Q_{env}	energy loss from the tank to the surrounding environment [kJ/hr]
Q_{gain}	heat gains within the room [kJ/hr]
$Q_{heating}$	heat supply to load [kJ/hr]
Q_{in}	rate of energy input to tank from hot fluid stream [kJ/hr]
Q_{loss}	heat loss of the house [kJ/hr]
Q_s	rate at which sensible energy is removed from the tank to supply the load [kJ/hr]

Q_{sens}	cooling input to room [W]
Q_{source}	heat supply from source [kJ/hr]
Q_c	heat supply from condenser [W]
Q_e	heat absorption from evaporator [W]
Q_u	useful solar heat [W]
q	power pulse per unit length [kJ/(hr m)]
R_b	borehole thermal resistance per unit length [m K/W]
t_0	phase constant day of minimum surface temperature [day]
t	day of a year [day]
T_a	ambient air temperature [K]
$\overline{T_b}$	average temperature on borehole wall [K]
T_{ci}	condenser inlet water temperature [K]
T_{co}	condenser outlet water temperature [K]
T_{ei}	evaporator inlet water temperature [K]
T_{eo}	evaporator outlet water temperature [K]
$T_{load,in}$	inlet load water temperature to the heat pump [K]
$T_{load,out}$	outlet load water temperature from the heat pump [K]
T_f	average temperature of exhaust flue when heater is not operating [K]
$\overline{T_f}$	average fluid temperature [K]
T_i	inlet temperature of fluid to collector [K]
T_R	room temperature of the residence [K]

T_{si}	solar loop inlet water temperature [K]
T_{so}	solar loop outlet water temperature [K]
$T_{source,in}$	inlet source water temperature to the heat pump [K]
$T_{source,out}$	outlet source water temperature from the heat pump
UA	overall heat conductance [kJ/(hr K)]
U_L	overall heat loss coefficient of solar collectors per unit area [kJ/(hr m² K)]
V_s	ground storage volume [m³]
V_t	tank volume [m³]
W_{hp}	power consumption of the heat pump [W]
W_{cp}	power consumption of the circulating pump [W]
X_i	the ith independent measured parameter
Z	depth from the ground surface [m]

Greek letters

α	thermal diffusivity of the soil [m²/day]
$(\tau\alpha)$	product of the cover transmittance and the absorber absorptance
β	accuracy grade [%]
γ	a control function with the value between 1 and 0
θ_i	accuracy grade
σ	uncertainty
σR	relative uncertainty
ρ_f	fluid density [kg/m³]

$\mathit{\Delta E}$	change of internal energy of the tank [kJ]
$\mathit{\Delta T_i}$	temperature change of an element [K]
ε	heat exchanger effectiveness

CHAPTER 1 INTRODUCTION

1.1 Backgrounds and motivations

In recent years, a lot of work has been done to incorporate renewable applications into residential and commercial buildings. This concern is prompted by the ever-aggravating energy crisis and the global warming problem all over the world.
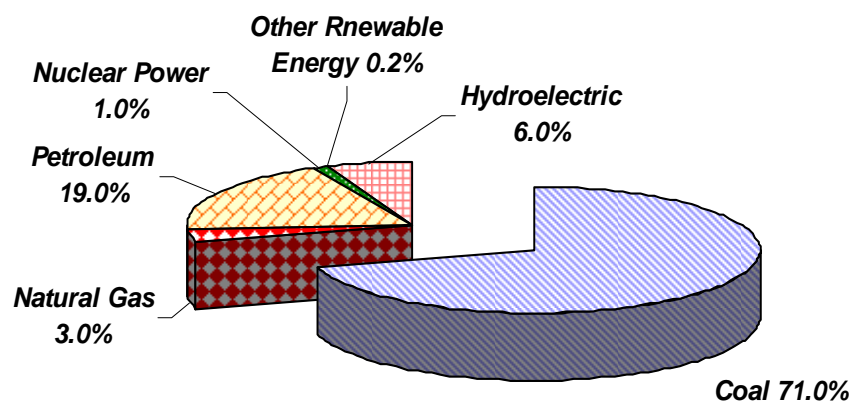
Figure 1.1 Energy consumption situations in China (2008)

According to statistics from Energy Information Administration (EIA), as shown in Figure 1.1, development of China' s modern industry and civil construction still largely depends on the consumption of fossil fuels, among which coal has contributed the largest part of 70%. Renewable energy sources only contributed no more than 7% of the total national energy requirement, of which over 90% derives from hydropower applications.

The technology for utilizing other renewable energies is still economically non-practical or needs further development.

The building sectors are expected to account for more than 35% of the national energy use by 2020, where heating, ventilation and air-conditioning would contribute more than 65% of the consumption (Yang, Lam et al. 2008; Wan, Li et al. 2011). Especially in northern areas, most space heating plants are still predominantly fueled by coal and DHW is widely provided by electric resistance water heaters. Ever since China's participation in Kyoto Protocol, reducing carbon dioxide emission as well as energy saving have been propelling researchers to explore substitutes for traditional heating and water heating systems in northern areas. Therefore, renewable energy sources have a great application potential for constructing low-carbon buildings.
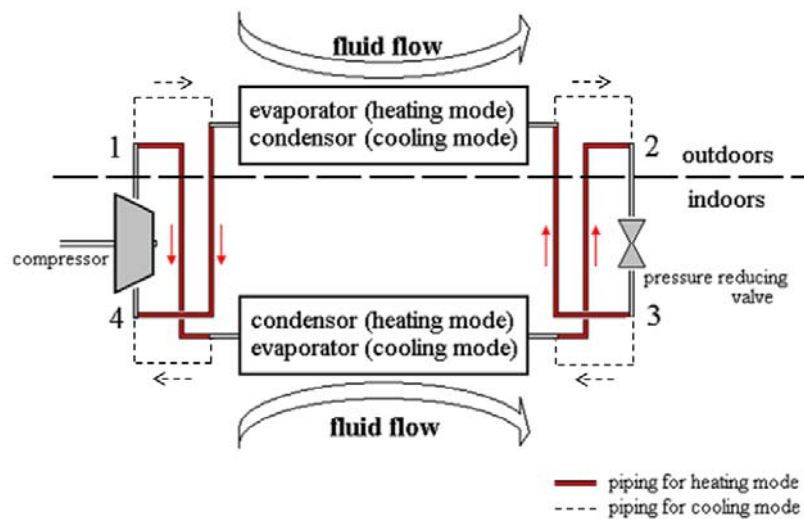
Figure 1.2 Theoretical circulation of a heat pump

Since 1852, the heat pump has been proposed as an energy-saving technology, which could provide space heating and hot water. In the essence, the heat pump, mainly consisting of a compressor, an evaporator, an expansion valve and a condenser, operates as a reversed refrigeration cycle (Figure 1.2), which supplies heat, several times of the consumed work, from sources to loads. The heating efficiency is measured by the COP (coefficient of performance), defined as "Heat supply divided by the consumed work". Usually, the COP could reach 3 ~ 4 or even higher values based on refined designs, which makes the heat pump far more efficient than traditional electrical heating systems, whose heating efficiency could not exceed 1. Although ambient air is a routine source for the heat pump, the COP descent as well as the frosting problems with the outdoor heat exchanger limits its application in cold winter of northern China.

In order to overcome the limitation of air-source heat pumps, geothermal resource is proposed as an alternative renewable heat source for the heat pump. It has great advantage over the air source heat pump because underground soil temperature is rather constant compared with ambient air temperature, which leads to higher heating efficiency as well as more stable operational performance compared with traditional air source heat pumps. As a result, geothermal heat pump systems with vertical/horizontal heat exchangers, also called ground coupled heat pump (GCHP) systems, are considered relatively efficient for heating supply in cold areas of northern China. However, geothermal potential for heat extraction or rejection could be impaired under short-term continuous operation or seasonal unbalanced-load conditions, which has been observed and discussed by many researchers (Gao, Zhang et al. 2008; Li, Yang et al. 2009; Fujimitsu, Fukuoka et al. 2010; Yang, Cui et al. 2010). For example, if the cooling load

of a building in summer could not balance the heating load in winter, which is the case in most cold areas in northeast China, long term operation could bring an irreversible temperature drop of underground soil so that the COP of the heat pump could be reduced significantly. Even when the heating and cooling load is balanced around a year, if the instantaneous heating load is too large, the temperature of heat transfer fluid (HTF) inside the ground heat exchanger may drop quickly under continuous working conditions, which might lead to a low heat pump COP and even possible system breakdown if the ground loop is not properly sized.

Consequently, a combination of solar thermal collectors and conventional GCHP, called the solar assisted ground coupled heat pump (SAGCHP) system, provides a possible solution to the abovementioned problems and is expected to improve the stability and efficiency of the heat pump. Solar radiation is considered to be an economical, readily available and non-polluting renewable source, despite the fact that its intensity is unstable due to variable weather conditions and its seasonal distribution is inconsistent with the heating requirement. Collected solar heat can be used for direct space heating, elevating evaporating temperature of the heat pump, providing domestic hot water (DHW), recharging the soil for temperature recovery, and short-term or long term thermal storage. In addition, the collecting efficiency would increase with reduced collector surface temperature due to the heat absorption by the evaporating process.

1.2 Objectives of studies

There are already many researches concerned with various aspects of the GCHP system, including simulative and experimental studies of the integral system, analytical

and numerical modeling of the ground heat exchanger (GHE), as well as economical and exergical analyses (Zeng, Diao et al. 2003; Cui, Yang et al. 2006; Esen, Inalli et al. 2007; Sanaye and Niroomand 2010). Standard design guidelines (Bose, Parker et al. 1985) and practical projects for the GCHP have already existed for years, whereas there is nearly no uniform criterion for the SAGCHP. A couple of simulative studies have been carried out on the SAGCHP system, which needs further verifications from field studies.

The main challenge of designing a high efficient SAGCHP system lies in optimized match between the collector area and the GHE loop length. There should be an equilibrium point for acquiring higher energy efficiency and better underground thermal balance. The connection mode of the two energy sources could also affect the system performance significantly under specific weather conditions. The optimization process should also consider the major design parameters in the solar collection and water storage loop, which should have influences on the system solar fraction and heating efficiency. In

Domestic hot water (DHW) is another important requirement in daily life. However, traditional hot water supply is usually performed by fossil fuel-fired or electrical boilers, which not only consume a great deal of energy but emit substantial volume of poisonous gases and greenhouse gases to the atmosphere. At the same time, solar collectors integrated to the GCHP system could be designed to meet part of the hot water load beside space heating requirement. Considering the two issues together, an economical and practical way to make full use of the collected solar heat and simultaneously decrease the energy consumption for DHW heating is to incorporate the water heating function

into the SAGCHP system, which has already been named "GEOSOL" (Trillat-Berdal, Souyri et al. 2007).

In view of the above technology backgrounds and research topics, this thesis will mainly focus on the optimization, parametric and experimental studies on a proposed SAGCHP system. The major aims and objectives are specified as follows:

1) A SAGCHP system with functions of space heating, air conditioning, heat storage and water heating will be proposed. The control strategies and working modes will be designed and modeled with the transient simulation software-TRNSYS to perform multi-functions with flexibility.

2) Optimization of the designed system, including the optimization of the connection mode and the solar collecting and water storage subsystem will be performed under the TRNSYS simulation environment. We will also investigate the systems with different collector areas and corresponding borehole lengths. The optimized ratio will be determined for the design heating load by comparing the change of major parameters.

3) Long-term simulation results of the optimized SAGCHP system will be presented. Effects of different control strategies together with comparison of various working modes are also under discussion.

4) Simulations will be carried out under different meteorological conditions to explore the applicability of the proposed SAGCHP system in northern China.

5) Energy conservation of the compound system will be validated by simulation.

6) Experiments will be performed to explore the applicability of the SAGCHP system in the target area. The heat pump performances, borehole temperature distributions and solar colleting characteristics are mainly used to analyze and compare different working modes. Furthermore, preferable utilization method of the solar thermal energy is under discussion.

1.3 Organization of the Thesis

The first Chapter presents the energy consumption situation in China and features of renewable energy sources including solar and geothermal energy. The theoretical basis of the heat pump technology is briefly introduced and the limitation in the development of traditional ground source heat pump (GCHP) is explained. Then the SAGCHP system for providing space heating and hot water is proposed. The main challenge in the design and modeling of the system and corresponding research objectives in this thesis are also discussed.

Chapter 2 includes a comprehensive literature review with regard to the SAGCHP system. Research findings related to various aspects of the system is introduced and analyzed through a critical perspective. Long-term seasonal storage in the soil and short-term PCM (phase changing material) storage is also reviewed. The developing trend of the SAGCHP system is anticipated based on a few tentative researches.

Detailed instructions of the components and working functions of the proposed SAGCHP system are stated in Chapter 3. Mathematical models used for simulation are described and control strategies are applied to realize different operation modes.

In Chapter 4, the optimization process performs to explore better coupling method between solar collectors and the GHE loop. Parametric studies involving solar collecting and heat storage subsystem as well as the ratio of the collector size and the ground loop length are under discussion. Variable control strategies are also subject to comparison.

Chapter 5 presents the long-term simulation performances of the system with optimal design derived from Chapter 4. The working characteristics of each mode are analyzed in contrast with the combination of an electric heater and a traditional GCHP system. The SAGCHP is also simulated to prove the systematic energy conservation and test its applicability in different meteorological regions.

In Chapter 6, experimental investigation is carried out to explore the difference between four working modes of the SAGCHP system under the climatic conditions of Shijiazhuang. System performances are analyzed based on borehole temperature changes, heat pump performances and solar collection characteristics.

Finally, Chapter 7 concludes the main findings in this thesis and makes suggestions for future work.

CHAPTER 2 LITERATURE REVIEW

As early as 1956 (Cube and Steimle 1981), Penrod proposed the concept of combining a solar collector with a coil of pipes buried in the soil, which enables solar energy to be stored in the soil. Continuous depletion of conventional fossil fuels, sustainability and environmental concerns are urging the world to utilize renewable energy as alternative energy sources. Especially since the oil crisis in 1980s, the combined system utilizing both solar and geothermal thermal energy was gradually recognized and more investigations have been conducted by researchers.

Most researchers before 2000 focused on using solar heat for seasonal ground storage, which was usually designed for large-scale central heating. However, in the last ten years, solar collectors began to serve as supplementary source to the ground coupled heat pump (GCHP), which came out to be the solar assisted ground coupled heat pump system (SAGCHP). The collector was usually sized to meet the excessive heating load of the GCHP system and decrease the length of the ground heat exchanger (GHE). Furthermore, design guidelines of the SAGCHP system were extended to the hybrid ground coupled heat pump (HGCHP), which could be used for satisfying both heating and cooling dominated conditions. Finally, some innovative explorations on solar collectors and GHEs are introduced to enlighten on the developing trend of the compound system.

This Chapter will present a detailed literature review with respect to the abovementioned aspects of the SAGCHP technology.

2.1 Ground-duct seasonal storage of solar heat
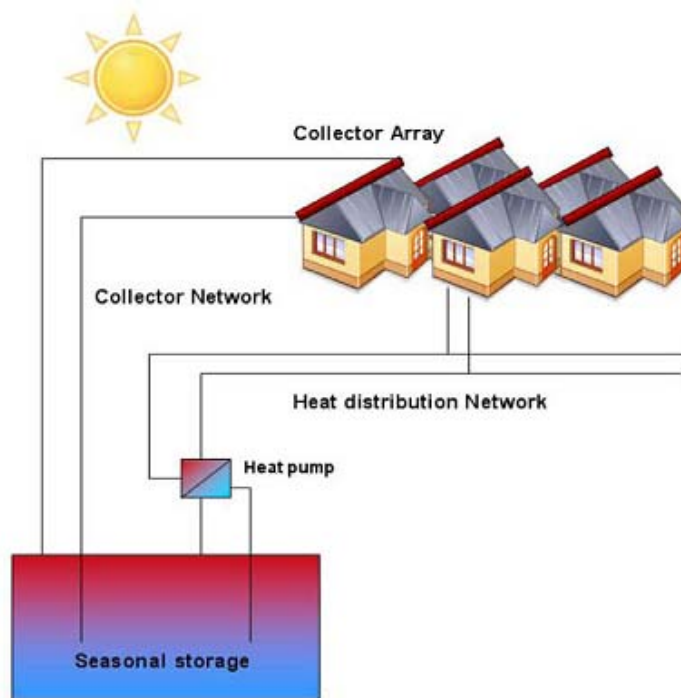
Figure 2.1 Schematic of the CSHPSS

A commonly recognized limitation of large solar heating system in the high latitude cold areas is the seasonal phase lag between the heating requirement and solar radiation availability. Storage of heat in summer that could be extracted for use in winter was believed to contribute a lot to energy savings for sustainable development. The thermal storage volume might be large aquifers, earth pits, rock caverns, underground water tanks or in-ground pipes (Novo, Bayon et al. 2010). Among various kinds of storages, the underground duct storage draws more interests in both practical engineering and

academic research field, owing to its advantage of less land occupation and wider range of application areas, especially in regions without rich water sources.

The technology of long-term seasonal heat storage has been investigated in many European countries since mid-1970s through large-scale central solar heating plant with seasonal storage (CSHPSS). The CSHPSS is usually designed to meet a high yearly solar fraction over 70~80% or no less than 50% in high north areas. In order to secure the high solar fraction, seasonal storage unit becomes crucial, whose storage capacity has to be able to hold all the summer-time solar energy and fully match the winter-time heating load. Therefore, a semi-analytical mathematical model to determine the optimal ratio of the collector area to the storage volume was developed and solar fraction was found to be in linear relation to the collector area under a fixed climate (Lund 1989).

As shown in Figure 2.1, heat production of the CSHPSS system could be used to provide either high temperature direct heating (less than 100 ℃) or low temperature requirement for the heat pump.

2.1.1 CSHPSS providing direct heating

When a CSHPSS system performs direct heating, the temperature of duct seasonal storage could vary in the range of 0~90 ℃. For that reason, the thermal performance of such systems is greatly influenced by the moisture and heat movement in the soil surrounding the ground heat exchanger (GHE) (Reuss, Beck et al. 1997).

A heat transfer simulation model of borehole and U-tubes called DST (duct storage), which is compatible with TRNSYS and MUSIN (design software for the CSHPSS), was compared with analytical solutions and finite-element models. The DST model proved to

produce reasonable accurate results over the simulation periods (Breger, Hubbell et al. 1996).

Buffer tanks were also added to the CSHPSS to realize short-term storage and the optimal ratio between the tank volume and the collector area was obtained by simulation to maximize the solar fraction (Pahud 2000). Pilot CSHPSS systems were constructed in high latitude areas like German and Sweden (Pahud 2000; Schmidt, Mangold et al. 2004; Lundh and Dalenback 2008), and it was found that the system needed 3 ~5 years preheating of the storage volume before operating efficiently as expected.

The thermal loss from the ground storage was observed to be 42 % of the collected solar heat in an experimental study (Nordell and Hellström 2000), even when the storage temperature was kept between 30 ~ 45 ℃ for a low temperature heat supply. It could be clearly seen that the seasonal heat storage for a direct solar heating system is not energy efficient due to the large heat loss. However, as mentioned before, the thermal storage could be alternatively used as the low temperature source of the heat pump. The thermal loss of the collected solar heat is expected to reduce with lower storage temperature.

2.1.2 CSHPSS providing low temperature to heat pump

Three-dimensional duct storage models were incorporated with popular commercial software, MINSUN and SOLCHIPS, which were proved to be reliable design-tools for the CSHPSS system by comparing the practical design data with the simulation results. Technical and economic feasibility of system was also subject to simulative verifications (Schlosser and Teislev 1979; Lund and Ostman 1985; Zinko and Perers 1985; Argiriou 1997).

A Poland researcher (Olszewski 2006) conducted simulations on long-term thermal storage with seasonal regeneration. A numerical code called GENOCOP with a designed pipe-in-pipe GHE mode was developed and used for optimization and parametric studies.

Experimental studies were carried out on a CSHPSS system in Belgium (Nicolas and Poncelet 1988). Annual collecting efficiency was about 0.41 and the heat pump COP ranged around 4.0. Important heat loss in the seasonal storage process was observed, while the storage efficiency reached 0.7 because of natural soil temperature recovery. Developing a control strategy that could achieve both good heating effect and high solar fraction simultaneously was found to be quite challenging. Similar experiment was recorded in Tianjin University (Wang and Qi 2008; Wang, Qi et al. 2009). It was found that the performance of the underground thermal storage of a solar-ground coupled heat pump system depended largely on the intensity of solar radiation and the storage factor (the volume of the storage water tank divided by the area of the collector). The underground storage efficiency based on the useful absorbed solar energy also reached 70% and the storage factor was suggested a value of 20~40 l/m^2 under the specified weather conditions of Tianjin.

In Harbin, an experimental rig of the CSHPSS was designed for meeting the heating load as well as the small cooling load in summer (Wang, Zheng et al. 2010). A satisfactory system heating efficiency of 6.55 was obtained, because 49.7% heating load was supplied directly by solar collectors. And the system achieved an even higher cooling efficiency of 21.75 as floor radiant cooling is provided by the GHEs bypassing the heat pump.

2.2 Solar assisted ground coupled heat pump (SAGCHP) system

Although field studies on the CSHPSS system showed high solar fraction up to 70%, it was admitted that the large loss of useful solar energy was still an unsolved problem and preheating of the storage area was prerequisite. As a matter of fact, due to the enormous large ground thermal capacity, the seasonal natural recovery of soil temperature could almost keep the constant soil temperature after single year operation. It is the continuous heat extraction in the middle of the heating period that reduces the soil temperature and system efficiency conspicuously. Therefore, the solar collectors are recommended to be used as auxiliary source for on-site heating, which forms the basic ideas of the SAGCHP (as describe in Figure 2.2).
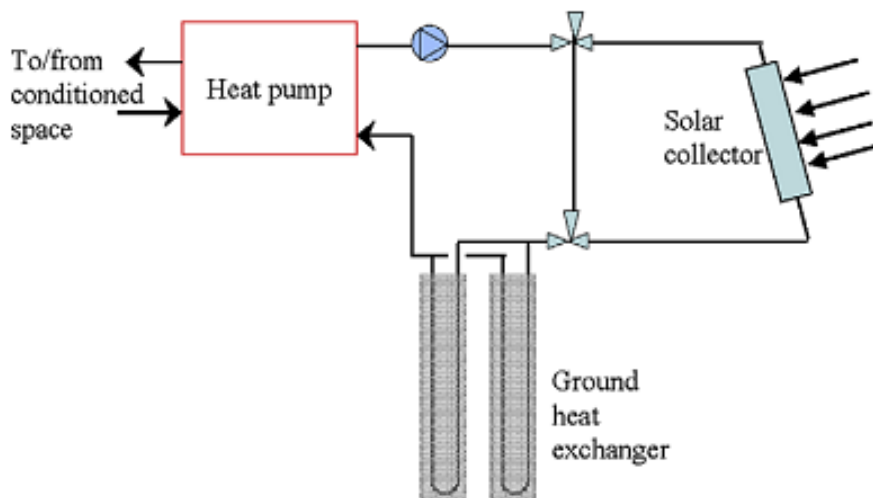
Figure 2.2 A flowchart of the SAGCHP

Comparisons of system performances were made among three simulation models: an air to air heat pump, an earth source heat pump and a solar assisted earth source heat pump. It was found that the earth source heat pump system consumed less power to

perform the same duties required from the air to air heat pump, while the solar loop did not show the expected effect of increasing heat pump COP, even though the borehole well temperature ascended to a level much above freezing during winter operation (AL-Juwayhel 1981). This is a rather early record concerned with simulation of the SAGCHP, whose results were never confirmed by experiments.

Mathematical model for the solar fraction of a SAGCHP is formulated based on the balance of energy (Yu, Ma et al. 2004). At the same time, the operation/shutdown ratio of the system in various operating conditions was also presented. The restoration of the ground temperature field was found to depend on the operation/shutdown ratio, and the optimum operating ratio of the ground coupled heat pump was about 33% to 50%, so that the system could achieve a solar fraction of 50~70 %.

The Southeast University carried out numerical simulation on different working modes of a solar-earth source heat pump (SESHP) (Yang, Shi et al. 2006). In a 20-day simulation, it was found that the SAGCHP system achieved the highest COP of 3.46 and energy saving rate of 14.5% when the solar collector and ground heat exchanger (GHE) were in series connection and the heat transfer fluid flowed through the solar collector first. This result was acquired under climatic condition of Qingdao, while different conclusions could be obtained in other areas. Similar simulation studies also existed in Sweden (Kjellsson, Hellström et al. 2010). Computational optimization was carried out under TRNSYS environment to study different combination of the system and the optimum design is when solar collectors were used for water heating in summertime and recharging the borehole in wintertime. COP improvement over the conventional GCHP was not apparent because of the extra power consumption from the circulating pumps. So

the major advantage of the SAGCHP system lies in the decrease of heat extraction rate from soil and the alleviation of thermal influence between closely neighbored boreholes.

Theoretical and experimental studies were performed for a solar-ground source heat-pump (SGSHP) system with a vertical double-spiral coil (VDSC) ground heat exchanger (GHE) (Bi and Chen 2002, 2004, 2005). The COP of the two heating modes including a SSHP (solar energy-source heat-pump) and a GSHP (ground-source heat-pump) was recorded as 2.73 and 2.83 respectively. The SSHP mode showed better collecting efficiency compared to solar direct heating systems and the GSHP's COP increased by 21% over the traditional single-pipe horizontal heat-exchanger system. VDSC-GHE was also proved to mitigate the temperature interference between the interior and exterior coil pipe.

Some researchers in Turkey presented energetic and exergetic modeling and experimental study of a solar assisted ground-source heat pump system (SAGSHPS) for system analysis and performance assessment (Ozgener and Hepbasli 2005, 2005, 2007). The SAGSHPS system was designed for greenhouse heating with a 50 m vertical 32 mm nominal diameter U-bend ground heat-exchanger under local weather conditions. The COP_{hp} (coefficient of performance of the heat pump) was about 2.00 at the end of cloudy day compared to 3.13 at the end of a sunny day. Average exergy efficiency was found to be 68.11%, with the peak value of 75.6% on a fuel basis.

As mentioned before, V. Trillat-Berdal et al. proposed the concept of GEOSOL, a process of combining the solar water heater with the GCHP system. The combined system was under 11-month operational tests in a 180 m^2 private residence (Trillat-Berdal, Souyri et al. 2006). During the system operation, energy injected into the ground

recovered 34% of the heat extracted, and the heat pump's coefficient of performance (COP) in heating mode had an average value of 3.75. However, the solar fraction for domestic hot water (DHW) was only 0.60 because of the solar heat recharged to the soil.

Due to the instability of solar radiation intensity, short-term storage is still required to maximize the function of solar heat. Latent heat energy storage tank (LHEST) is able to enhance the reliability and flexibility of the SAGCHP system, which was demonstrated by simulation under the severe cold climatic conditions of Harbin (Han and Zheng 2007; Han, Zheng et al. 2008). From simulation results, the average COP of the SAGCHP system in the whole heating period was 3.28 compared to 2.16 of the GSHP, and the effect of the LHEST becomes especially obvious in the initial and latter heating period. Experimental rigs were also constructed for further investigation (Han, Zheng et al. 2006; Wang, Zheng et al. 2006). $CaCl_2 \cdot 6H_2O$ was used as the PCM (phase changing material) in the LHEST and the maximum COP of the system achieved a value of 6.48, which was higher than common heat pumps. However, long-term operational characteristics and under-ground thermal balance were not verified.

Jilin University and Hebei engineering university in China also carried out simulations and experiments on the SAGCHP system under local climatic situations (Wang, Li et al. 2008; Wu 2008).

2.3 Hybrid ground coupled heat pump system (HGCHP)

Researches concerned with the SAGCHP system still needs standard design guidelines and optimization procedures based on more experimental proofs. Currently,

most studies still focus on the modeling and simulation, and there is no uniform criterion for the assessment of the system performances.

The Oklahoma State University has been exploring the GCHP applications for decades and some researchers (Hern 2004; P 2005; Xu 2007; Cullin 2008) tried to figure out a standard design and optimization methodology for hybrid ground coupled heat pump systems (HGCHP) with either an auxiliary heating (e.g. solar collector) or cooling (e.g. cooling tower) source to balance the underground thermal condition in any cases of load requirements. Based on former studies, a practical method for designing stand-alone and hybrid geothermal heat pump systems that use closed-loop vertical GHEs was developed (Chiasson 2007). Flat plate solar collectors and direct-contact evaporative cooling tower were used as supplement equipment for minimizing the size of borehole heat exchanger (BHE). Through detailed computer simulation, dimensionless groups were introduced in order to determine the total ground loop length and supplement equipment capacity required to balance the annual ground load. Especially, transient effects of the thermal mass of heat transfer fluid in the U-tube heat exchanger are calculated by finite difference method and the whole heat exchanger is modeled with an equivalent diameter approximation, whose results were compared with two analytical solutions and field study data.

Usually, the cooling tower is used as supplementary heat rejecter to the GHE in a cooling dominated situation. A practical hourly simulation model of the HGCHP system with cooling tower was built to calculate the operating data of the HGCHP system according to the building load. The design methods and running control strategies of the HGCHP system for a case study were also investigated (Man, Yang et al. 2008; Man,

Yang et al. 2010). The DHW tank was also incorporated into a HGCHP system as auxiliary heat rejecter (Cui, Yang et al. 2008). A mathematical model for this hybrid system as well as a traditional GCHP system were established within the HVACSIM+ environment and comparative simulation was carried out base on TMY weather data in Hong Kong. The system proved to effectively alleviate the imbalanced loads of the GHE and save 70% energy compared to an electric water heater.

2.4 Summary and prospect

According to aforementioned literatures, it can be clearly seen that the SAGCHP technology needs further improvement from the following aspects:

(1) The best utilization method of the solar energy has to be determined. Although seasonal solar storage for central heating system could achieve a high solar fraction over 70%, yet the large storage heat loss is still a problem. Alternatively, solar heat could be used to recharge the borehole, to provide direct floor heating, as the low temperature source for the heating pump, or for short-term storage. If the above methods are used in a multi-modes system, applying an optimal control strategy would be a challenge.

(2) Investigations on the important parameters that could influence the performances of the SAGCHP system are required. After taking the heating efficiency, solar fraction, soil thermal balance and economic factors into consideration, the systematic guidelines should be developed for the optimization procedures.

(3) To estimate the performance of a SAGCHP system and validate the design methodology, both long-term and short-term simulations and experiments should be conducted. Long-term researches include the underground thermal balancing verification, the energetic & exergetic calculation and life-cycle economic assessment; while short-term studies involve heating efficiency evaluation for single heating period, instant temperature changes and heat transfer analysis between modules of the system.

(4) When the DHW supply module is integrated to the SAGCHP system, it has to be redesigned for the interests of both sides. Studies has shown that DHW load profiles, control methods and ratios of collector area to water tank volume have great effects on water heating performances (Jordan and Vajen 2000; Lima, Prado et al. 2006; Badescu 2008), which are also significant factors influencing the performances of the SAGCHP system.

Apart from the above directions, there have already been new interests with respect to primary components of the SAGCHP system: the solar collector and the GHE.

2.4.1 PV/T panels in SAGCHP system

A photovoltaic/thermal (PV/T) panel is a combination of photovoltaic cells with a solar thermal collector, generating solar electricity and solar heat simultaneously. Because the conversion rate of a single PV cell is usually no more than 20 %, most of solar thermal energy is wasted and has to be removed by other ways to keep the PV cell from high temperature. By utilizing this part of solar heat to elevate the evaporating

temperature of the heat pump, both the PV conversion efficiency and the COP of the heat pump could be improved (Ji, Liu et al. 2008; Ji, Pei et al. 2008).

A sample system, consisting of 25 m^2 of PV/T panels and a ground coupled heat pump, has been built for space heating of a typical single-family in Dutch, and operational performances were simulated in TRNSYS. It has been found that this system could not only cover 100% of the total heating demand, but also produce all the electricity for system consumption and keep the long-term average ground temperature constant at the same time (Bakker, Zondag et al. 2005).

Economic analysis was conducted to compare the cost of the sample system to that of a system comprising a separate PV panel and a SAGHHP, but which is otherwise identical. The two systems yielded equal electrical and thermal energy, and required nearly the same initial investments. The system discussed in this reference shows a prosperous future for SAGCHP system with PV/T panels.

2.4.2 Pile-pipe GHE in the SAGCHP system

Recently, foundation piles of buildings are used to partly take the place of boreholes in the GHE, which is called pile-pipe GHE. Appling this new GHE to the SAGCHP system is also a promising developing direction.

Classical approaches of the line heat source model and the ''hollow'' cylindrical heat source model fails in the design and heat transfer analysis of the pile-pipe GHE. Therefore, a new ''solid'' cylindrical source model was presented to consider both the radial dimension and the heat capacity of the piles (Jun, Xu et al. 2009; Man, Yang et al. 2010).

Analytical solution derived for 1-D and 2-D pile-pipe models by means of the Green's function method was compared with the classical line source and ''hollow'' cylindrical source models, and validated by a numerical solution of the same model. It was proved that the 1-D and 2-D solid cylindrical source models can provide adequate tools for design and simulation of the pile-pipe GHE.

CHAPTER 3 DESIGN AND MODELING

This chapter presents the design of a new SAGCHP system, mainly consisting of a ground heat exchanger (GHE) subsystem, a solar collecting subsystem with heat storage, a water to water heat pump and a DHW supply subsystem, which could achieve multi-mode space heating, water heating, heat storage as well as soil recharging. The system could switch between six primary working modes with flexibility under the specified control strategies in relation to the environmental conditions. Mathematical modeling is completed in TRNSYS with detailed explanations on the main components.

3.1 Proposed design of the SAGCHP

3.1.1 Overview of the system

The proposed SAGCHP system combines a solar collecting system with a GCHP system through a water storage tank and plate heat exchanger as shown in Figure 3.1. A DHW tank is added to the coupled system, which could be heated by the solar collectors or the GCHP. The components 17 and 16 are valves used for switching between the two heat sources (solar thermal and geothermal energy). The whole system could be divided into five main modules, including the solar collecting subsystem (A), DHW supply subsystem (B), indoor heat exchanging subsystem (C), reversible heat pump subsystem (D), and close loop GHE subsystem (E). The main specific design parameters are listed in Table 3.1.
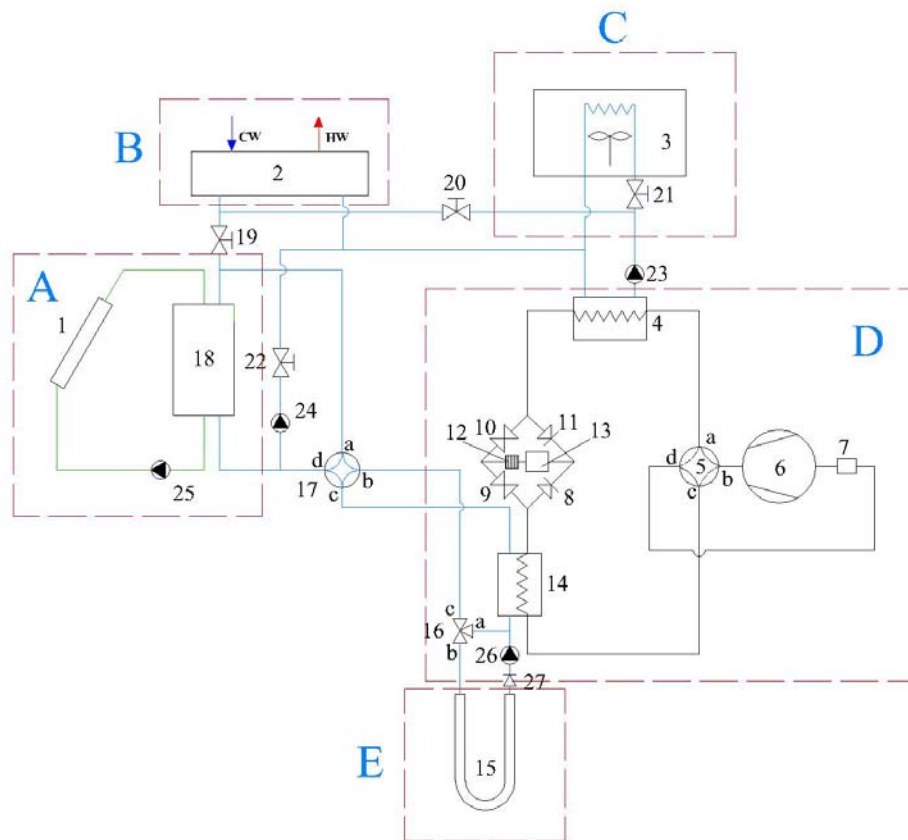
1. Solar collector 2. DHW tank 3. Indoor heating terminal 4. Indoor heat exchanger (HEX) 5. Four way valve（for refrigerant）6. Compressor 7. Separator 8&11. Check valves 9&10. Throttle valves 12. Filter-drier 13. Accumulator 14. Outdoor HEX 15. VGHX (vertical ground heat exchanger) 16. Three way valve 17. Four-way valve (for anti-freezing fluid) 18. Storage water tank 19-22. Control valve 23-26. Liquid pump 27. Check valve (for water and anti-freezing fluid) (**CW: cold water, HW: hot water**)

Figure 3.1 The system schematic diagram

The solar collection subsystem includes a 30 m^2 flat plate solar collector system, a plate heat exchanger, two circulation pumps and a 0.75 m^3 water storage tank. The heat transfer fluid in the solar collector is an anti-freezing fluid of 23.6% ethylene glycol (freezing point: -13 ℃, density: 1030 kg/m^3, specific heat capacity: 3.81 kJ/kg・K). In this simulation, the effectiveness of the plate heat exchanger is assumed as a constant of

0.8 for simplification. An ON/OFF differential controller with hysteresis effect is used to model the practical operation of the two circulation pumps subjected to temperature control.

The 0.35 m^3 DHW tank is also connected to the storage tank with the aid of flow diverters and mixers, and an additional controller is used for switching between hot water production and heat storage based on the system's load requirement, tank water temperature and solar radiation conditions. The electrical auxiliary heater is in series connection to the upper outlet of the tank, and is triggered whenever hot water is needed.

The ground heat exchangers with total borehole length of 270 m are coupled directly with the water storage tank. High conductivity grout materials (2.3 W/m·K) and HDPE pipes (0.42 W/m·K) with nominal outer/inner diameters of 40/32 mm are chosen for the GHE borehole and pipes. A constant flow rate of 1700 kg/m^3 is set for the circulation pump connected to the source side of the water to water heat pump, which is selected according to the maximum heating load. The inlet temperature to the heat pump is kept over 6 ℃ for freezing protection and reliable operation.

The load side heat exchangers together with temperature controllers keep the temperature over 18 ℃, and the load side water circulation pumps are subjected to intermittent control determined by heating requirement. The value of $\varepsilon C_{min}/UA$ (the product of heat exchanger effectiveness and the minimum capacitance rate of the two heat exchanging fluids, divided by the overall room heat loss coefficient) is set at 1.81, which is in reasonable range of 1-3, according to recommendations from previous researches (Klein 1976; Klein 2007).

Table 3.1 Basic system design parameters for simulation

Site location: Beijing (lat. N39°56', long. E116°20')

- *Building and heating load*
  Indoor/outdoor winter design air temperatures: 18℃/-9 ℃
  Average heating load in the coldest month: 12.44 kW
  Overall conductance of the building: 1600 kJ/(h・K)
  Building Thermal Capacitance: 15 MJ/K

- *Water to water heat pump*
  Rated heating capacity of heat pump: 14 kW (TRANE-EXWE-060)

- *Underground loop and soil characteristics*
  Thermal conductivity of ground soil: 2.1 W/(m・K)
  Inside/outside diameters of HDPE pipes: 32/40 mm
  Borehole number:　3
  Borehole depth:　90 m

- *Flat plate solar collector*
  Collector area:　30 m^2
  Bottom & edge loss coefficient:　10 kJ/(hr・m^2・K)
  Absorber plate emittance:　0.11
  Absorber plate absorptance:　0.90

- *Storage tank:*
  Tank volume:　0.75 m^3
  Heat loss coefficient:　1.2 kJ/(hr・m^2・K)

- *DHW tank:*
  Tank volume:　0.35 m^3.
  Heat loss coefficient:　1.2 kJ/(hr・m^2・K)

3.1.2 Working principles of main operational modes

The working principles of the main control modes are given as follows based on Figure 3.1.

(1) Mode 1 for solar direct heating

When water temperature in the storage tank is high enough for space heating (35 ℃ for a floor heating terminal and 45 ℃ for a fan coil heating terminal), the system can

deliver hot water directly to the indoor heat exchanging unit (component 3) by turning on valves 19, 20, 21, 22 and pump 23, while turning off other pumps.

(2) Mode 2 for solar heat pump heating

When the outlet water temperature in the storage tank is 2 ℃ higher than the average soil temperature, solar collectors are used as the only heat source for the system and the ground loop are bypassed with control valve 17 connecting "d c" and control valve 16 connecting "a c". Hot water can also be supplied at the same time if solar radiation is intensive. The pump 26 and valves 19, 20, 22 are closed while other pumps and valves are kept open.

(3) Mode 3 for ground-source heating

When the water outlet temperature from the tank is lower than the average soil temperature, the heat pump is working with the GHE as the only heat source. The control valve 17 connects "c b" while control valve 16 connects "a b". The working conditions of the circulation pumps 24, 25 are determined by the temperature difference of the solar collectors.

(4) Mode 4 for solar coupled ground source heating

When solar energy is abundant, the inlet water temperature to the heat pump might exceed the maximum allowed inlet temperature according to the product specifications (29 ℃ in this simulation). Therefore, the ground heat resource as well as solar energy resource is used as heat sources of the heat pump and extra solar heat is stored in the tank as well as recharged to the soil. Control valve 17 connects "d c", and valve 16 connects "b c" in the working modes.

(5) Mode 5 for solar energy storage and recharging

Once the collector outlet temperature is 10 ℃ higher than the average temperature of the storage tank, the system starts collect solar energy and keeps transferring energy to the tank until the outlet temperature drops back to the average storage tank temperature. Recharging and storage could be achieved together with the heat pump, or could work only between space heating intervals in wintertime. In non-heating seasons, when the outlet temperature of the storage tank is 15 ℃ higher than the average soil temperature, valve 17 connects "b c" and "a b", delivering the energy stored in the tank 18 to soil.

(6) Mode 6 for DHW production

Hot water production could be achieved by opening valve 19 & valve 22 and the solar water heating process begins as soon as the outlet collector temperature exceeds the average DHW temperature by 6 ℃. The solar collectors are then switched off when the outlet temperature drops to 2 ℃ over the average tank temperature or the tank temperature reaches 55 ℃ (the high limit alarm temperature).

3.2 Mathematical modeling of the SAGHCP

Modeling of the designed system is achieved in the TRNSYS (Transient System's Simulation Program) simulation studio. The TRNSYS is a comprehensive and extendable modeling environment for transient simulation of various energy conversion systems. Its development was originally initiated by the Solar Energy Laboratory in 1974 at University of Wisconsin, USA, and was continuously improved by users and programmers all over the world. It is widely used by engineers and researchers to validate new energy concepts like various solar thermal engineering systems to provide space heating and domestic hot water. Design and simulation of building installations, control strategies, occupant behaviors, and renewable energy systems such as photovoltaic, wind and hydrogen systems are also available under the TRNSYS modeling environment. Up to 40 units were connected on the simulation deck in order to perform numerical modeling of the designed SAGCHP system under specified conditions. Theoretical models of the important components used in the system are described in details and their relative control methods are introduced.

3.2.1 The solar collector

The theoretical flat plate solar collector model, Type 73, is adopted to model the performance of the solar collectors. The total collector array may consist of collectors connected in series or in parallel. The thermal performance of the total collector array is determined by the number of modules in series and the characteristics of each module (transmittance, absorptance of the glazing, overall heat loss coefficient, etc.). The flat-plate solar collectors were used in this system because it is well-developed, economical and suitable for application in middle and low temperature solar thermal systems. The

Hottel-Whillier steady-state model is used for estimating its thermal performance. The useful energy gain (Q_u) by the collectors is shown as follows:

$$Q_u = \frac{A_C}{N_S} \sum_{j=1}^{N_S} F_{R,j}(I_T(\tau\alpha) - U_{L,j}(T_{i,j} - T_a)) \tag{3.1}$$

where A_C is the collector area; N_S is the number of identical collectors in series; I_T is the global radiation incident on solar collectors; U_L is the overall heat loss coefficient of solar collectors per unit area; T_i is the inlet temperature of fluid to collector; T_a is the ambient air temperature; ($\tau\alpha$) is the product of the cover transmittance and the absorber absorptance; F_R is the overall collector heat removal efficiency factor, which is calculated by:

$$F_{R,j} = \frac{N_S m_f C_{pf}}{A_C U_{L,j}}\left(1 - \exp(-\frac{F' U_{L,j} A_C}{N_S m_f C_{pf}})\right) \tag{3.2}$$

where m_f is the collector mass flow rate; C_{pf} is the specific heat of collector fluid; F' is the collector efficiency factor determined in a manner given by Klein S. A. (1976).

3.2.2 The water-to-water heat pump

Type 668 is a single-stage water-to-water heat pump used in this simulation which is linked with the load-side and source-side subsystems. This model is based on user-supplied data files containing the catalog data for heating or cooling capacities with power consumptions, and is able to perform linear interpolating according to the entering source and load temperatures. Type 668 could operate with temperature level control and perform heating or cooling modes in response to the input control signals. When the user-defined control signal indicates that the unit should be on in either heating or cooling mode, the Type 668 operates at its rated capacity level until the control signal switches to "off". Type 668 can interpolate data within the range of input values specified in the data

files, but it is not able to extrapolate beyond the data range and will return the values of the dependent variables with regard to the maximum or minimum of the range. The COP of the heat pump and outlet conditions can be derived from:

$$COP_{hp} = \frac{Q_{heating}}{W_{hp}}$$ (3.3)

$$Q_{source} = Q_{heating} - W_{hp}$$ (3.4)

$$T_{source,out} = T_{source,in} - \frac{Q_{source}}{m_{source}C_{p,source}}$$ (3.5)

$$T_{load,out} = T_{load,in} - \frac{Q_{heating}}{m_{load}C_{p,load}}$$ (3.6)

where $Q_{heating}$ is the heat supply to load; Q_{source} is the heat absorption from source; $T_{source,in}$ is the inlet source temperature to heat pump; $T_{source,out}$ is the outlet source water temperature from the heat pump; $T_{load,in}$ is the inlet load water temperature to the heat pump; $T_{load,out}$ is the outlet load water temperature from the heat pump; W_{hp} is the power consumption of the heat pump; m_{source} is the source water mass flow rate; m_{load} is the load water mass flow rate; $C_{p,load}$ is the specific heat of load fluid; $C_{p,source}$ is the specific heat of source fluid.

3.2.3 The ground heat exchanger (GHE)

The vertical ground heat exchanger model, Type 557, is the most commonly used model in ground-source heat pump applications. Up to 10 U-tubes per borehole is allowed for user's convenience (Klein 2007). The program assumes that the boreholes are placed uniformly within a cylindrical storage ground volume (V_s), which can be calculated by:

$$V_s = \pi N_b H (0.525B)^2$$ (3.7)

where N_b is the number of boreholes; H is the borehole depth; B is the borehole spacing.

The borehole thermal resistance (R_b) is defined as:

31

$$R_b = \frac{\overline{T_f} - \overline{T_b}}{q} \qquad (3.8)$$

where $\overline{T_b}$ is the average temperature at borehole wall; $\overline{T_f}$ is the average fluid temperature in tubes; q is the power pulse per unit length.

There is a convective heat transfer within the pipes and conductive heat transfer between the pipe and surrounding soil. The calculation of the ground temperature is a superposition of three parts: a global temperature, a local solution and a steady-flux solution. The global and local problems are solved with the use of an explicit finite difference method. The steady state flux solution is obtained analytically and the temperature is then calculated using the superposition methods (Hellström 1991). The computer code of the Type 557 was initially written by the Department of Mathematical Physics in Lund University.

3.2.4 The building load

A simple degree-day model, Type 12c, is chosen to simulate the building load instead of a detailed multi-zone building model like Type 56, because the objective in the present research was to investigate the optimization of the SAGCHP system instead of simulating any building energy system. In this Type, an hour by hour structured load of a simple building space is estimated. Mode 4 of this Type models a single lumped capacitance house which allows the indoor temperature to float while compatible with the temperature level control. The total heat loss (Q_{loss}) of the house could be calculated according to the overall conductance (UA) by equation (3.9). The overall conductance and the house thermal capacitance (C) are given parameters, and the different building

loads are modeled by varying these values. The house thermal capacitance (CAP) is the sum of the products of mass, heat capacity and temperature changes of all the elements in a building, as shown in equation (3.10). For computational stability, the thermal capacitance should be chosen so that the maximum swing of room temperature in a time step is on the order of the controller dead band ranges. Then, the temperature change in the room is expressed in equation (3.11).

$$Q_{loss} = UA(T_R - T_a) - Q_{gain} \tag{3.9}$$

$$CAP = \sum (m * C_P)_i \Delta T_i \tag{3.10}$$

$$CAP \frac{dT_R}{dt} = \varepsilon C_{min}(T_i - T_R) + Q_{gain} - UA(T_R - T_a) + Q_{aux} - Q_{sens} \tag{3.11}$$

where T_R is the room temperature of the residence; Q_{gain} is the heat gains within the room; m is the mass flow rate; C_p is the specific heat; ΔT_i is the temperature change of an element; ε is the heat exchanger effectiveness; C_{min} is the minimum fluid capacitance rate of the load heat exchanger, Q_{aux} is the auxiliary energy to the room, Q_{sens} is the cooling input to room.

3.2.5 Weather data model

The component to provide weather data for the simulated system is Type 109, which combines data reader and solar radiation processor. This Type serves the main purpose of reading weather data at regular time intervals from a data file, converting the weather data to the desired data units and generating direct and diffuse solar radiation outputs for an arbitrary number of surfaces with specified orientation and inclination. Perez model, usually considered to be the best available model, was chosen for the combined solar

radiation processor to calculate sky diffusive radiation. This model accounts for circumsolar, horizon brightening, and isotropic diffuse radiation by empirically derived "reduced brightness coefficients", which are functions of sky clearness and brightness. In the simulation, the Type 109 gives input to the solar collector, the building load and the GHE model. The typical meteorological year (TMY) data of Beijing and Harbin is obtained from the Metronome weather documentations.

3.2.6 Water storage tank

A stratified tank with auxiliary electric heater is modeled by the Type 4 for both the heat storage tank and the DHW tank. It can be modeled by assuming a composition of N (less than 15) fully-mixed equal volume segments, which would determine the degree of stratification. In this simulation, the inlet of heat source was fixed at the segment under the auxiliary heater and the load side inlet was at the bottom, while the outlet of heat source and load were fixed at the bottom and top segments, respectively. Because the heat transfer fluid in solar collectors differs from that in the water tank, a zero capacitance sensible heat exchanger with a constant effectiveness (0.80) was connected to the source side of the water tank. Options of temperature dead band on heater thermostats, incremental loss coefficients, and losses to gas flue of auxiliary heater are all available for user setting.   Energy exchange between the tank and environment, inlet energy from the heat source and outlet energy for the load are calculated by the following equations:

$$Q_{env} = \sum_{i=1}^{N} UA_i(T_i - T_{env}) + \gamma_f \sum_{i=1}^{N} (UA)_{f,i}(T_i - T_f) \qquad (3.12)$$

$$Q_s = m_L C_{pf}(T_i - T_L) \qquad (3.13)$$

$$Q_{in} = m_h C_{pf}(T_h - T_i) \tag{3.14}$$

$$\Delta E = \frac{V_t \rho_f C_{pf}(\sum_{i=1}^{N} T_i - \sum_{i=1}^{N} T_i\big|_{t=TIME0})}{N} \tag{3.15}$$

where Q_{env} is the energy loss from the tank to the surrounding environment; γ_f is the control function to define if the auxiliary heater is on or off; T_f is the average temperature of exhaust flue when heater is not operating; Q_s is the energy removed from the tank to supply the load; m_L is the fluid mass flow rate to the load; T_L is the temperature of the fluid replacing that extracted to supply the load; T_h is the temperature of the fluid entering the storage tank from the heat source; Q_{in} is the energy input to tank from hot fluid stream; V_t is the tank volume; ρ_f is the fluid density; ΔE is the change of internal energy of the tank [kJ].

3.2.7 Differential controller

The Type 2 simulates a differential temperature controller with hysteresis effect. This controller generates a control signal γ_o with only zero or one as its value. The value is decided by a function of the difference between upper and lower temperatures, T_H and T_L, compared with two dead band temperature differences, ΔT_H and ΔT_L. The new value of γ_o also depends on whether the old value γ_i equals zero or one and the hysteresis effect is realized by connecting γ_o to γ_i. For safety considerations, a high limit cut-out is also included with the controller to arbitrarily set the control output to zero once the high limit condition is exceeded. Specific working functions are explained as follows:

If the controller was previously ON ($\gamma_i = 1$):

If $\Delta T_L \leq (T_H - T_L)$, $\gamma_o = 1$

$$\text{If } \Delta T_L > (T_H - T_L), \gamma_o = 0$$

If the controller was previously OFF (γ_o =0):

$$\text{If } \Delta T_H \leq (T_H - T_L), \gamma_o = 1$$

$$\text{If } \Delta T_H > (T_H - T_L), \gamma_o = 0$$

3.2.8 Control settings

Mathematical modeling of the SAGCHP system is finally completed by combing above mentioned components with the following settings of the control card. And a sample flowchart constructed in the TRNSYS simulation studio is displayed by Figure 3.2. The following parameters are used in the simulations.

(1) Simulation time step: 1 min ~ 15 min;

(2) Error tolerance for integration and convergence: 0.001 (relative);

(3) Indoor temperature: Upper limit: 20 ℃; Lower limit: 18 ℃;

(4) Solar collector: ΔT_{on} = 10 ℃; ΔT_{off} = 0.5 ℃ (ΔT: the difference between the collector outlet temperature and the average storage tank temperature);

(5) Water storage tank as the heat source for the heat pump: ΔT_{on} = 2 ℃; ΔT_{off}=0 ℃ (ΔT: the difference between the storage tank temperature to load and the average ground storage temperature);

(6) Activation of direct space heating without the heat pump: T_{on}=35 ℃, T_{off}=30 ℃ (T: the storage tank temperature to load);

(7) Operation of the DHW tank: ΔT_{on} = 6 ℃; ΔT_{off}=2 ℃ (ΔT: the difference between the collector outlet temperature and the average storage tank temperature);

(8) Soil recharging in non-heating period: ΔT_{on} = 15 ℃; ΔT_{off}=10 ℃ (ΔT: the

difference between the average storage tank temperature and the average ground storage temperature).
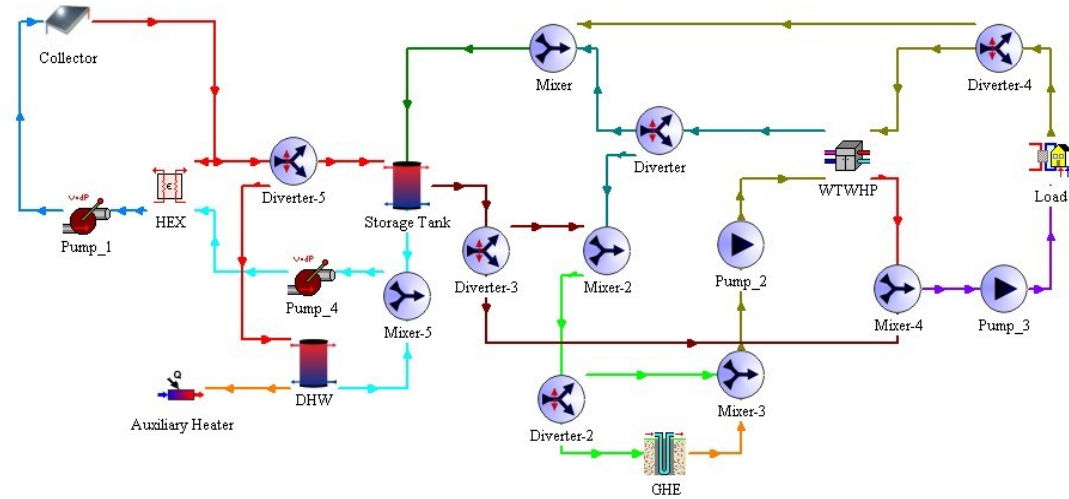
Figure 3.2 Overview of a sample SAGCHP system in the TRNSYS studio (WTWHP: Water-to-Water Heat Pump)

CHAPTER 4 OPTIMIZATION AND PARAMETRIC STUDIES

The system's optimization process starts with the comparison between different combining modes of the solar collector and the GHE. Based on the weather condition of the coldest period, the most appropriate coupling method will be determined. Then, a parametric investigation is performed to optimize the space heating efficiency and the solar fraction. Furthermore, the optimal ratio of the collector area and GHE loop length is studied for long-term system operation and its diverse control strategies are under discussion.

4.1 Weather condition and load characteristics

The simulation process in a year could be divided into two periods: Stage 1 starts from 1st November and ends on 1st April, in which space heating is the major load of the system, and the modes 1-5 are in alternate operation. The rest time belongs to Stage 2, when the system is primarily working for the DHW and soil recharging for mode 5 or mode 6, and the recovery of soil temperature largely depends on this period. During the heating session, the average outdoor temperature is about 0.16 ℃, with a yearly space heating load of 109 GJ.
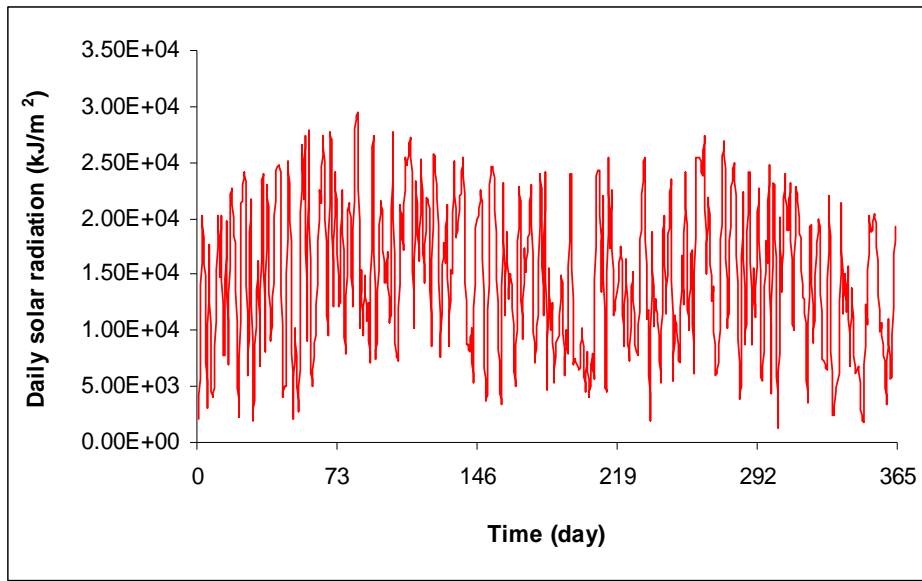
Figure 4.1 Solar radiation conditions in a TMY
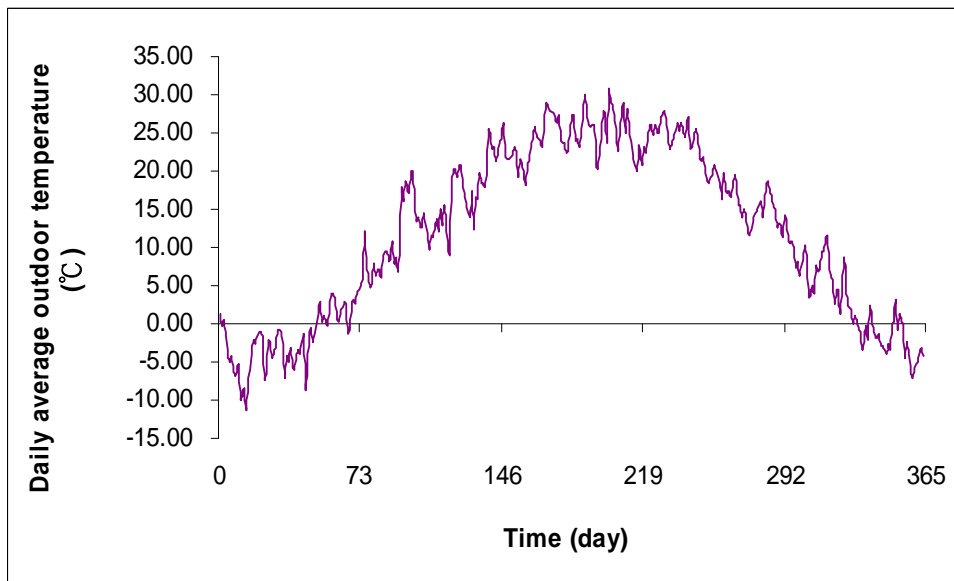
Figure 4.2 Ambient temperatures in a TMY

Figure 4.1 shows the whole year hourly solar radiation in Beijing. From this figure, we can draw the conclusion that solar radiation reaches the highest level at the beginning

and the end of the heating period, and in the middle of non-heating seasons, the radiation is as weak as the level in the middle of the heating period. Low solar incident angle in cold winter and more rainy days in hot summer might explain such solar radiation distribution. From Figure 4.2, the lowest outdoor temperature is observed at the same period (December and January) when solar radiation is weak, which challenge the reliability of the system in winter operation. Therefore, comparison between different coupling methods of the system is carried out with regard to the weather condition in January. Furthermore, the peak heating load occurs at the same time with the adverse environmental conditions because of the largest difference between the outdoor and indoor temperatures (from Figure 4.2 and Figure 4.3), which could strongly explain the necessity of the solar collectors. By adding solar collectors to the GCHP, the peak heating load is partly afforded by the collected solar heat, and the inlet temperature could also be increased by a certain level to avoid freezing problems in maximum load occasions.
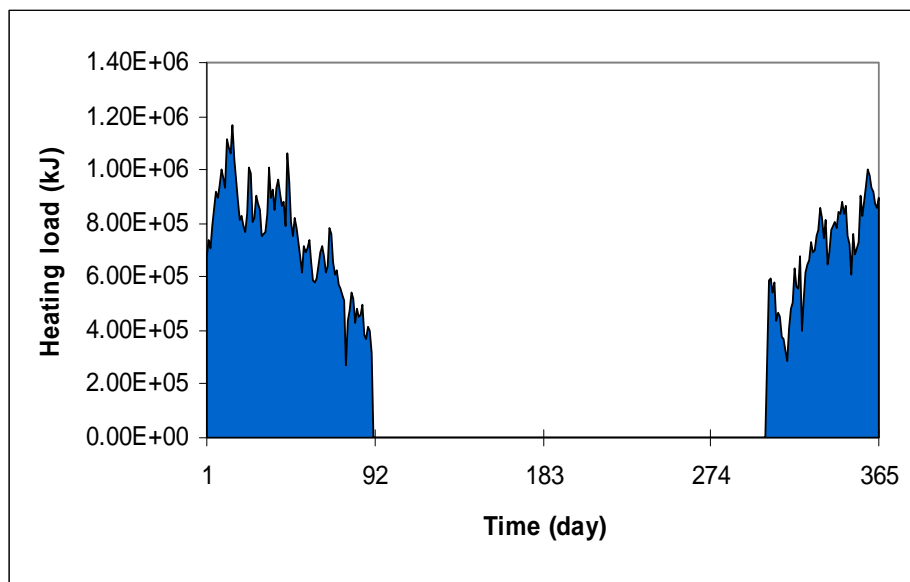
Figure 4.3 Yearly heating load distributions
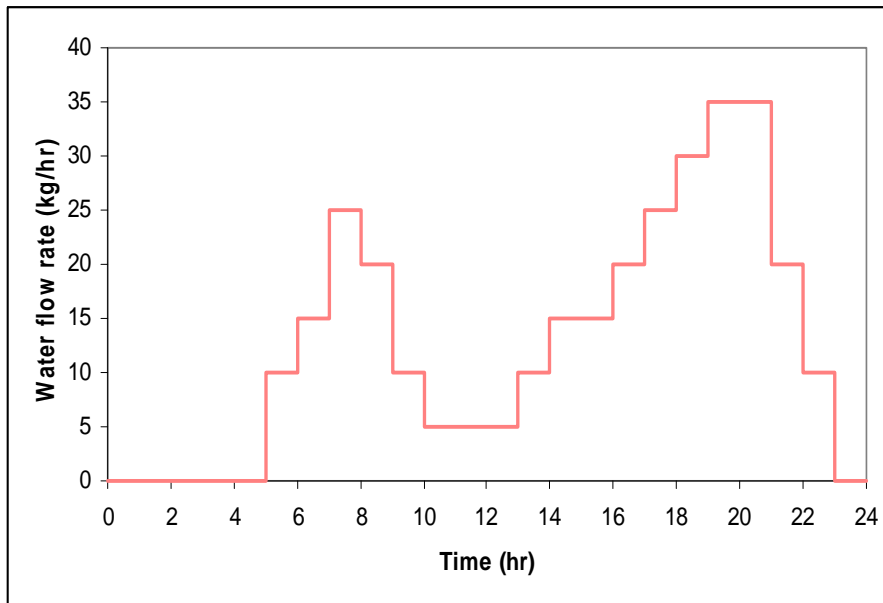
Figure 4.4 Daily DHW flow rate profiles

The water flow rate distribution of the DHW is described by Figure 4.4, in which most of the hot water requirement occurs at around 8:00pm when solar radiation is not available. This situation proves the need for storage tank and auxiliary heating instruments. If a phase changing material (PCM) is used instead of water as storage material, solar energy could be utilized more efficiently. However, taking initial cost into consideration, the simulation still performs with traditional water tank. The cold water inlet temperature is set to 5 ℃ from November to March, 20 ℃ from June to August and 15 ℃ through the rest time in a year. The required hot water temperature is 45 ℃ from June to August and 50 ℃ during other operation periods. As a result, the total hot water heating load in a year is up to 8861 MJ.

4.2 Optimization of the combination mode

4.2.1 Model definition and classification

The operation of a SAGCHP system can be divided into alternate operation mode and combined operation mode (Yang, Shi et al. 2006). The ground heat exchanger (GHE) only works as heat source when solar energy is not available in an alternate mode, while solar collectors and GHE work simultaneously in the combined mode. In this simulation, the combined working mode is our main investigating target. The combined working mode can be further classified by direct-coupled mode and indirect-coupled mode. The direct-coupled mode uses the collected solar energy immediately for heating. On the other hand, the indirect-coupled mode allows the collector to be combined with the GHE through a fluid tank, which means solar thermal storage is available for balance of difference in the short-time heating requirement. In addition, as the performance of the direct-coupled mode could be influenced by different system configurations, two direct-coupled models with different combination sequence of collectors and GHEs are contrasted.

As a result, five models are constructed to compare the heating performances of the GCHP system and different other combination modes of the SAGCHP system. Model 1 is the GCHP system used as the base case in the following analysis and comparisons. Model 2 is a direct-coupled SAGCHP system: the outlet source HTF from the heat pump passes through the solar collectors first and then to the GHE. Model 3 is the other connecting sequence of the direct-coupled SAGCHP system: the outlet source HTF from the heat pump passes through the GHE first and then to the solar collectors. Model 4 adds a water storage tank for energy storage and solar direct space heating based on the model with

better performance between Model 2 and Model 3. Model 5 is an indirect-coupled system SAGCHP system with water storage tank for both energy storage and solar direct space heating.

4.2.2 Comparison between Models with different coupling modes

The simulation results of the base case (Model 1) and two directly coupled SAGCHP systems (Model 2 & Model 3) are first compared as shown in Figure 4.5, Figure 4.6 and Figure 4.7. The COP_{sys} is calculated with the total supplied useful heat divided by the total power consumption of the system over a specified time period.
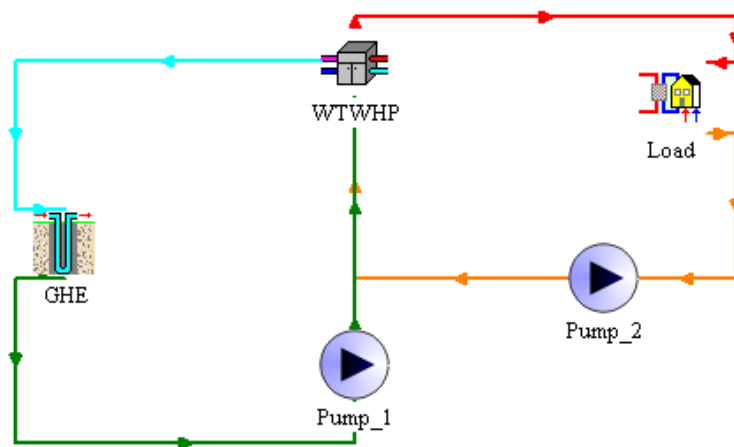
Figure 4.5 TRNSYS layout of model 1 (WTWHP: water-to-water heat pump)
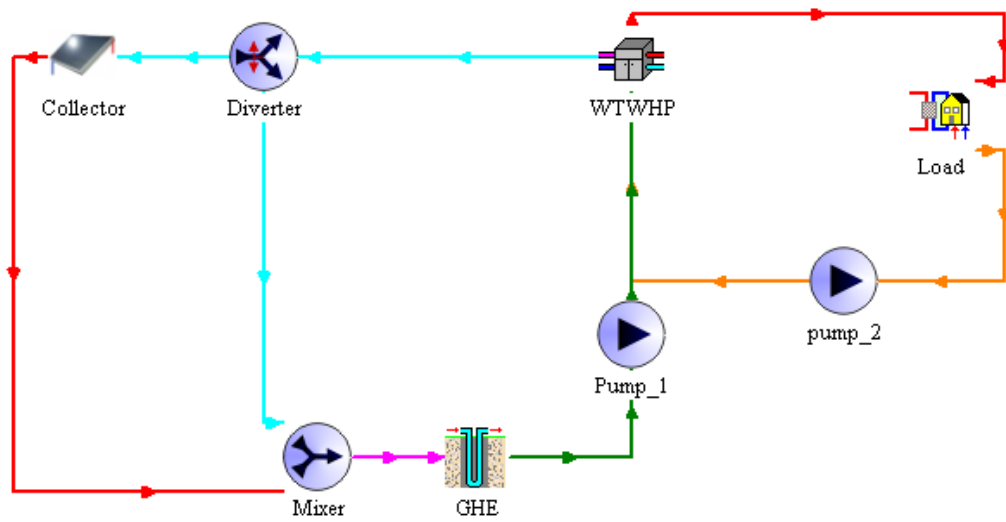
Figure 4.6 TRNSYS layout of model 2 (WTWHP: water-to-water heat pump)
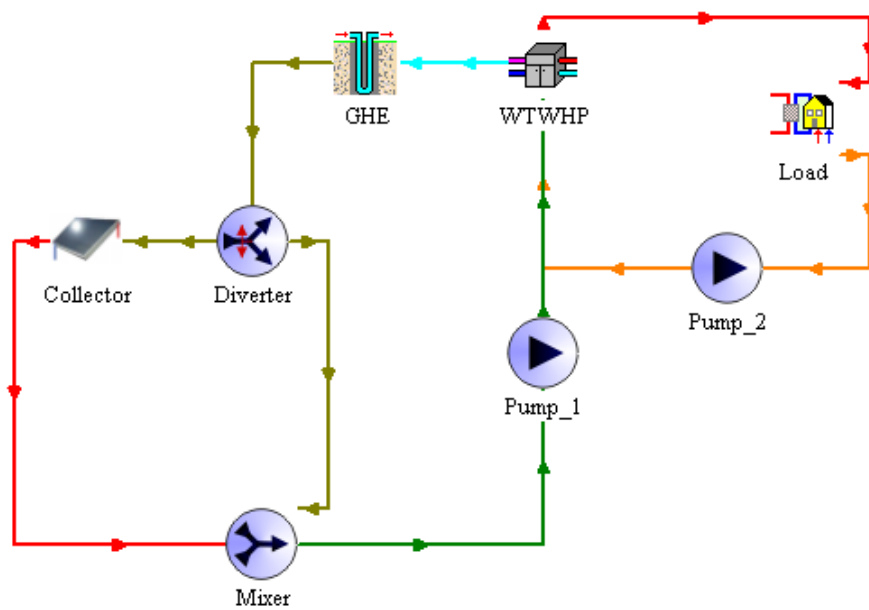
Figure 4.7 TRNSYS layout of model 3 (WTWHP: water-to-water heat pump)
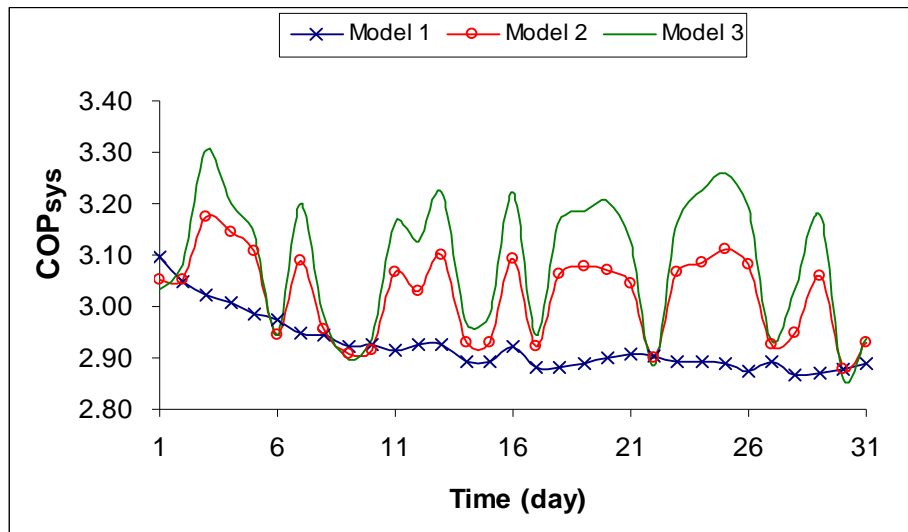
Figure 4.8 Daytime COP$_{sys}$ comparison of Model 1, 2, 3 (daytime: 8:00 AM ~ 17:00 PM)
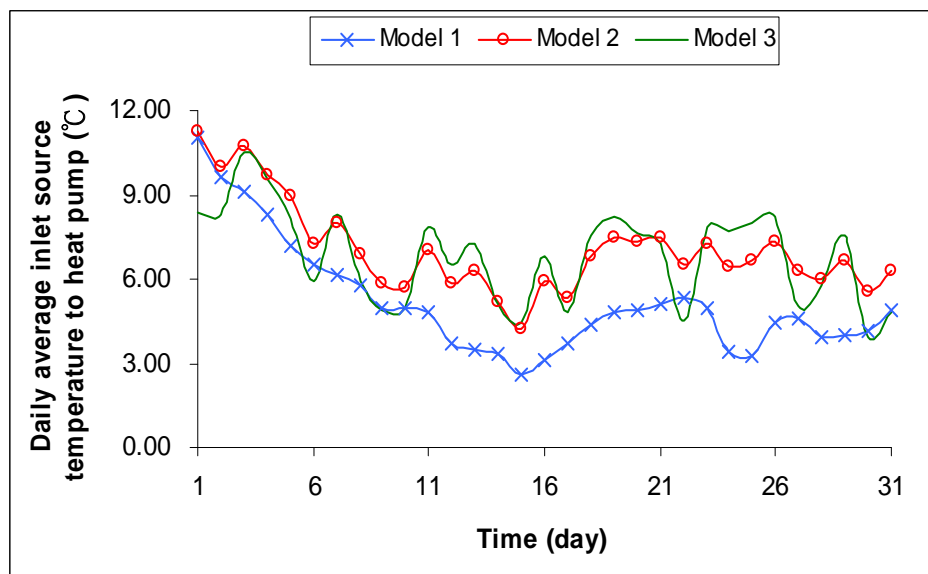
Figure 4.9 Daily average inlet source temperatures to the heat pump of Model 1, 2, 3

From Figure 4.8, the daytime COP$_{sys}$ of the Model 3 is always higher than that of other models because high temperature HTF from the solar collectors flows directly back to the heat pump whenever heat collection is available. However, the average inlet

temperature of the Model 2 is the highest and is most stable in the three models, because part of the solar radiation is used to recover the soil temperature drop which makes the inlet temperature higher when solar radiation is not available. The tendency can be clearly observed from the curve in Figure 4.9. Whereas both curves of the COP_{sys} and inlet source temperature displayed several fluctuations owing to the solar assisted heating process, they kept an overall declining trend throughout January. Such situation results in the decreasing soil temperature in the simulation period (described in Figure 4.10), which leads to 2.15 ℃ drop in Model 2 in contrast with the 2. 23 ℃ and 2.55 ℃ in Model 3 and Model 1.
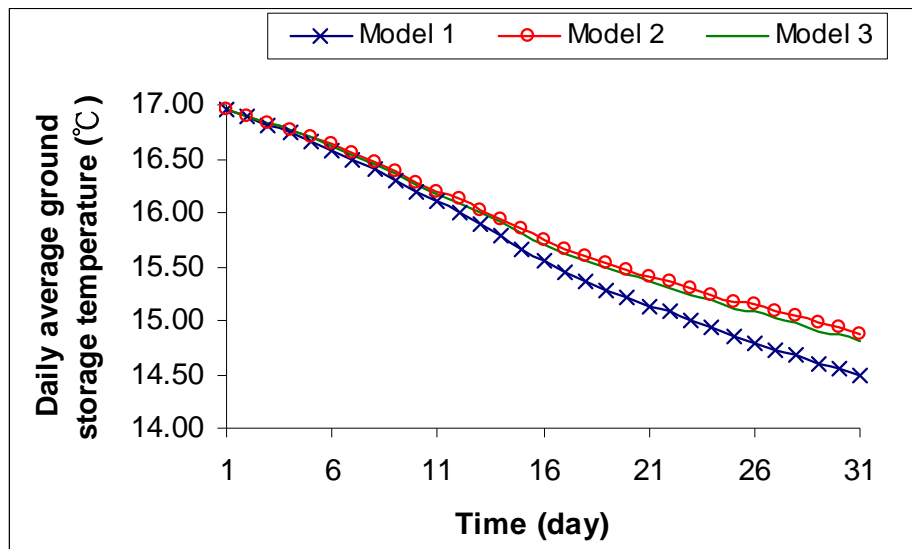
Figure 4.10 Daily average ground storage temperature comparison of Model 1, 2, 3

Both Model 2 and Model 3 exhibited improved system efficiency and reduced soil heat extraction with solar energy as an alternative heat source. Although the monthly average COP_{sys} of the Model 2 in January is 0.68% lower than the Model 3, the soil heat

extraction of Model 2 still achieved a 3.39% reduction. In addition, the average and minimum inlet source temperature of the Model 2 was improved by 3.07% and 4.01%, respectively compared with Model 3. Furthermore, if the whole heating period is taken into consideration, the inlet source temperature of Model 3 might exceed the upper limit (29 ℃) provided by the producer's data file at the beginning and the end of the heating period. Therefore, in spite of the higher COP_{sys} of Model 3, Model 2 is considered to be the preferable combination in the direct-coupled systems.
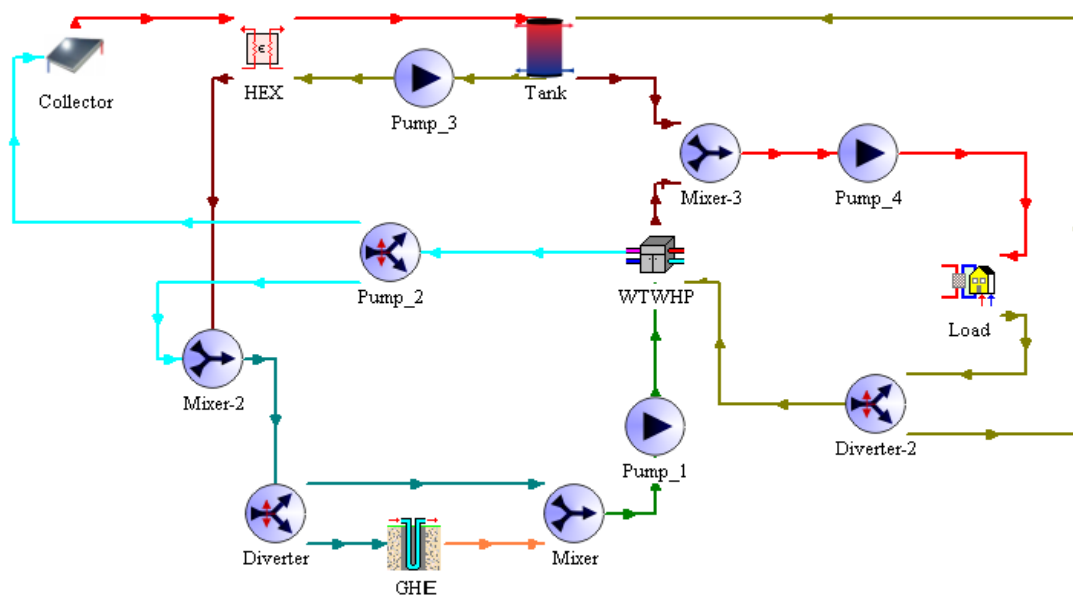
Figure 4.11 TRNSYS layout of Model 4

According to the above analyses, Model 2 is consequently used as the optimum combining sequence to construct Model 4 (Figure 4.11), a directly coupled system with extra water storage tank to perform the solar direct heating function of the SAGCHP system. Control strategies were also added to the model in order to control the inlet source temperature under the upper limit specified by the product manual. The indirect-

coupled system, known as Model 5 (Figure 4.12), is also simulated and compared with
Model 4.
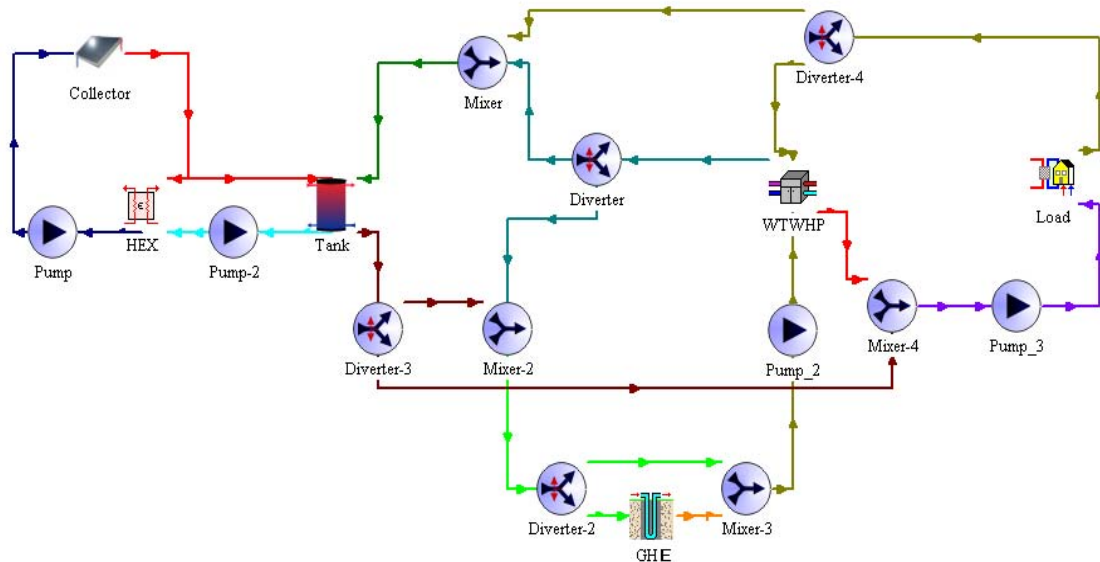
Figure 4.12 TRNSYS layout of Model 5

The main operation characteristics of direct-coupled and indirect-coupled operation
mode can be summarized from Table 4.1. The COP_{sys} of Model 5 is obviously higher than
that of Model 4, with a monthly average increment of 4.90% and a maximum daily
promotion of 25.48%. On the contrary, the soil heat absorption of Model 5 is 8.15%
higher than that of Model 4, because solar heat is allowed to recharge the ground even
after the heat pump stops working, which consumes more power consumption of the
circulating pumps. Most of the solar energy collected by Model 4 is used to increase soil
temperature, so that the solar direct heating mode of the designed system is not available
as the temperature in the storage tank could not reach the minimum temperature required

for direct space heating. If the decrease in heat extraction has already been enough for keeping the thermal balance in soil, Model 4 is not as economical and practical considering its low heating efficiency even compared with the base case.

Table 4.1 Performance analysis results of Model 4 and 5 in January

Operation model	Monthly Average COP	Average inlet source temperature (℃)	Minimum inlet source temperature (℃)	Heat extraction (kJ)	Temperature drop of soil (℃)
4	2.86	7.79	3.26	1.681E7	1.99
5	3.00	7.21	2.23	1.818E7	2.15

4.2.3 Optimization on Model 5 through parametric studies

Optimization of the selected Model 5 from the above comparison and analysis focuses on the parameter settings of the solar thermal collection subsystem, including the adjustment of physical characteristics of solar collectors, the mass flow rate and the storage factor. First of all, some parameters of the theoretical solar collector model and the storage tank model are changed to model a solar collector with higher efficiency. The collector fin efficiency and absorptance of the plate are increased to 0.95 and 0.90, while the absorber plate emittance and the bottom & edge loss coefficient are reduced to 0.1 and 10 kJ/(h m^2 K), respectively. The tank loss coefficient was decreased to 1.2 kJ/(h m^2 K). With the above parameter resetting, the system could get a reasonable and higher solar collecting efficiency.

● *Optimization of collector mass flux in the solar collecting subsystem*
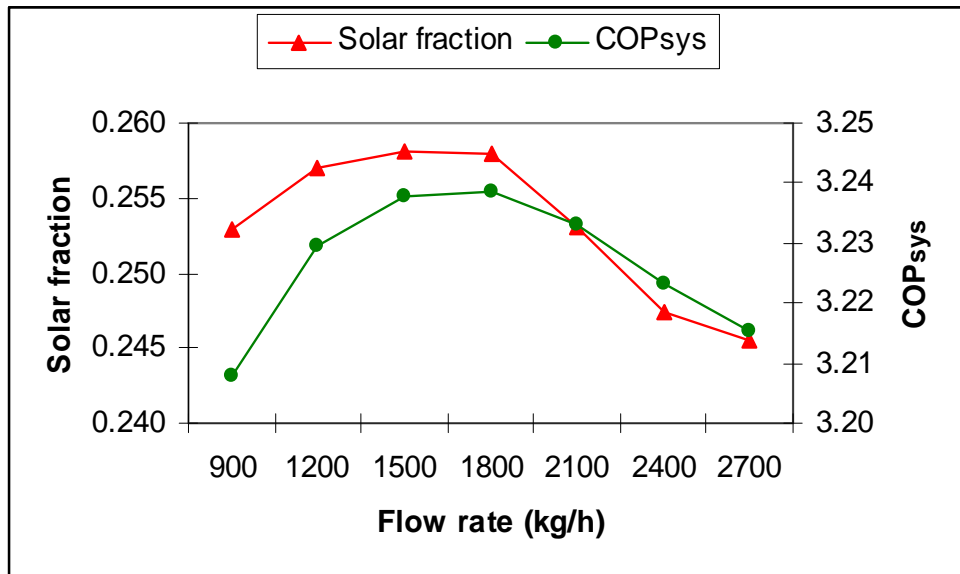
Figure 4.13 COP$_{sys}$ & Solar fraction (Useful solar heat collected/total system load) of the system with mass flow rates of solar collectors

The optimization procedure of the solar collecting subsystem starts with the test on different mass flow rate while other parameters kept unchanged. When the solar collector area and storage tank volume were kept at 30 m^2 and 0.75 m^3, the solar fraction of the system for different mass flow rates ranging from 900 kg/h to 2700 kg/h with an increment of 300 kg/h were simulated and the results are shown in Figure 4.13.

At the beginning, both the COP$_{sys}$ and solar fraction increase with mass flow rate because a lower flow rate results in the development of high temperatures in the solar collectors which would bring down the collecting efficiency. However, when the mass flow rate becomes too large, the outlet temperature of the collector will be too low to elevate the evaporating temperature of the heat pump and also handicap the efficiency of heat recharging to the soil due to a lower temperature difference. It can therefore be

clearly seen that both the COP_{sys} and solar fraction reached the maximum value with a mass flow rate of around 1500 kg/h, which means that the optimum collector mass flux is approximately 50 kg/(h·m^2). When the mass flow rate was at a level of 50 kg/(h·m^2), the heat extraction rate is reduced for about 30% compared with a traditional ground source heat pump system. The optimum collector mass flux acquired from this simulation coincides with relevant researches on solar heating systems (MICHAELIDES 1993).

● *Optimization of water tank storage factor*

The storage factor is defined as the tank volume per collector area, which could have effect on the thermal performance of the solar heating systems, according to Klein, S. A. (1976). In this part the storage factor was investigated when the solar collector area is 30m^2 and the mass flow rate at the aforementioned optimal value of 50 kg/(h·m^2), and its effects on system performances are shown in Figure 4.14.

The COP_{sys} reaches a peak of 3.24 with 0.75 m^3 tank volume before decreasing. The ascending COP_{sys} when tank volume is under 0.75 m^3 can be explained by the fact that the tank volume beneath 0.75 m^3 is too small and the temperature drop in the tank would be too fast when it is used as the heat source of the heat pump. So, an undersized tank is insufficient for making full use of the collected heat. As the tank volume becomes larger, the COP_{sys} comes to decline because lower average storage temperature failed to measure up to the standard (35 ℃) for the direct space heating mode (direct space heating mode could achieve higher COP_{sys} than other working modes). On the other hand, the solar fraction keeps increasing with larger tank volume, because the larger tank contributes to higher collecting efficiency. However, the increasing rate slows down between 1 m^3 and

1.25 m^3, and the curve almost levels off after the volume reaches 2.5 m^3. From the above results, the optimum storage factor should be within the range of 33.33 l/m^2 to 42 l/m^2, when system efficiency and solar fraction are taken into consideration simultaneously. For the following simulation, 40 l/m^2 is chosen as the optimal storage factor for further simulation and comparison.

- *Optimization of collector size*

After the optimal mass flow rate and storage factor are determined from the above simulation, the results can be used to investigate appropriate collector size for the combined SAGCHP system. The collector areas from 10 m^2 to 80 m^2 at an interval of 10 m^2 are simulated with other parameters set at the optimized values from former conclusions.
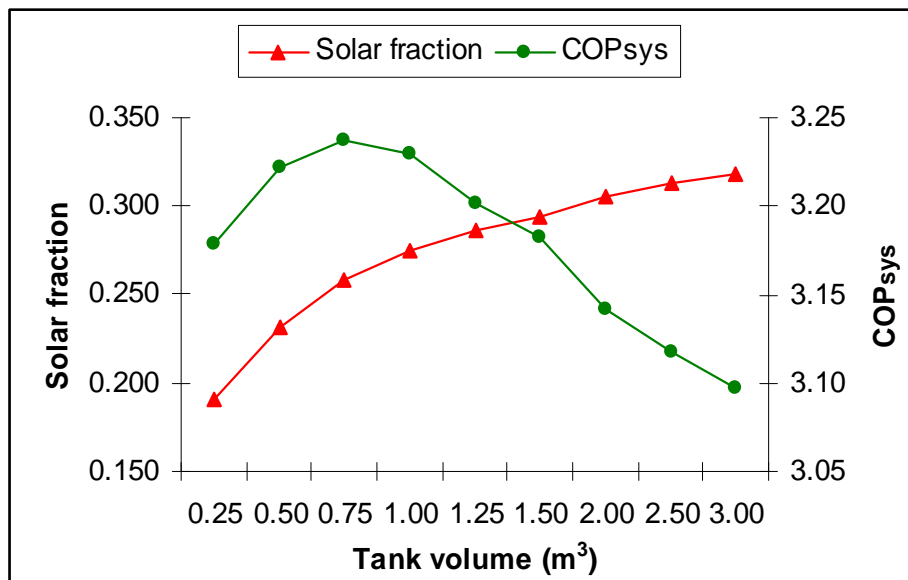
Figure 4.14 Average COP$_{sys}$ & solar fraction changed with tank volume
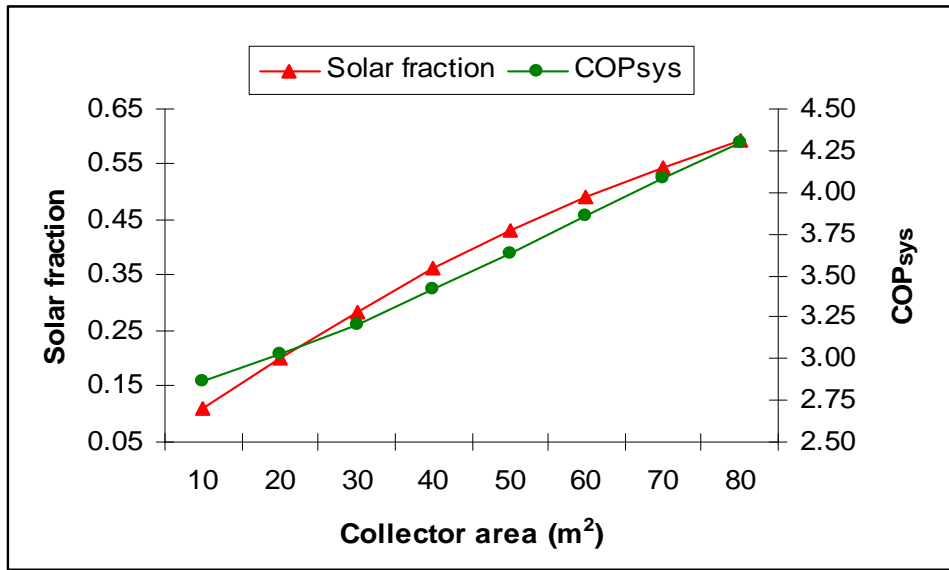
Figure 4.15 Average COP$_{sys}$ & solar fraction for different collector areas

A continuous increment of an average COP$_{sys}$ with extended collector areas is depicted by Figure 4.15. The increasing keeps until the collector area exceeds 30m^2, whereas the curve of the solar fraction shows declination. The optimum collector area could not be chosen until the economic factors, availability of installation area and long term soil thermal balance are confirmed, which will be covered in the following section.

4.3 Optimization on the ratio of the collector area to the GHE length

Based on the optimized solar loop parameters in the last section, further simulations are carried out to investigate the performances of the system with different collector areas and corresponding borehole lengths. The optimal ratio will be determined for the whole year space heating and hot water supply by comparing the energy efficiency, solar fraction, soil thermal balance and economic factors.

Table 4.2 Required solar collector area and borehole length

Collector area (m^2)	Total borehole length (m)	Minimum inlet source temperature in the operation (℃)
0	420	6.07
10	396	5.92
20	330	5.98
30	294	6.04
40	264	6.08
50	255	6.07
60	252	6.05
70	246	5.99
80	243	6.10
90	240	6.06

When the collector area (A_C) is changed from 0 to 90 m^2, the minimum inlet source temperature to the heat pump is secured for freezing protection in the range of 6 ± 0.1 ℃ (based on the assumption of a 5 ℃ temperature drop through the evaporating process), and the required borehole lengths are listed in Table 4.2.

The decreasing rate of the borehole length with enlarged A_C (shown in Figure 4.16) is about 2.4 m/m^2 at first and reaches its peak value of 4.5 m/m^2 when the A_C is enlarged to 20 m^2. The declining rate of the borehole length is kept at around 4 m/m^2, until a sudden drop occurred after the A_C reaches 40 m^2. When it exceeds 50 m^2, the relative decreasing rate of the borehole length almost stops changing and falls back to a 2.0 m/m^2. Therefore, when the saving of the borehole length is taken into major consideration, the A_C should be within the range of 20 to 40 m^2. However, the collectors under 20 m^2 could not balance the heat extraction by the heat pump, which leads to a total heat absorption of over 517 GJ from the ground storage volume. Even though net heat rejection is produced when A_C is up to 30 m^2, both the monthly minimum and average inlet source temperature to the heat pump are reduced by 1 ℃. The thermal loss from the storage volume by

conductive and convective heat transfer to the peripheral area accounts for the descent of the inlet source temperature. The total thermal loss of the soil storage volume to the surrounding is about 475 GJ when A_C is 40 m^2, which is well balanced with overcharged solar heat. Therefore, in spite of the most remarkable reduction rate of borehole length when A_C is 20 m^2, the system with 40 m^2 is more preferred for optimization in the view of operating safety of the source side heat transfer fluid (HTF).
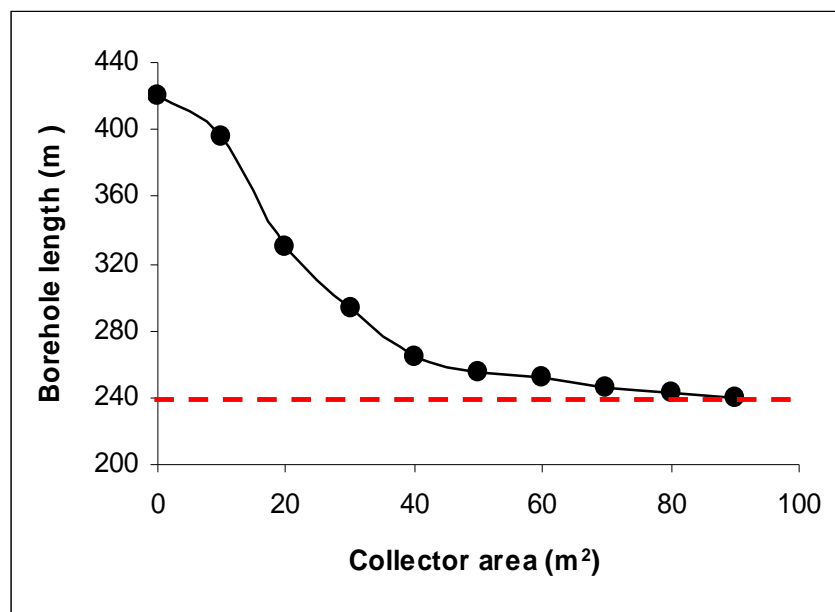
Figure 4.16 Relation between the collector area and borehole length

The change of system efficiency is shown in Figure 4.17. Minor increment ratio in the average heat pump efficiency is observed, because the design source inlet temperature exceeds the usual standard to maintain the operating stability, which makes the temperature elevation inconspicuous compared to the original high value. If an anti-freezing HTF is used in the source pipelines, the minimum inlet source temperature to the heat pump could be set below zero and the system performance should be improved more

obviously with the increased evaporating temperature.
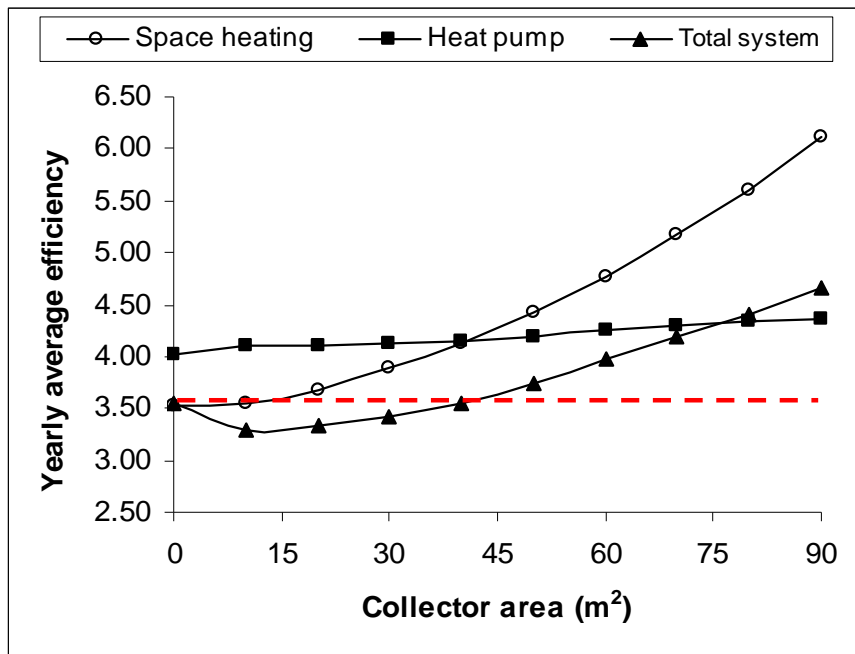
Figure 4.17 The heat pump and system efficiencies with the collector area

In addition, the promotion of space heating efficiency and total system efficiency is significant and they are even approximately linear with the A_C larger than 50 m^2. The annual average space heating efficiency with the A_C of 40 m^2 reaches the same level of the heat pump efficiency (4.12) and continues its increasing tendency till the end of the simulation. Because there is extra power consumption by operating the circulation pumps in the solar collection and water heating subsystem, the total efficiency of the SAGCHP system (3.29) is initially inferior to that of the GCHP system (3.55) and does not surpass this value until the A_C is enlarged to 40 m^2. The pump power is carefully calculated by interpolating pump its curve according to product manuals and is automatically modulated with mass flow rate.
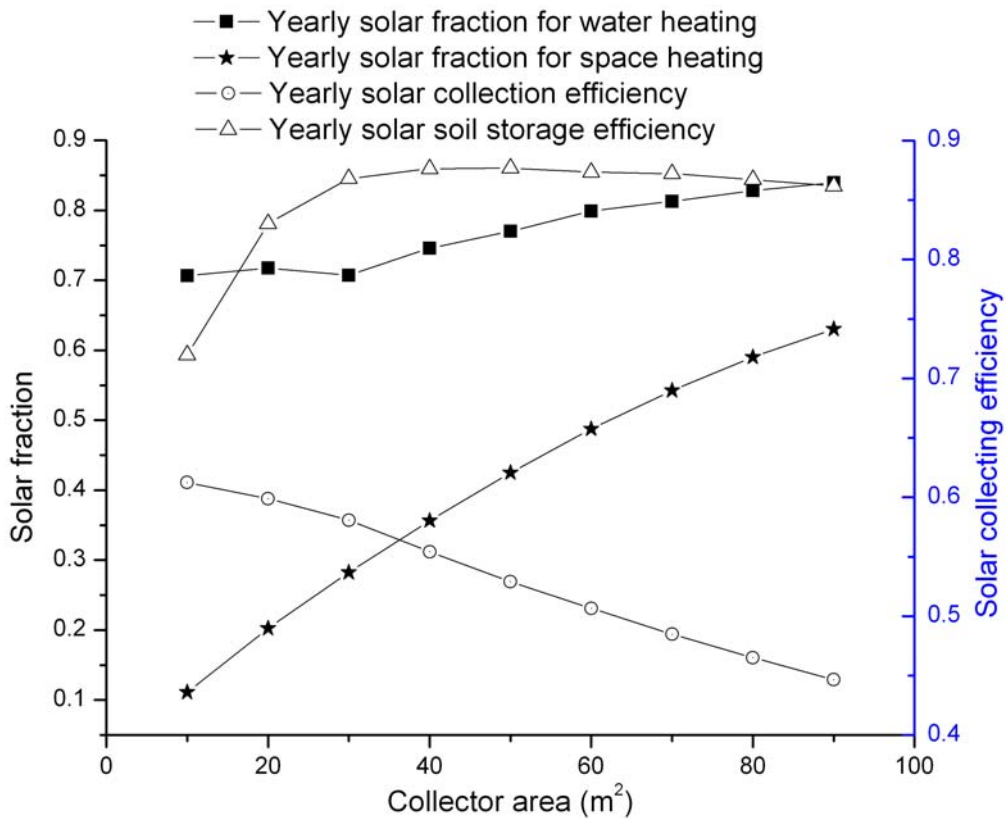
Figure 4.18 Change of the solar collection efficiency and fraction with the collector area

The reason why the total efficiency of the SAGCHP could surpass that of the GCHP system lies in the larger solar fraction due to the increasing area, as shown in Figure 4.18. The extra power consumption from DHW production and soil recharging could be compensated by energy savings due to solar energy use as long as the collector area is large enough. The solar fraction for space heating and the DHW are both improved with extended collector area. However, the space heating solar fraction ascends from 11% to 63% nearly at the same speed, while the DHW solar fraction starts escalating only after

the area exceeds 30 m^2, from 71% to 84%. The larger thermal loss caused by higher water temperature in oversized collectors could limit the increase of solar fraction for the DHW. Contrary to the solar fraction, the collecting efficiency drops from 61% to 45%, when the collector area increases from 10 to 90 m^2. The peak decreasing rate is about 0.27% per unit area with the collector area between 30 and 40 m^2. In order to study the seasonal storage effect, the storage efficiency defined as the fraction of solar energy stored into soil is also calculated from the simulation. The storage efficiency increases with the collector area from 72% to 78% in the initial stage, whereas the increasing curve immediately levels off after the area reaches 30 m^2. The increased soil temperature around the borehole impairs the recharging efficiency of the solar heat, which provides a possible explanation for the storage efficiency changes.
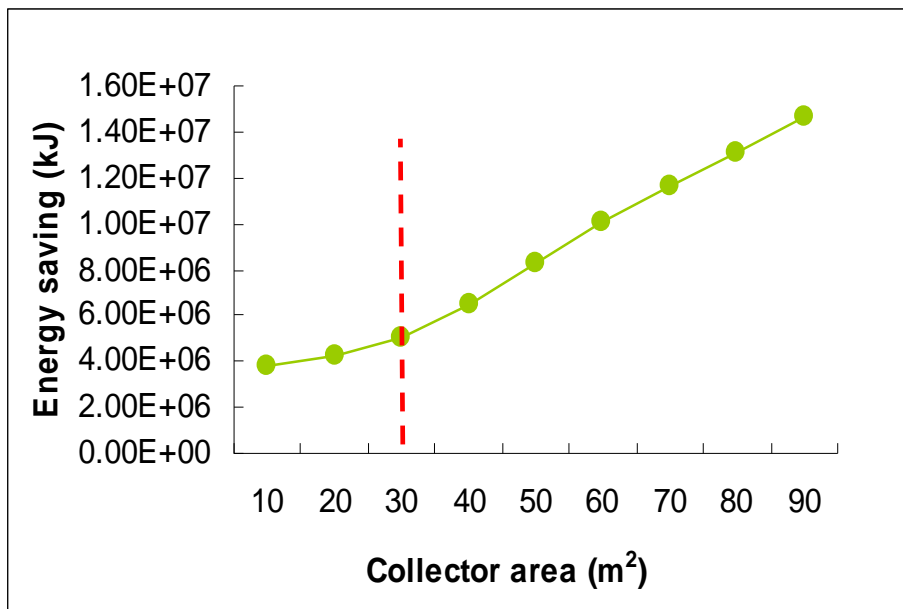
Figure 4.19 Change of energy savings with the collector area
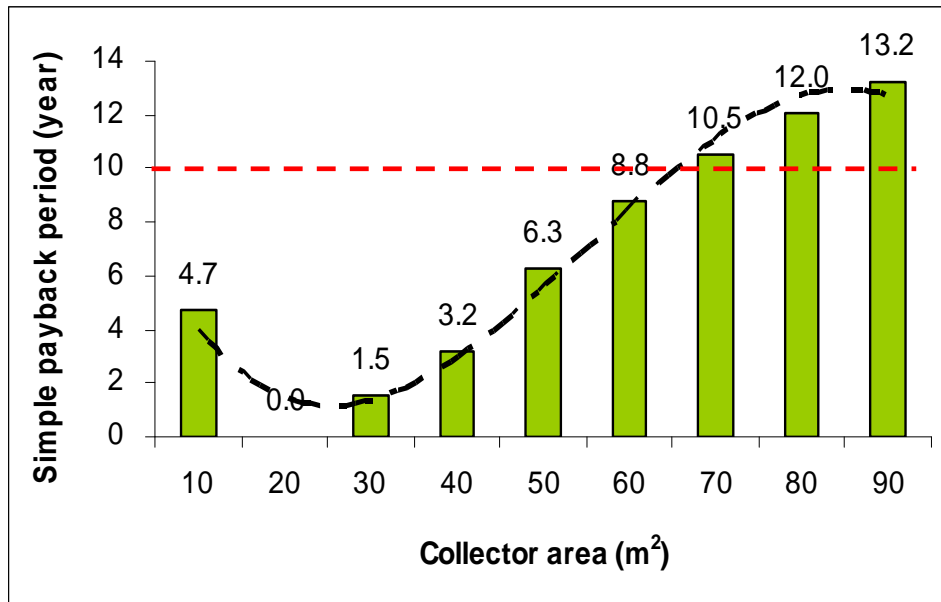
Figure 4.20 Change of relative payback period with the collector area

The energy savings compared to the combination of a GCHP system and an electric water heater becomes larger when the A_C is increased as depicted in Figure 4.19, owing to the contribution of solar energy in the total heating load. The increasing rate is relatively low at the beginning until a sudden acceleration occurs when the area is over 30 m^2. The increase is maintained till the largest area in the simulation with an average of 160 MJ/m^2. Furthermore, a relative payback period (RPB) is calculated based on the energy savings and increment of the initial cost, whose result is briefly described in Figure 4.20. The combination of a GCHP for space heating and an electric water heater is used as the base system for comparison. The relative payback period is defined by: RPB = C/S (C: The extra initial cost of the SAGCHP system; S: The annual cost savings compared to a traditional GCHP system with an electric water heater). The additional initial cost is acquired with parameters listed in Table 3, and the annual cost savings is the

multiplication of the electricity price and the energy savings.

According to the results in Figure 4.20, the RPB is 5 years for the system with the smallest A_C, and is further shortened to zero because larger savings of borehole length with 20 m^2 offsets the extra cost of collectors. Accompanied with the increase of the A_C, the extra cost of the SAGCHP system ascends faster than the increment of annual cost savings, which results in longer RPB. In this study, RPB within 10 years is considered to be cost effective, so the system with the A_C more than 60 m^2 is not recommended.

Table 4.3 List of parameter used for estimating the increment of initial cost

Items	Cost for calculation (RMB)
The collector cost per unit area (m^{-2})	450
The ground loop cost per unit length (m^{-1})	120 (Wu 2008) (including the cost of HDPE pipes, filling materials, fittings, construction fee of borehole etc.)
The extra cost of pumps and storage tanks (m^{-2})	90 (20% of the collector cost in this study)
Extra cost of hot water tank, auxiliary heaters, and required pipe lines (together with fittings and valves) for installation	0 (the cost of electric water heater etc. is considered equal to the DHW subsystem in the SAGCHP system)
The electricity tariff (kWh^{-1})	0.5 (for Beijing)

From the analysis of the optimization procedures, the optimum system design under the specified load conditions should be the system when A_C is 40 m^2 and the 2 borehole length is 64 m total. The optimized system could not only balance the underground thermal load by maintaining a constant inlet source temperature to the heat pump, but also achieve comparatively large energy savings within acceptable relative payback period.

4.4 Optimization of control strategies

After the optimization on the main components, four control strategies are investigated in this section: CTR 1 performs soil recharging and DHW heating only in non-heating periods; CTR 2 allows soil recharging but not DHW heating in the heating period; CTR 3 allows both soil recharging and DHW heating in the heating period; CTR 4 allows DHW heating but not soil recharging in the heating period. The comparisons of the four control methods are listed in Table 4.4.

Table 4.4 Performance comparisons for different control strategies

Mode	Total COP_{sys}	COP_{sys} for space heating	Minimum inlet temperature (℃)	Solar fraction for space heating	Total solar collecting efficiency	Collecting efficiency during space heating
CTR 1	3.17	3.89	6.34	0.39	55.7%	44.8%
CTR 2	2.75	3.22	6.37	0.46	58.6%	52.5%
CTR 3	2.71	3.23	6.02	0.41	58.2%	50.8%
CTR 4	2.96	3.64	5.88	0.38	56.0%	46.9%

The table shows that the overall collector efficiency could be improved by nearly 8% with additional soil recharging in the heating period. If soil recharging is not allowed in winter, the temperature of the collecting plates might rise over 70 ~ 80 ℃ whenever solar energy is abundant, which in turn brings down the collecting efficiency. In reverse, if this extra heat is used for soil recharging, the collector efficiency could be elevated. On the other hand, since soil recharging consumes extra electricity, the space heating efficiency could be decreased by 17.2%. Similarly, if the DHW load is added to the space

heating period, the solar collecting efficiency would be increased for the same reason while the space heating efficiency declines slightly by 6.4%. However, for the CTR 4, the minimum inlet temperature to the heat pump falls under 6 ℃ and impairs operational stability. In regard of the CTR 3, the collector efficiency cannot be further increased, which is limited by the total amount of solar radiation. As a result, the solar fraction increases with the descending of system efficiency, which demonstrates again that the power input for collecting and transporting solar thermal energy cannot be neglected in an active solar system. In addition, minor improvement of the solar collecting efficiency and the fraction of DHW are observed, which explains the similarities in the overall collecting efficiency.

Taking both energy saving and system stability into consideration, the CTR 1 is the most appropriate control method for the SAGCHP system. However, if DHW supply is needed in winter, the system should be redesigned to add a few more collectors for the operation reliability, though a little decrease in space heating efficiency would be accompanied.

4.5 Summary

In this chapter, optimization and parametric studies of the solar assisted ground coupled heat pump (SAGCHP) system are performed, which could be useful for guiding system design, experiments and possible industrial applications in northern China. Models with different system configurations are investigated under the weather conditions of Beijing area, and further comparative studies concerned with the solar collector, storage tank and GHE loop were carried out to refine the simulation model.

Influences from control methods were also studied. Some preliminary points are made as follows:

(1) Different coupled method has great influence over system performance, when solar energy resources, characteristics of earth and system components are fixed. From the comparison of several indicators of system performances, the indirect-coupled SAGCHP system (Model 5) was found to be the most practical combination strategy with best system efficiency. The optimal mass flow rate in the solar collect system was determined to be 50 kg/(hr·m^2), and the storage factor should be around 40 l/m^2 for increasing solar fraction and system efficiency while reducing heat extraction from the ground.

(2) By modifying the collector area and the corresponding borehole length under the climatic conditions of Beijing, system performances are analysed based on the saving rates of the borehole length, characteristics of each subsystem, as well as energy and economy factors. The optimal design can reduce the GHE loop of 3.9 m/m^2 by adding solar collectors.

(3) Four control strategies are investigated on the SAGCHP system and their performances are compared. Solar collecting efficiency could be increased by 8% if wintertime DHW and recharging are allowed. However, the extra power consumed by circulation pumps could impair the system efficiency by 17.2%. No significant change in solar fraction of the DHW is observed in the simulation and the overall solar collecting efficiency keeps at a level of 55%~58%. If wintertime hot water is required, the total area of collectors should be enlarged to secure the stability of the SAGCHP system.

CHAPTER 5 LONG-TERM PERFORMANCE ANALYSIS

A 20-year long term simulation of the optimized SAGCHP system is carried out under the TRNSYS environment with 15-minute time interval. Another model of a traditional GCHP system is used under the same environmental conditions and load characteristics as references for comparison. The short term operation features in one simulation year are also investigated with specific analysis on each working mode. Energy conservation is proved by calculating the total input and output energy for the optimized system. Furthermore, in order to explore the application of the system in further north areas, the system performances under the environment conditions of Harbin are used for comparison.

5.1 Simulative results for 20-year operation

5.1.1 Long-term operational effects

The operational performance of the SAGCHP system demonstrated good consistence throughout the 20-year simulation. During each heating period, the indoor temperature is about 19 ℃, and the temperature distribution for a single heating season is presented in Figure 5.1. The temperature fluctuates between 19.1 ℃ and 18.9 ℃, which perfectly satisfies the space heating requirement with minimum room temperature of over 18 ℃. As shown in Figure 5.2, the COP_{sys} is compared to that of the GCHP system with the same borehole length and load conditions.
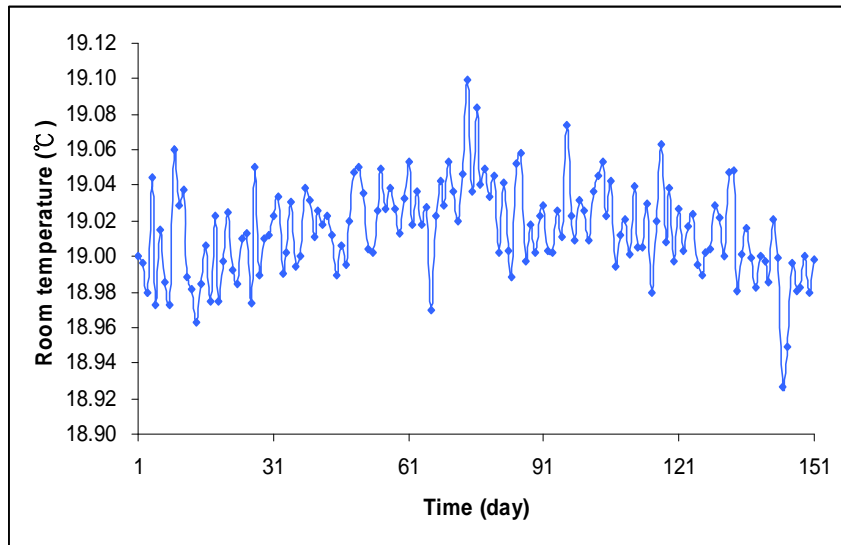
Figure 5.1 Indoor air temperature
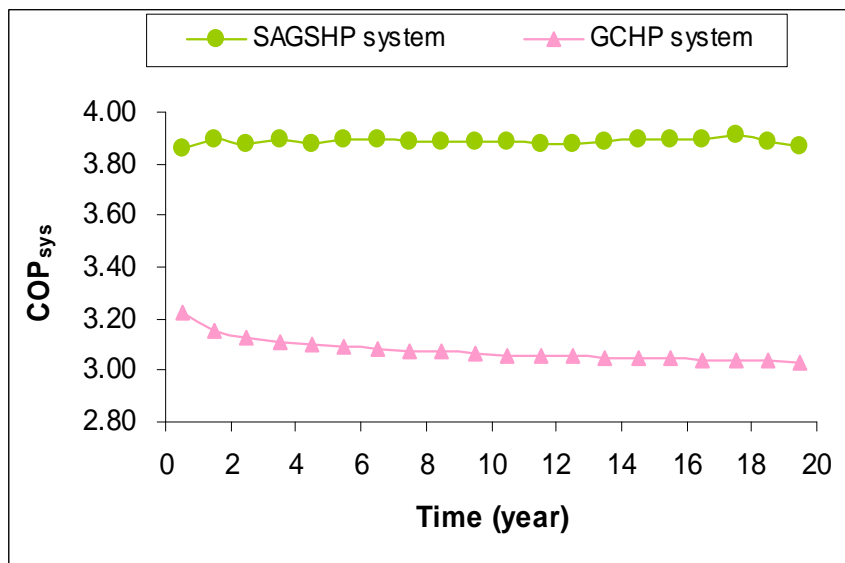
Figure 5.2 Comparison of COP$_{sys}$ for space heating between SAGSHP and GCHP system
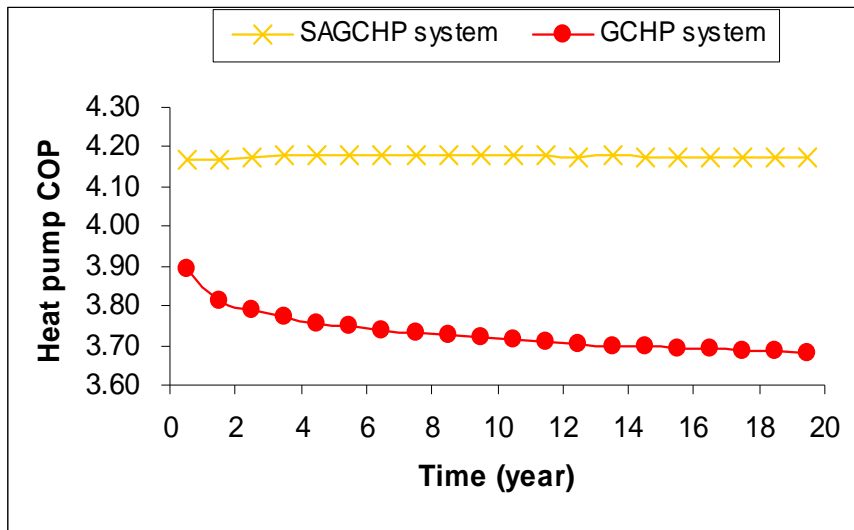
Figure 5.3 Comparison of COP_{hp} for space heating between SAGSHP and GCHP system
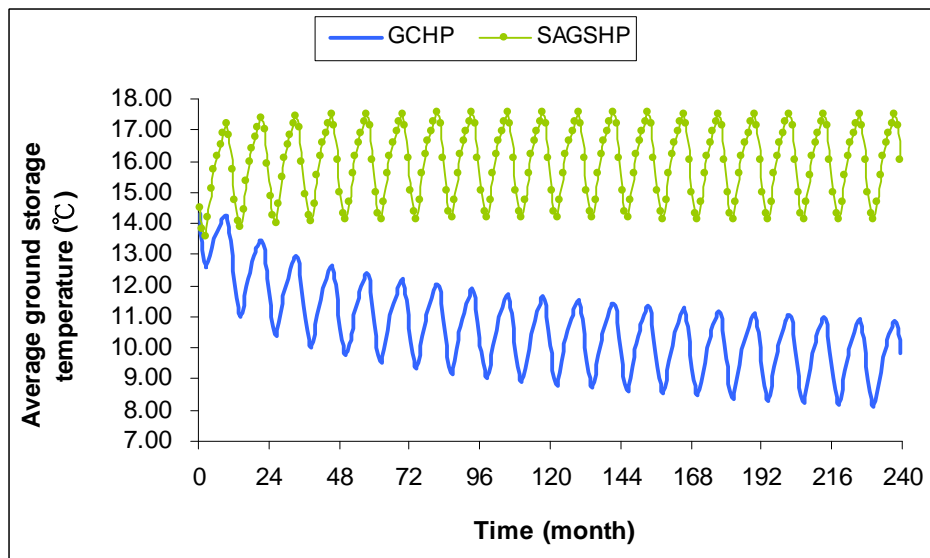
Figure 5.4 Comparison of average soil temperature around GHE

The COP_{sys} of the SAGCHP system for space heating is around 3.89, improved by 26.3% in contrast with 3.08 of the GCHP system. The system efficiency as well as the heat pump efficiency of the GCHP system declined in continuous operation mode in both

Figure 5.2 and Figure 5.3 because long term heat extraction from the ground soil lowers the average soil temperature around the GHE and in turn reduces the inlet source temperature to the heat pump. The average COP_{hp} of the SAGCHP is 4.18, which is 12.1% higher than the average heat pump COP of the GCHP system (3.73). The improvement of the COP_{hp} is not as conspicuous as COP_{sys} because the direct heating working mode could achieve efficient space heating without activation of the heat pump for improving the overall system performance. If the electricity consumed for DHW and soil recharging is also counted in, the total COP_{sys} over 20 years falls to 3.17, which is still more efficient than a traditional space heating system.
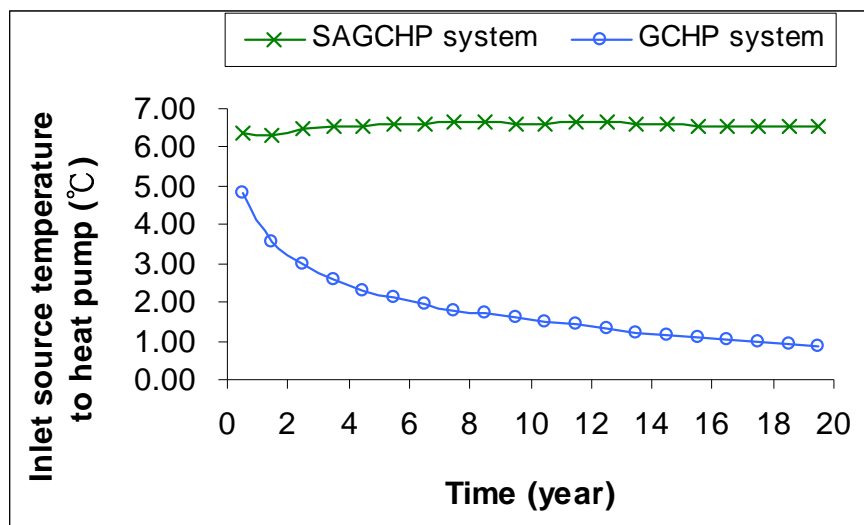
Figure 5.5 Yearly minimum inlet source temperature to the heat pump

As shown in Figure 5.4, the average soil temperature around the GHE of the SAGCHP at end of the heating period is nearly the same as that in the initial year while the soil temperature drops by 3.17 ℃ for the GCHP. Consequently, the heat transfer

driving-force between the GHE and surrounding soil decreases, which leads to a descending inlet source temperature (described in Figure 5.5) year by year. At the end of the simulation, the yearly minimum inlet temperature has already fallen to 0.87 ℃, which not only affects the system efficiency but also put the GHE pipes in danger of freezing. On the other hand, the minimum inlet temperature of the SAGCHP system is kept at over 6 ℃ due to the soil recharging and solar assisted heating process. Usually, the inlet temperature to the evaporator of the heat pump should be over 6 ℃ for pure water HTF to protect the system from freezing problems, assuming a 5 ℃ temperature drop after evaporation process. On an average basis, there is 32.3GJ solar heat injected into the soil storage each year during the simulation period for the SAGCHP system, while the GCHP system extracts 80.1 GJ each year. Therefore, approximately 112.4 GJ solar heat is delivered by the solar-soil recharging function at the cost of only 6.5 GJ electricity. Solar fraction is derived from the useful collected solar heat divided by total thermal load in this study. According to the definition, solar energy is fully used for space heating in winter under current control strategy with a solar fraction of nearly 40%, while in non-heating periods the system deliver all collected solar heat for DHW or soil recharging with a solar fraction of 75% (for DHW).

5.1.2 Detailed system performance in a typical year

The aforementioned data provides a general idea of long term systematic performance of the systems, while the following part focuses on daily or monthly operational characteristics in an average year.
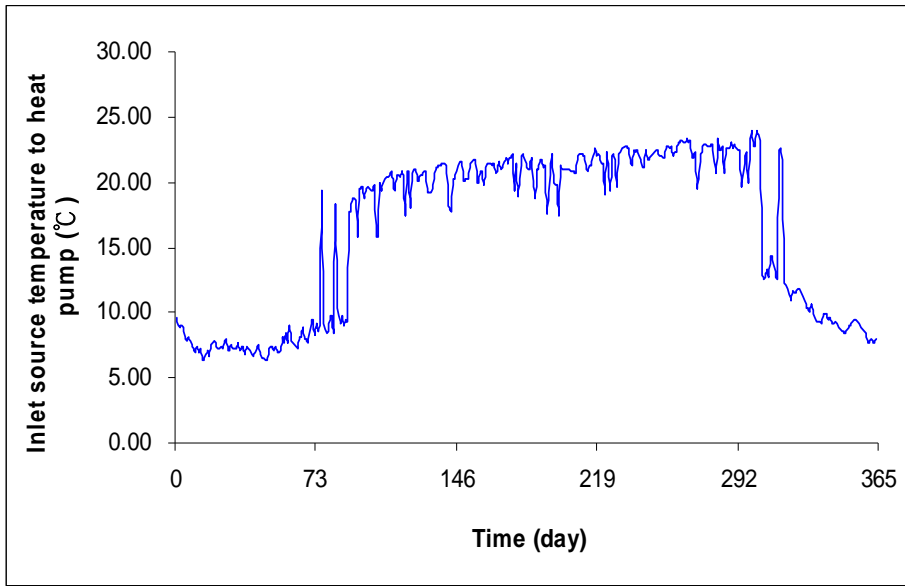
Figure 5.6 Daily inlet temperature to the heat pump
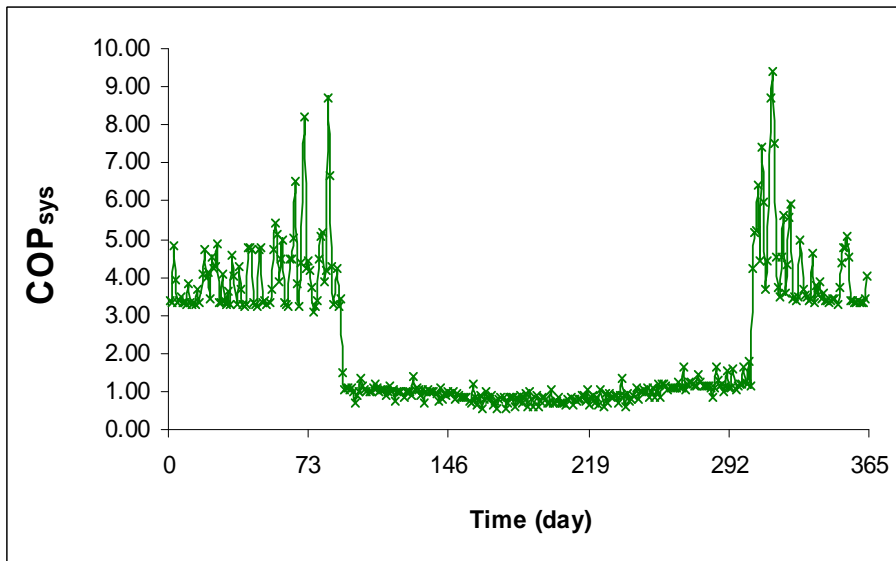
Figure 5.7 Daily system performances

As shown in Figure 5.6, the daily minimum inlet source temperature to the heat

pump keeps decreasing at the beginning of the simulation and reaches the lowest point in

the middle of January. The inlet temperature rebound a little at the end of January possibly because of the soil recharging effect and solar assisting working modes for space heating. The descending tendency of the inlet temperature does not cease until the beginning of March, when higher ambient temperature alleviates the heating load and solar radiation is stronger. At the end of the heating periods the minimum inlet temperature exceeds 19 ℃, which explains the high system efficiency in Figure 5.7. During non-heating seasons, the inlet temperature fluctuates at around 20 ℃, which is the temperature of the HTF after soil recharging. At the beginning of November, space heating is activated and high inlet temperatures are observed for the same reason at the end of the heating periods. The temperature will then decrease to the level at the beginning of January. In the heating periods, the system efficiency depicted by Figure 5.7 showed the same tendency as inlet temperature, and could reach as high as 9.41 when direct solar heating is the dominating working mode at the beginning and end of the heating periods. There are totally 64 days in a heating period when the COP_{sys} exceeds 4, which manifests comparatively high system performance over the GCHP system and other traditional heating systems. On the other hand, the system efficiency drops below 2 in non-heating periods, because the power consumption for continuous soil recharging and auxiliary heating of DHW is added. It is clearly seen that the power consumption of the circulating pumps cannot be neglected especially in a small scale heating system. Sometimes, a SAGCHP system might even save zero electricity compared with a GCHP system if soil recharging is allowed in the whole year.

The performance of a SAGCHP system depends heavily on the useful thermal energy acquired from solar collectors, which is the product of total radiation on the

collectors and the energy collecting efficiency. The daily collecting efficiency could reach as high as 78.2%, according to Figure 5.8, when the temperature difference between the absorber plate and ambient air is small in summer. The high environmental temperature as well as the low required temperature for soil recharging (10~15 ℃ higher than average soil temperature) contributes to the low temperature difference. Based on Figure 5.9, solar fraction of the system almost shows the same changing tendency as collecting efficiency, except in July, when total solar radiation is not enough due to rainy days in summer. The lowest monthly solar fraction of 0.27 occurs in December in the middle of the heating periods, while the highest monthly solar fraction of 0.78 belongs to September when clear and sunny days dominates the early fall.
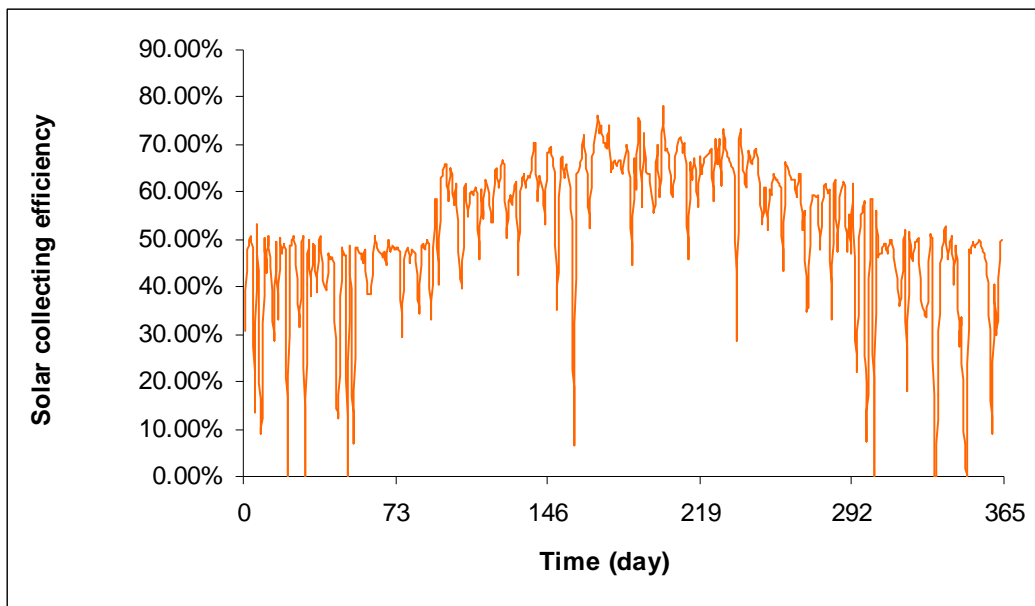
Figure 5.8 Daily solar collecting efficiency

For space heating, the more heat the solar collecting system provides, the less energy the system extracts from the soil heat exchangers, which is proved by comparing Figure 5.9 and Figure 5.10. The decreasing trend of the soil extraction during the first half of the heating period (from January to March) coincides with the increasing solar fraction showed in the same session. The heat extraction is reduced by 77.5% from January to March, while the solar fraction increases from 30.3% to 64.4%. The soil temperature near the borehole recovers by 3.6 ℃ after the soil recharging period from April to October. Averagely, 11.1 GJ solar heat is stored in the soil in each month and the heat storage is a little smaller in July for the same reason with solar fraction.
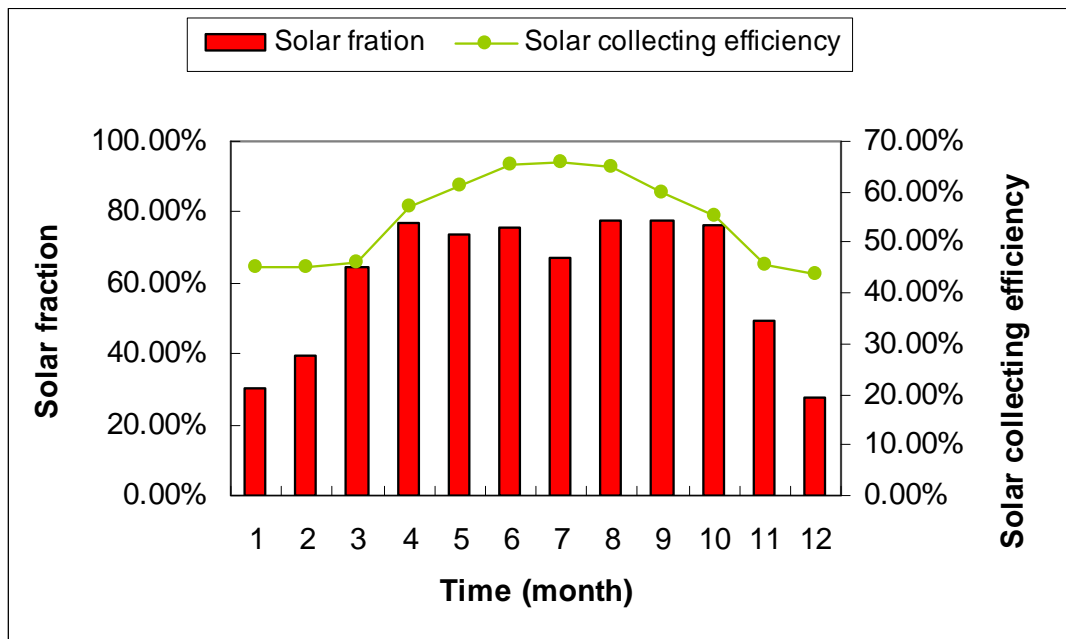
Figure 5.9 Monthly solar collecting features

The solar collector area in this system is mainly designed for space heating, which leads to more energy loss for production of DHW. The actual energy delivered to the

DHW tank could fully meet the total hot water load if the tank is completely adiabatic. Auxiliary heaters are required because approximately 46.4% monthly heat loss is observed in the DHW tank. Beside water tanks, heat loss from the heat exchangers, solar collectors and pipelines (which is not included in the simulation) adds up to the total heat loss of the system. The yearly average system efficiency for water heating alone is about 2.27 (calculated with the total DHW load divided by electricity consumption for water heating), and the combined energy efficiency of the DHW and soil recharging achieves reaches to 9.73 (calculated by the sum of the DHW load and the heat stored in soil divided by the total power consumption during non-heating period).
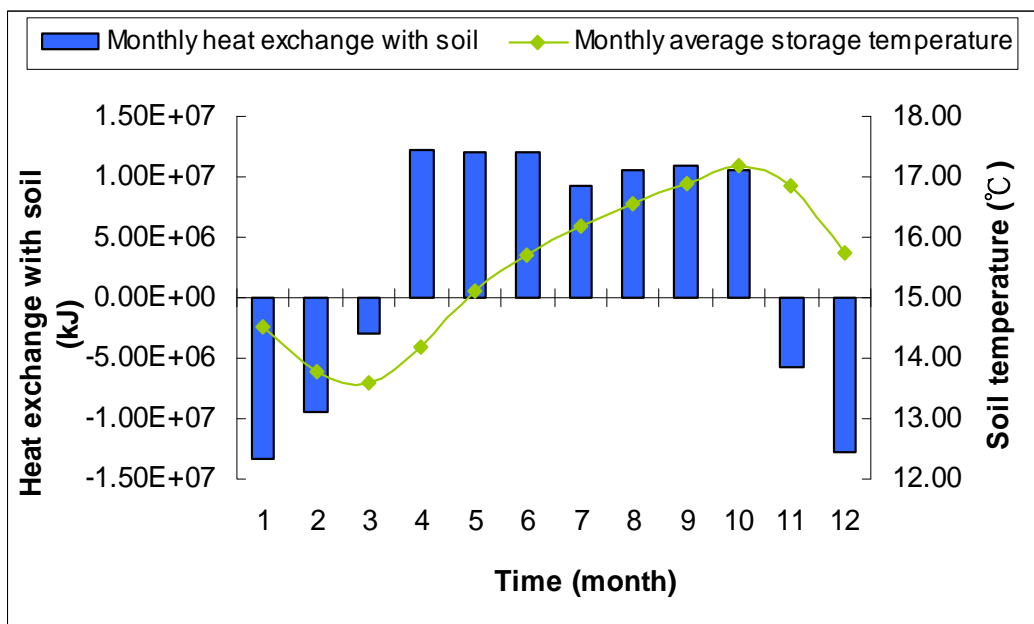
Figure 5.10 Monthly soil heat exchange and soil temperature
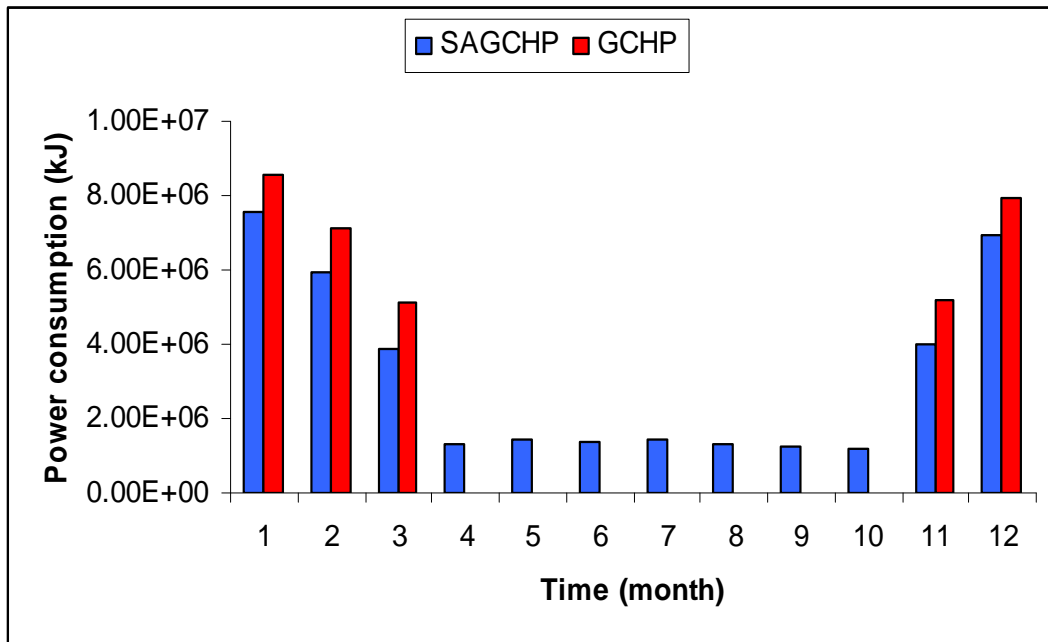
Figure 5.11 Comparison of monthly power consumption

The total energy saving in a space heating season compared with the GCHP system without solar collectors, as presented in Figure 5.11, amounts to 5.6 GJ per year. However, there is unavoidable energy consumption for the circulation pumps and auxiliary heaters in non-heating seasons which adds up to 9.25 GJ. If the DHW load is calculated with pure electricity consumption by an electric resistance heater with 100% energy efficiency, another 8.85 GJ should be added to the annual energy consumption. As the result, there is still 5.20 GJ electricity saved in contrast to a traditional GCHP with an electric resistance water heater for DHW.

5.1.3 Simulation results for each working mode in a typical heating period

There are totally five working modes in wintertime operation and the results for each working mode is listed in Table 2. The average water supply temperature for space

heating is 35.42 ℃ which is high enough for floor radiation heating, while the GCHP system could only supply hot water at temperature of 32.54 ℃. As a result, the SAGCHP system performs space heating more efficiently for better resting of the heat pump and self-recovery of the ground temperature field. The annual total operating time of the heat pump in the SAGCHP system is 1425.5 hr, reduced by 26% in contrast to the GCHP system.

Table 5.1 Simulation results for each mode in a heating period

Mode	Operational time (hr)	Percentage (%)	Supplied heat (MJ)	Percentage (%)	Power consumption (MJ)	Average COP_{sys}
Mode 1	235.1	10.26	1.75 E+4	16.02	4.79 E+3	3.66
Mode 2	277.8	12.12	1.90 E+4	17.34	5.52 E+2	34.39
Mode 3	1104.3	48.20	6.67 E+4	60.96	1.97 E+4	3.39
Mode 4	86.2	3.76	6.22 E+3	5.69	1.71 E+3	3.63
Mode 5	587.7	25.65	0	0	1.57 E+3	—

Mode 1: solar assisted heat pump heating; Mode 2: direct space heating; Mode 3: GCHP heating; Mode 4: solar assisted ground coupled heating; Mode 5: heat storage.

From the table, it can be concluded that the ground coupled heat pump heating mode occupies nearly half of the total operation time and supplies over 60% of the heating load. When there is no need for space heating, the system could store the collected solar heat to the water tank, which amazingly accounts for one fourth of the heating period. Sometimes, with certain control strategies, the SAGCHP system could consume more electricity than a traditional GCHP system, just because of the extra power consumed by the heat storage or soil recharging modes. Among the five working modes, the system

efficiency of the direct heating is the highest since only circulation pumps are needed for providing space heating. However, the heat supplied from solar energy for this working mode is only 17.34% because it works mostly at the beginning or end of the heating period when heating load is smaller than other sessions. Mode 1 and Mode 4 are also efficient working modes which could operate during the middle of the heating periods, and could afford 22% of the total heating load with no more than 14% operating time. In wintertime operation, soil recharging at heating intervals is not allowed under current control strategy for elevating system efficiency and saving electricity, but soil temperature recovery could be realized by the intermittent operation of the system depending on indoor temperature (the heating system stops as soon as the indoor temperature exceeds 20 ℃ and restarts once the temperature falls below 18 ℃). Even for the traditional GCHP system, the total operating time adds up to 1926.9 hours, taking up only 53.2% of the length of a heating season.

5.2 Energy balance analysis

The result of energy conservation analysis is presented in Figure 5.12. The 4329 GJ total radiation exposed on the 40 m^2 solar collectors is changed to 2399 GJ useful heat and delivered to the system with a thermal loss ratio of 44.58%. Electrical power of 666 GJ (including the power input to the heat pump, circulation pumps and auxiliary heaters for hot water), heat absorption of 947 GJ from the ground storage volume and the collected useful solar heat contribute to the whole energy input of the SAGCHP system. The main outputs of the system consist of the 2366 GJ heat for hot water and space heating, 259 GJ thermal loss of the system (from tanks and plate heat exchangers), and

1417 GJ heat rejection to ground seasonal storage. There is a 0.75% small difference in the thermal balance calculation, which is considered acceptable.
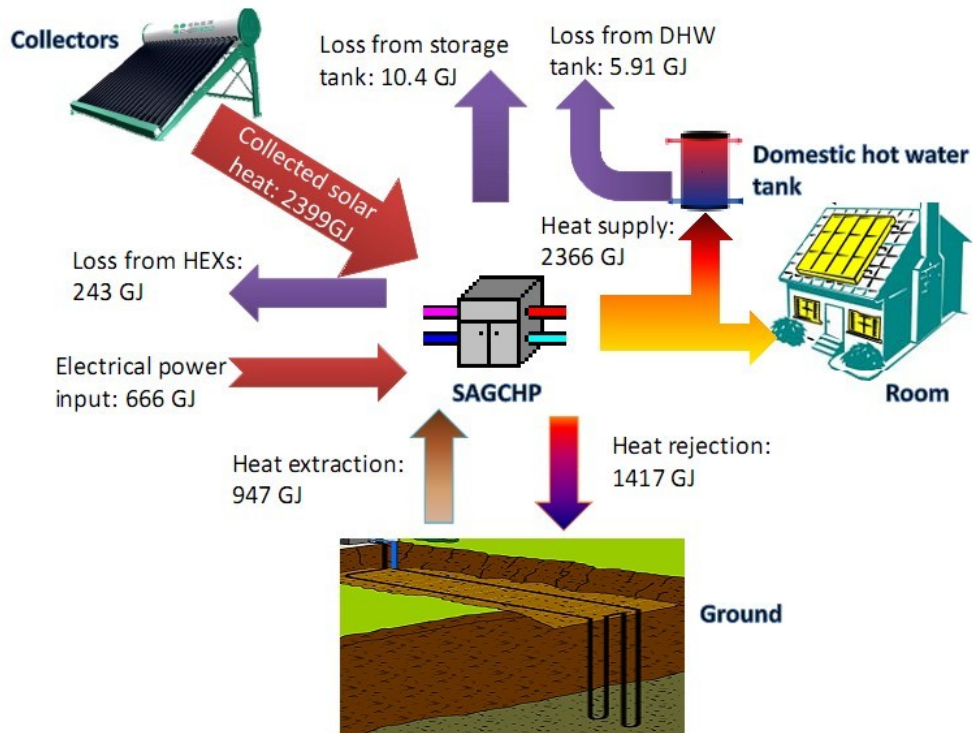
Figure 5.12 Energy balance of the optimized system

5.3 Performance comparison under diverse weather conditions

The applicability of the optimized system in Beijing has been proved by its efficient performance. For the purpose of investigating its application in far north areas in China, the performance of the SAGCHP system under environmental inputs of Harbin is simulated and compared with the performance of system in Beijing.

Table 5.2 Comparison of design parameters in Beijing and Harbin

Design parameters	Beijing	Harbin
Design space heating load (kW)	12.44	12.44
The length of heating period	Nov. 1st to March 31st	Oct. 16th to Apr. 15th
Design outdoor temperature (℃)	-9	-26
Collector slope (°)	45	55
Undisturbed soil temperature (℃)	15	7.1
Soil conductivity (W/m・K)	2.1	2.44
Soil heat capacity (kJ/m3・K)	2500	4187
Cold water temperature to water tank (℃)	June to Aug. : 20 The rest : 15	June to Aug. : 15 The rest: 10
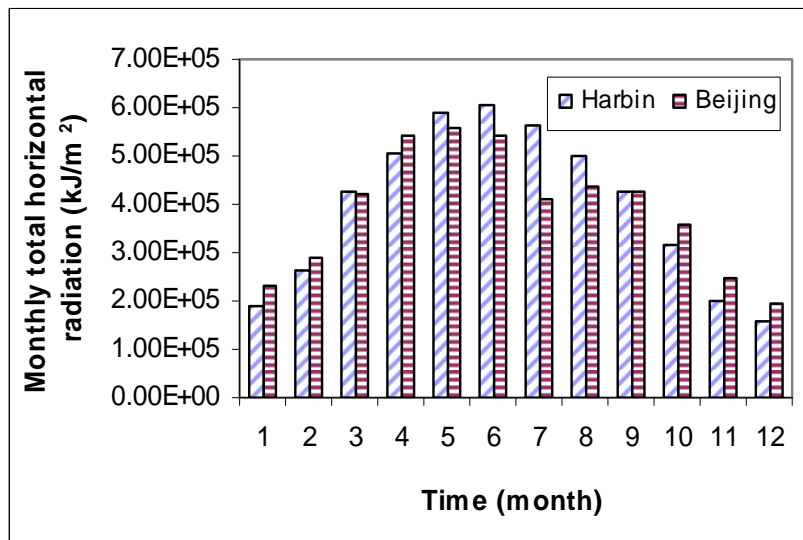
Figure 5.13 Comparison of monthly total radiation level in Beijing and Harbin

The model used for Harbin's case is basically the same as the optimized model from the former research, except that the weather data, soil properties, the collector tilt angle etc. are changed according to Table 5.2. It is important that the two systems are tested with the same design heating load. The collector slope is increased to 55° in Harbin in view of its local latitude, and the heating period is extended for its colder outdoor

ambient in late October and early April. Soil properties are selected from the geological

test results (Duan, Zhao et al. 2006). A tentative simulation revealed that the minimum

inlet source temperature to the heat pump could not measure up to the 6 ℃ standard due

to the limitation by low natural soil temperature so that an anti-freezing fluid has to be

used in the ground loop and a heat exchanger between the storage tank and ground loop is

added.
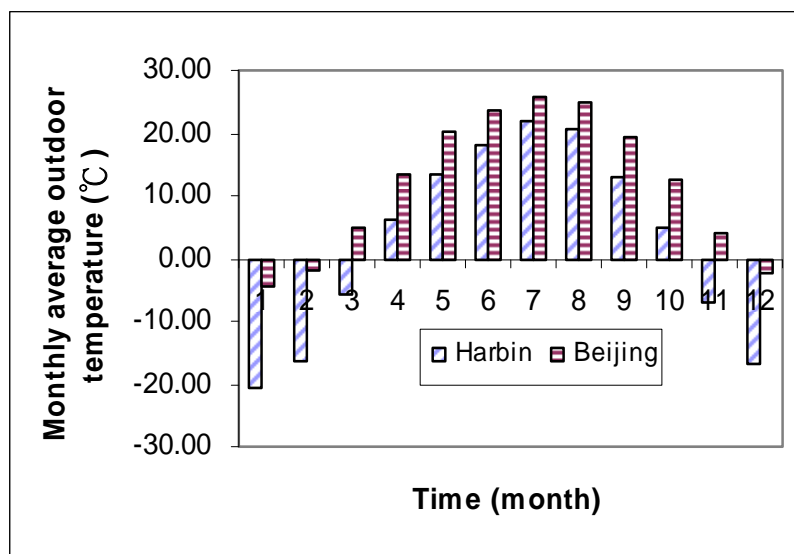
Figure 5.14 Comparison of monthly average outdoor temperature in Beijing and Harbin

Environmental conditions are shown in Figure 5.13 and Figure 5.14. The radiation

and temperature distributions in Harbin display similar tendency to that of Beijing.

Although the monthly average outdoor temperature is always lower, the radiation level in

Harbin is higher in summer because of its longer daytime hours, which could lead to

better efficiency for soil recharging and hot water production in non-heating periods. The

operating conditions for the system is far more severe in December and January in Harbin,

because the radiation level reaches only 80% of Beijing's level while the average ambient temperature descends to -16.77 in December and -20 ℃ in January. In addition, the average outdoor temperature of Harbin in April and October is about 8 ℃ below the level of Beijing in the same season in a year, which proved the necessity for extending the length of heating period. As a result, although the actual heat supply is similar in the distribution, as expressed in Figure 5.15, small difference in the total amount is observed for each month despite the same design heating load. The annual space heating load is 128 GJ for Harbin and 109 GJ for Beijing. On the contrary, the annual hot water load adds up to 8.55 GJ for both cases despite that the cold replacement water temperature and water heating periods are different.
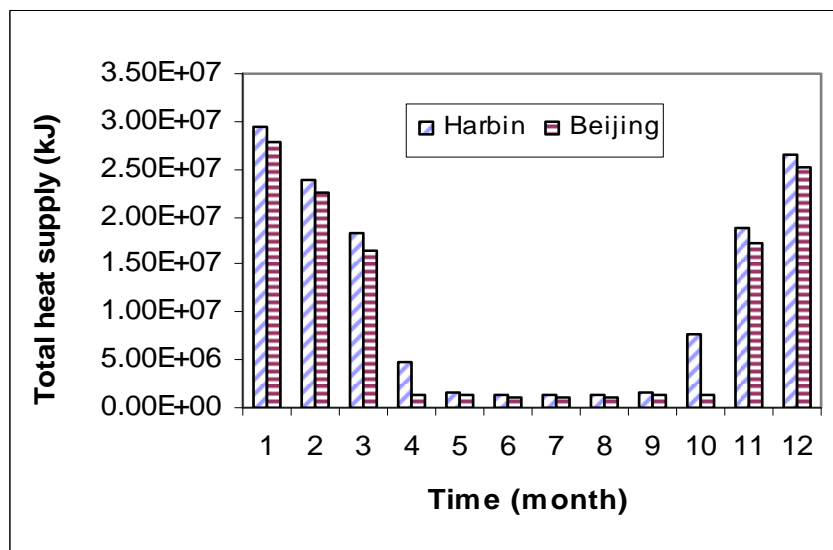
Figure 5.15 Comparison of monthly total heating load in Beijing and Harbin

The fluctuation of space heating performance in both cases, as described in Figure 5.16, shows the same changing trend with the average inlet source temperature to the heat

pump. In contrast to the case in Beijing, the monthly average inlet temperature in Harbin descends by 5 to 8 ℃, which results in a 21% drop in annual space heating efficiency. However, the average heating performance in early April has achieved a relatively superior efficiency of 5.18, which is attributed to the direct heating mode without starting the heat pump during light-load sessions.

Figure 5.16 Comparison of space heating efficiency in Beijing and Harbin

For the SAGCHP system, solar fraction is an important indicator on the system performance. As shown in Figure 5.17, the monthly solar fraction in the heating period of Harbin is always lower except in March and April. Especially in early April, most of the heating load is satisfied by the solar direct heating mode with little auxiliary energy consumption, contributing to an average fraction of 91%. Consequently, the average solar fraction for space heating is about 36% in both cases. Although solar radiation in non-heating periods is stronger in Harbin, larger heat used for seasonal storage lowered the

average solar fraction of non-heating periods to 65% compared with 75% in Beijing' case. Larger solar seasonal storage derives from the temperature difference control in the soil recharging mode. In Harbin, the system delivered about 94% of the solar heat to soil storage, increased by another 6% in contrast. Despite that comparatively low soil recharging temperature in Harbin elevates the average collecting efficiency from May to September by 3%, the greater temperature difference with the environment decreases the efficiency in the rest time by 1%. It is worth noticing that the average collecting efficiency in April in Harbin is 14% inferior to that in Beijing. This large difference results from the redundant solar heat beyond the heating load requirement, which is accumulated in the storage tank and elevates the collectors' working temperature in the first half of the month.
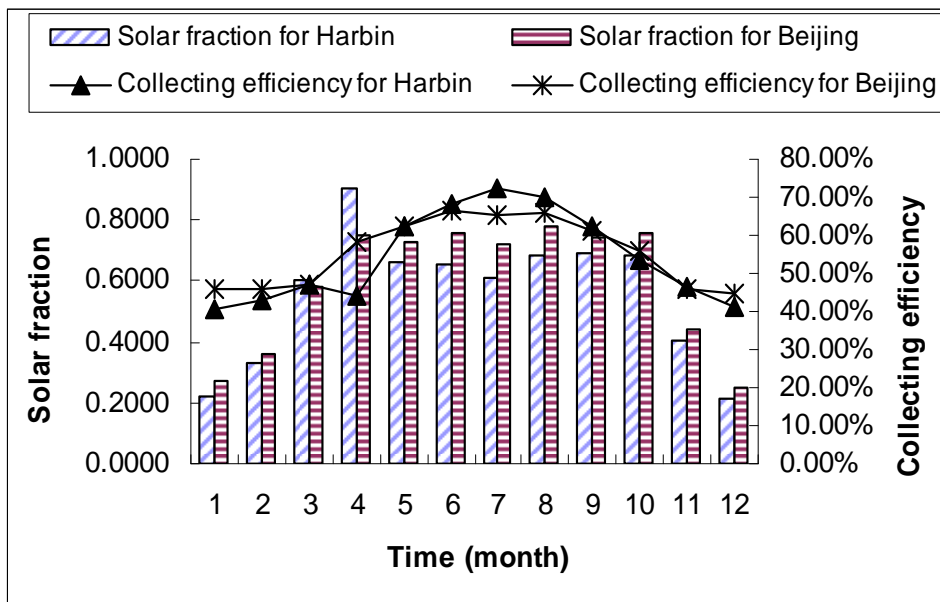
Figure 5.17 Comparison of solar fraction and collecting efficiency in Beijing and Harbin

The underground thermal balance is also compared for the two cases in Figure 5.18 for judging the applicability of a SAGCHP system. Even though better seasonal storage efficiency is observed from May to September in Harbin, the longer heating period with more heat extraction reduces the annual net heat rejection by 7.95 GJ. Therefore, the minimum monthly average inlet temperature is decreased by 0.55 ℃ after continuous operation for 20 years compared with the constant value in Beijing's situation.
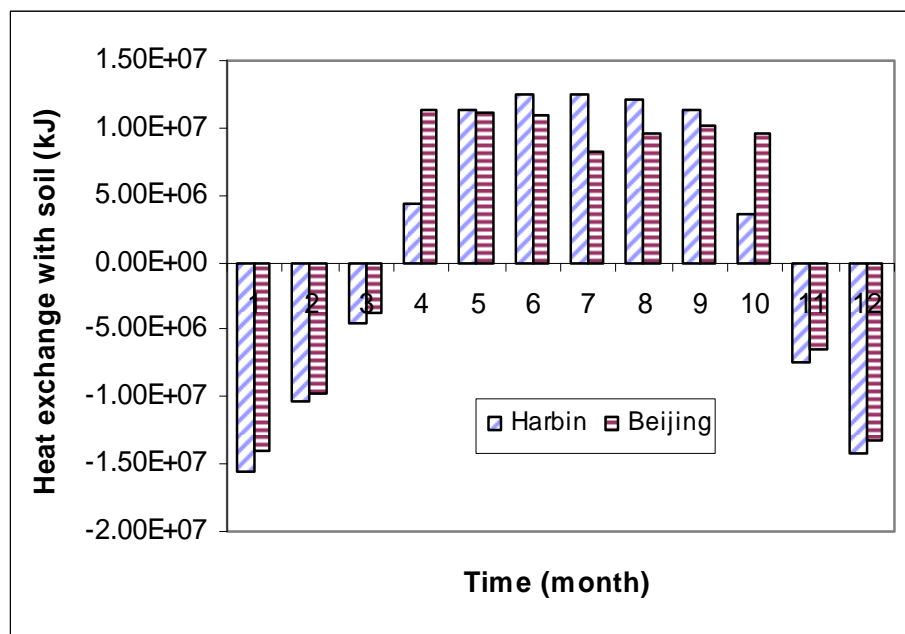
Figure 5.18 Comparison of soil heat extraction and thermal balance in Beijing and Harbin

The system could be feasible in Harbin with minor change in the collector area for the sake of underground thermal balance. Although the two cases is designed for the same peak heating load, the integrated heat requirement though the specified heating period should also be checked to secure the balance of the system. If the soil temperature is too low for freezing protection, the use of anti-freezing fluid could bring down the

system efficiency and raise the initial investment cost. The average system efficiency over 20 years is about 2.84 for the case in Harbin, but the efficiency under 3.00 is usually not considered economical for application compared to traditional central heating plants. In a word, the optimized design of the system should be adjusted according to the meteorological and geological situation, heating load distributions, solar fraction requirements and economic factors.

5.4 Summary

The long-term simulation was performed to investigate the advantage of the SAGCHP system over a conventional GCHP system under the climatic conditions of Beijing area. The operational performance for a typical year, the characteristics of each working mode and the applicability under diverse weather conditions were analyzed and discussed. Following conclusions can be drawn:

(1) In the 20-year simulation, the minimum inlet source temperature to the heat pump is kept over 6 ℃ for freezing protection. The SAGCHP system can have an average COP_{sys} of 3.89 for space heating, improved by 26.3% compared to a traditional GSHP, and electricity consumption reduction of 5.6 GJ for space heating per year can be achieved. The solar fraction is 0.40 for space heating and 0.75 for DHW, based on an average solar collection efficiency of 55.7%. On the other hand, the inlet temperature, the heat pump coefficient as well as the average soil temperature of the GCHP system decrease conspicuously after long term operation, which proves that adding solar collectors is quite necessary. The system performance within a typical year during the simulation is selected for further analysis. The daily or monthly

changes of solar collecting efficiency, solar fraction, inlet temperature, system efficiency, heat exchange with soil and average soil temperature are discussed. The annual total electrical energy saving compared with the combined system of a traditional GCHP with electric hot water heaters amounts to 5.20 GJ.

(2) The operational characteristics of each working mode for space heating are studied. The operation time, supplied heat, consumed power and solar fraction for each working mode are compared. Among the five working modes, direct heating is most efficient with only circulation pumps at work. The solar assisted heating and solar coupled ground heat pump heating modes are also the energy saving modes that supply 22% of the total heating load.

(3) Energy conservation of the system is also confirmed by comparing the total inputs and outputs between the ambience and objective system. The energy balance is just within 0.75%, which is acceptable for a complicated compound system.

(4) Furthermore, applicability of the designed system in severe cold areas is analyzed with weather conditions of Harbin. Restricted by the local soil and weather conditions, the underground loop has to be charged with anti-freezing fluid to secure operating stability. Higher seasonal storage efficiency as well as an enlarged heating load requirement due to prolonged heating period was observed. The overall thermal balance is maintained at the cost of a much lower system efficiency of 2.84. Consequently, the application in Harbin is not recommended for the sake of energy savings and economic factors.

CHAPTER 6 EXPERIMENTAL INVESTIGATION

In order to validate the simulations and obtain practical experience of the SAGCHP technology, an on-site experiment was carried out, because detailed experimental study on the performance of the SAGCHP system for different operational modes to provide space heating in cold areas of China is still not available. In this chapter, an experimental test rig with comprehensive data acquisition equipment installed at Hebei Academy of Sciences in China is reported. Based on the experimental data and relevant theories, the thermal responses of the borehole and heating performances of the system under different working modes are estimated and analyzed. Consequently, the application potential of the SAGCHP in the cold area of China is verified and preferable utilization method of solar thermal energy will also be discussed.

6.1 Description of the experimental installation

The SAGCHP experimental system is developed inside the renewable energy laboratory of the Academy. A schematic diagram of the system and the solar collector are shown in Figure 6.1 and Figure 6.2. The system consists of five main components, i.e. the ground heat exchanger (GHE), the water-to-water heat pump unit, fan coils, circulating water pumps and evacuated-tube solar collectors.

(1) The ground heat exchanger (GHE)

In the GHE, five single U-tubes in parallel were buried in the boreholes with 5 m interval and 21 m depth. High-density polyethylene (HDPE) tubes with 32mm outside

diameter and 25 mm insider diameter are used with water as heat transfer fluid. In order to prevent surface water penetration and potential groundwater contamination, all boreholes are completely backfilled by grout mixed with drilling mud, cement and sand in specific proportions. According to the geological report, the on-site geological conditions are: clay layer from surface to 28 m deep and pebble gravel layer from 28 m to 40 m deep. The thermal conductivity and diffusivity of soil around the boreholes are estimated to be 1.9 (W/m K) and 0.71×10^{-6} (m^2/s), respectively.
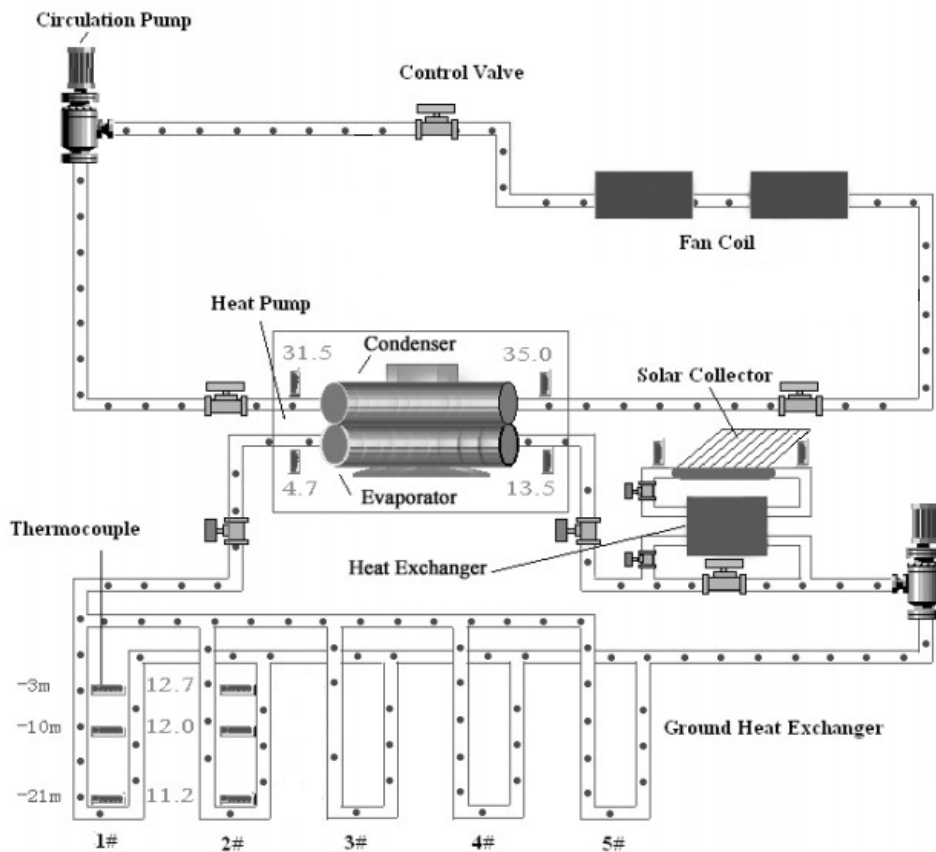
Figure 6.1 Schematic diagram of the experimental system

Figure 6.2 Solar collector used in the project

(2) The heat pump unit

The heat pump utilized in this experimental system is a water-to-water heat pump DNQWSR-4 manufactured by Lu Huan Company with R22 as refrigerant. The rated heating capacity is 4.6 kW with load side inlet water temperature of 40℃.

(3) The fan coil units

Two series-connected fan coil units (Model: FP-12.4LMZ; Production of GRAD) provide space heating for a single room of 36 m^2 area. The total rated air flow rate is 2500 m^3/h.

(4) Solar collectors

Four evacuated solar collector modules are mounted on the top of the laboratory building. Each module is composed of 25 pipes with 1800 mm length and 70 mm diameter. Solar collectors with gross area of 13.6 m^2 facing south are installed with 0° azimuth angle and 38° tilt angle (about the local latitude).

(5) The circulating water pumps

The water circulating loops consist of a GHE side loop, a fan coil side loop and a solar side loop. The circulating pumps chosen for the GHE and the fan coil side loops are constant-speed pumps with maximum head of 5 m and maximum flow rate of 65 l/min (Model: LRS40-6; Produced by Tianfeng Company). The solar loop circulating pump is a constant speed pump with maximum water head of 9 m and maximum flow rate of 95 l/min (Model: LRS40/9; Produced by BaiYi Company).

6.2 Measurement and Uncertainty analysis

6.2.1 Data acquisition system

The data acquisition system consists of the temperature measurement system, the flow rate measurement equipment, the power consumption measurement system and the solar radiation measurement equipment.

Temperature system: 6 Pt100 sensors are buried together with the GHE to measure the temperature distribution at the center of the boreholes. Borehole 1 and Borehole 2 are implanted with sensors at 3 different depths according to Figure 6.3. Beside underground part, there are additional 6 identical three-wire Pt100 temperature sensors installed at the water pipelines' inlets and outlets of the evaporator, the condenser and the solar collector array. The Pt100 sensors (Model: WZP-201) could be applied to the temperature range of -50 ~ 100 ℃ and the accuracy grade is 0.5 %.

Flow rate system: Because the SAGCHP system works with constant flow in all the water circulating loops, the flow rate is recorded by a ultrasonic flow meter (Model: JTLL-Ⅱ). The equipment could be applied to fluids with temperature range from -40 ℃

to +160 ℃ and the pipeline diameter from 50 mm to 1500 mm. The accuracy grade is 1.0 %.

Power system: The operational power consumption of three circulating pumps and the compressor in the heat pump can be measured and recorded by the system consisting of 6 current transformers and 3 tri-phase active power transmitters. Two current transformers combined with one tri-phase active power transmitter can generate 4~20 mA standard current signal at one of the three measurement points. The accuracy grade of the power consumption acquisition is 0.2 %.

Solar system: The total solar radiation on the inclined surface of solar collectors could be recorded by a pyranometer (Model: TBQ-2). The sensitivity of the pyranometer could reach 7 $\mu V/Wm^{-2}$, and the output current range is 0~20 mV corresponding to instant solar radiation of 0~2000 W/m^2.
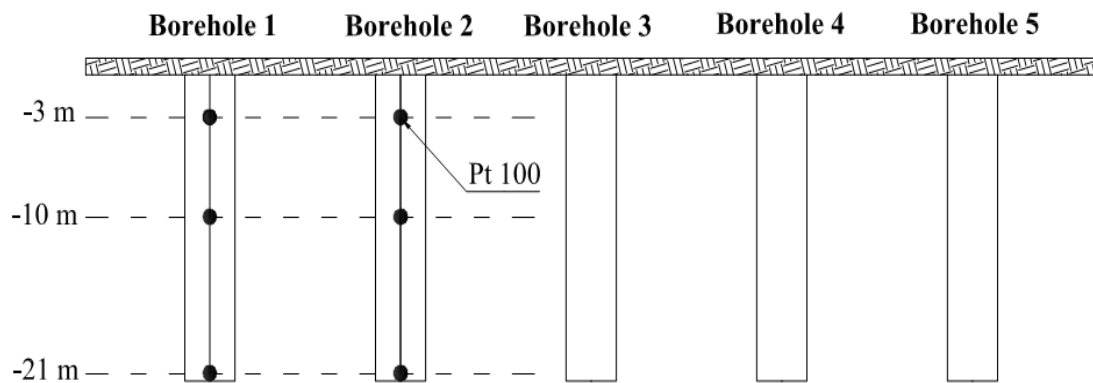

Figure 6.3 Borehole temperature sensor distribution
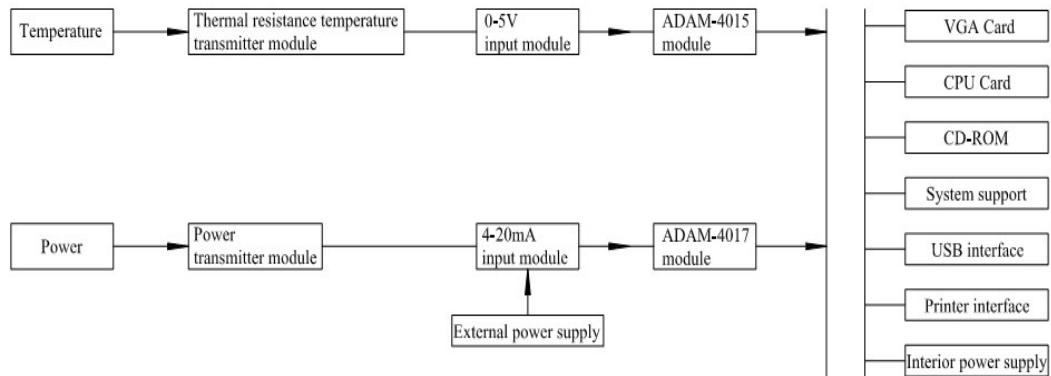
Figure 6.4 Schematic of the data aquisition hardware system

Data transmitted from the flow meter and the pyranometer could be logged by their implanted commercial hardware and software, while the temperature and the power consumption signals are processed by a special industrial control computer designed by the ADVANTECH Company with model number PCA-6175. The ADAM-4015 6-channel RTD module (Accuracy: 0.1 %) cooperates with the Pt100 temperature sensors for temperature acquisition. The ADAM-4017 16-bit 8-channel analog module which provides programmable input ranges on all channels is selected for power consumption acquisition, whose accuracy is within 0.2 %. The ADAM-4520 converter serves as a communication module with the computer. Owing to its advanced function, the acquisition system shows excellent performance in anti-vibration, anti-high/low temperatures and anti-interference aspects. The schematic diagram of the data acquisition system for the temperature and the power consumption is described in Figure 6.4. In addition, the HMI/SCADA program FIX, which is a real time information management and SCADA solution from GE Fanuc Intelligent Platforms, is utilized as the software for the temperature & power consumption acquisition system. The real time operation data,

historical data and flow chart of the experimental system could be processed, displayed and exported for further analysis.

6.2.2 Uncertainty analysis

Uncertainty analysis for this experiment includes error estimations for both measured and calculated parameters, which provides a statistical interpretation of the errors in well-replicated experimental results. The experimental result is meaningful only when its errors fall within the permitted scope of research. In this experiment, measurements were taken in every 5 minutes and the corresponding calculations were made to acquire other required parameters to evaluate system performances.

The measured parameters include the temperature, the power consumption, the flow rate and the solar radiation, whose uncertainties (δX_i) and relative uncertainties (δRX_i) could be obtained by the following equations:

$$\delta X_i = L \cdot \theta_i \tag{6.1}$$

$$\delta RX_i = \frac{\delta X_i}{X_i} \tag{6.2}$$

where L is the upper limit of the measuring range, and θ_i is the accuracy grade according to the manufacturer.

The calculated parameters include the heat supply from the condenser (Q_c), the heat absorption from the evaporator (Q_e), the COP$_{hp}$ (coefficient of performance of the heat pump), the COP$_{sys}$ (coefficient of performance of the whole system), useful solar heat (Q_s), solar efficiency (η), and solar fraction (f), which are calculated by equations (6.3)~(6.9):

$$Q_c = m_c C_w (T_{co} - T_{ci}) \tag{6.3}$$

$$Q_e = m_e C_w (T_{eo} - T_{ei}) \tag{6.4}$$

$$COP_{hp} = \frac{Q_c}{W_{hp}} \tag{6.5}$$

$$COP_{sys} = \frac{Q_c}{W_{hp} + W_{cp}} \tag{6.6}$$

$$Q_u = m_s C_w (T_{so} - T_{si}) \tag{6.7}$$

$$\eta = \frac{Q_u}{I_T A_c} \tag{6.8}$$

$$f = \frac{Q_u}{Q_c} \tag{6.9}$$

where Q_c is the heat supply from the condenser; Q_e is the heat absorption from the evaporator; Q_u is the useful solar heat; C_w is the specific heat of water flow; m_c is the condenser water mass flow rate; m_e is the evaporator water mass flow rate; m_s is the solar loop mass flow rate; T_{ci} is the condenser inlet water temperature; T_{co} is the condenser outlet water temperature; T_{ei} is the evaporator inlet water temperature; T_{eo} is the evaporator outlet water temperature; T_{si} is the solar loop inlet water temperature; T_{so} is the solar loop outlet water temperature; I_T is global radiation incident on solar collectors; A_c is the collector area; W_{cp} is the power consumption of the circulating pump; W_{hp} is the power consumption of the heat pump.

The basic root-sum-square (RRS) method introduced by Robert J. Moffat (Moffat 1988) is used to evaluate the relative uncertainty of the calculated parameters. The RRS method is briefly described as follows:

If a parameter F is a function of a series of measured independent variables, $F=F(X_1, X_2, X_3, \cdots, X_4)$, the relative uncertainty F (δRF) is acquired from:

$$\delta RF = \frac{\sqrt{\sum_{1}^{N}(\frac{\partial F_i}{X_i}\delta X_i)^2}}{F}$$
(6.10)

The relative uncertainties with regard to their typical values of the main parameters are listed in Table 6.1.

Table 6.1 Uncertainties of main parameters in the experiment

Item	Type of Data	Typical value	Unit	Relative Uncertainty
Average borehole temperature	Measured	9.83	℃	2.18 %
Average condenser outlet water temperature	Measured	33.79	℃	0.63 %
Average evaporator inlet water temperature	Measured	10.99	℃	1.95 %
Average flow rate of GHE loop	Measured	0.93	m^3/h	1.61 %
Average flow rate of Fan coil loop	Measured	1.04	m^3/h	1.44 %
Average flow rate of solar loop	Measured	0.60	m^3/h	2.50 %
Average total power consumption	Measured	887.45	W	1.02 %
Solar radiation on the tilted surface	Measured	431.12	W/m^2	2.53 %
Average heat supply from condenser	Calculated	4017.13	W	6.42 %
Average heat absorption from evaporator	Calculated	3377.68	W	6.71 %
Average useful solar energy	Calculated	3202.63	W	6.79 %
Average COP$_{hp}$	Calculated	6.22	—	6.81 %
Average COP$_{sys}$	Calculated	4.53	—	6.50 %
Solar collector efficiency	Calculated	0.51	%	7.24 %
Solar fraction	Calculated	0.35		9.34 %

6.3 Results and discussion

In this research, we investigated the space heating performances of the SAGCHP

system under four working modes during the heating period from Dec 5th to Dec 27th. Various parameters including representative temperatures, heat supply & absorption, power consumption, heating efficiency and features of solar thermal performance are calculated and compared to analyze the experimental results. Different effects from continuous operation, intermittent operation as well as solar assisted heating are discussed.

6.3.1 Environmental conditions
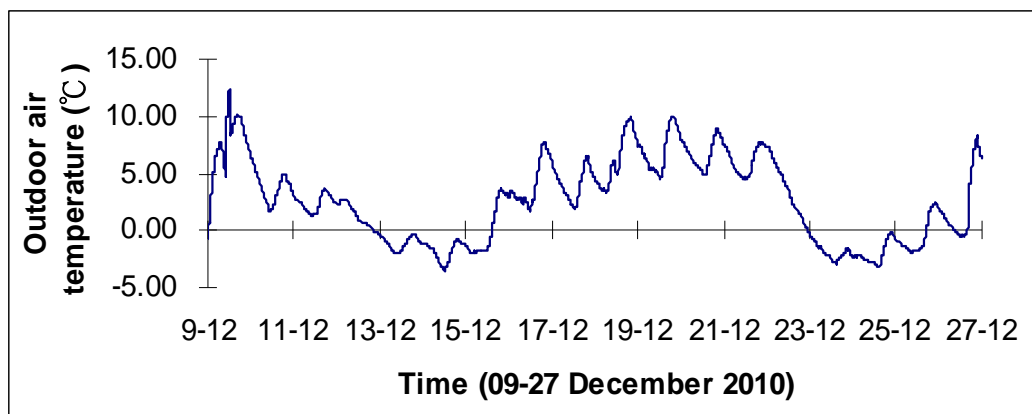
Figure 6.5 Outdoor ambient temperature when space heating is performed

The outdoor air temperature and the solar radiation level are recorded and shown in Figure 6.5 and Figure 6.6. The outdoor temperature was recorded from 9th Dec 2010 to 27th Dec 2010, whenever space heating is provided. However, solar radiation was only collected between 21st Dec and 27th Dec to evaluate the solar assisted heating process. The average outdoor temperature and solar radiation level in the specified periods are 2.6℃ and 358.5 W/m^2, respectively.

Figure 6.6 Solar radiation on the tilted surface when collectors are activated

6.3.2 Undisturbed soil temperature

Undisturbed borehole temperature is tested before activating the SAGCHP system. The borehole temperatures at different depths remain con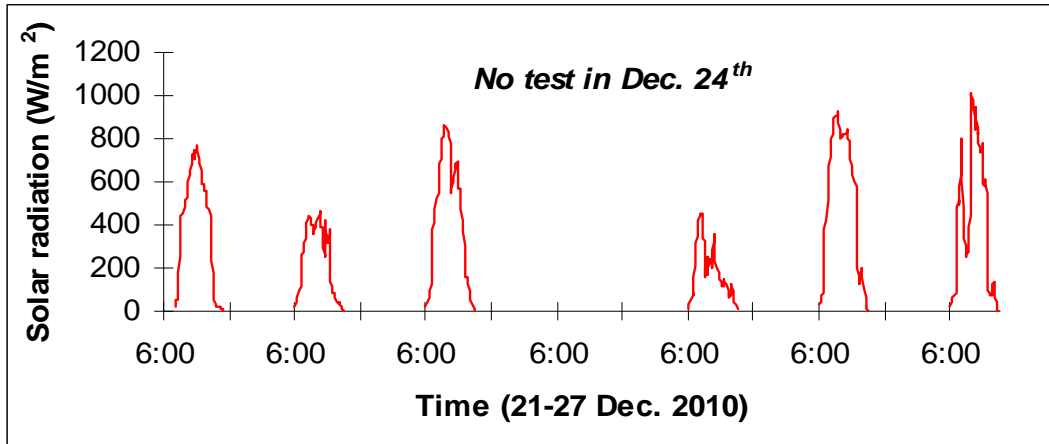stant from Dec 5th to Dec 7th, which could represent the local soil temperature. The recorded daily average temperature on Dec 6th at the depth of -3 m is 14.49 ℃. According to the simulation model proposed by Hart and Couvillion, the calculation of the undisturbed ground temperature filed is divided into two parts, i.e. the ground temperature rise below -45.7 m is calculated by a natural geothermal gradient of 0.01~0.03 ℃/m and at the region of the depth less than -45.7m, its initial temperature can be obtained from equation (11):

$$T(Z,t) = T_{ave} - A_S \cdot \exp\left[-Z\left(\frac{\pi}{365\alpha}\right)^{\frac{1}{2}}\right] \cdot \cos\left[\frac{2\pi}{365}\left(t - t_0 - \frac{Z}{2}\left(\frac{365}{\pi\alpha}\right)^{\frac{1}{2}}\right)\right] \qquad (6.11)$$

where T_{ave} is the annual mean ground temperature; A_S is the annual ground surface temperature amplitude; t is the time of year; t_0 is the phase constant day of minimum

surface temperature; α is the soil thermal diffusivity; Z is the depth from the ground surface. The daily air temperature of Shijiazhuang has an annual average temperature of 13.26 ℃ with a yearly amplitude of 20.9 ℃. Based on this model, the analytical solution of the soil temperature at the depth of -3m on Dec 6th is 14.89 ℃, which fits the practical situation.

6.3.3 Specifics of operation modes

Different control strategies applied to each working mode are explained as follows:

Mode 1: Intermittent space heating for 3 days (from 8:10 am to 17:30 pm) is provided with the soil as the only heat source. The indoor air temperature is controlled between 23 ℃ and 24 ℃.

Mode 2: Continuous space heating of 48 hours is provided with the soil as the only heat source while the indoor air temperature is floating freely.

Mode 3: Continuous space heating of 48 hours is provided with the soil and solar energy as heat sources while the indoor air temperature is floating freely. The solar collectors are turned on manually from 9:30 am to 15:30 pm.

Mode 4: Intermittent space heating of 3 days (from 8:10 am to 17:30 pm) is provided with the soil and solar energy as heat sources, while the indoor air temperature is floating freely. Solar collectors are turned on manually from 9:30 am to 15:30 pm.

6.3.4 System performances of Mode 1

The temperature distribution in the Borehole 1 through the three heating periods can be observed from Figure 6.7. Under intermittent operation, the borehole temperature

keeps decreasing as soon as the heat pump is activated and then recovers during the non-heating period due to the enormous heat capacity of the soil. At the beginning of a new heating session, the borehole temperature almost returns to the initial state of the last one. As a result, the daily average temperature of the Borehole 1 only decreases from 9.83 ℃ to 9.15 ℃ by 6.9 % for Mode 1.

The evaporator inlet temperature has similar changing tendency to the borehole temperature, which keeps declining through a single heating period, as depicted in Figure 6.8. At the end of the heating operation, the average evaporator temperature descends by 0.9 ℃ due to the reduced borehole temperature. On the other hand, the condenser outlet water temperature stops increasing within an hour since the activation of the system, and starts fluctuating between 34 ℃ and 35 ℃, which coincides with the variation of the indoor air temperature. The evaporator inlet together with the condenser outlet water temperature would determine the heating performance of a water-to-water heat pump.
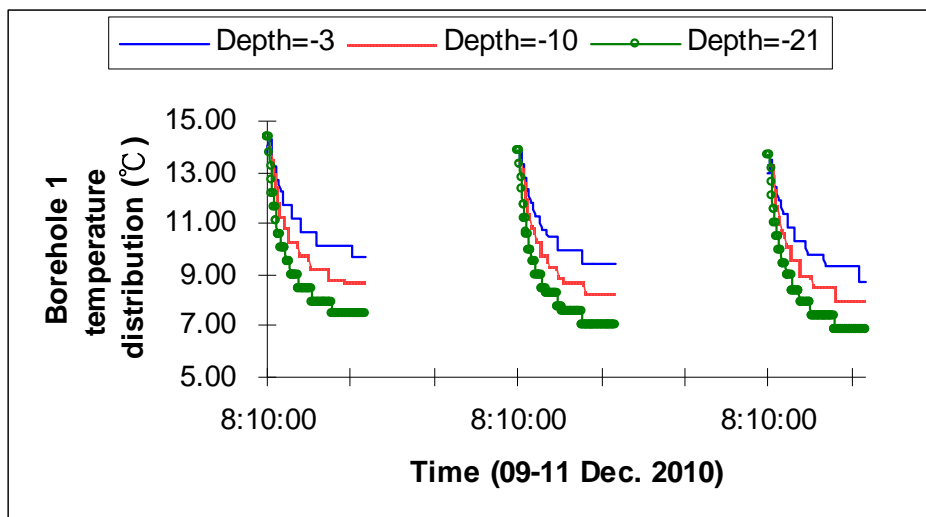

Figure 6.7 Borehole 1 temperature distribution for Mode 1
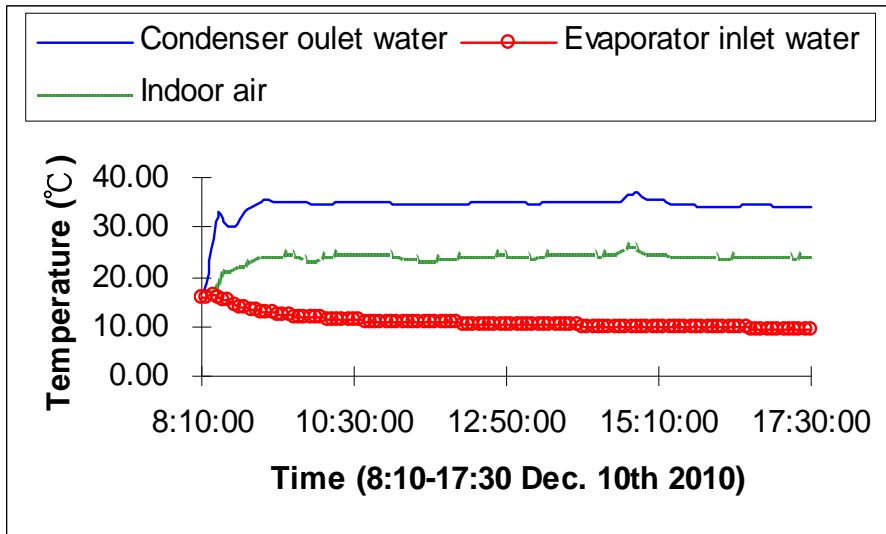
Figure 6.8 Condenser outlet & evaporator inlet water temperature on a typical day in
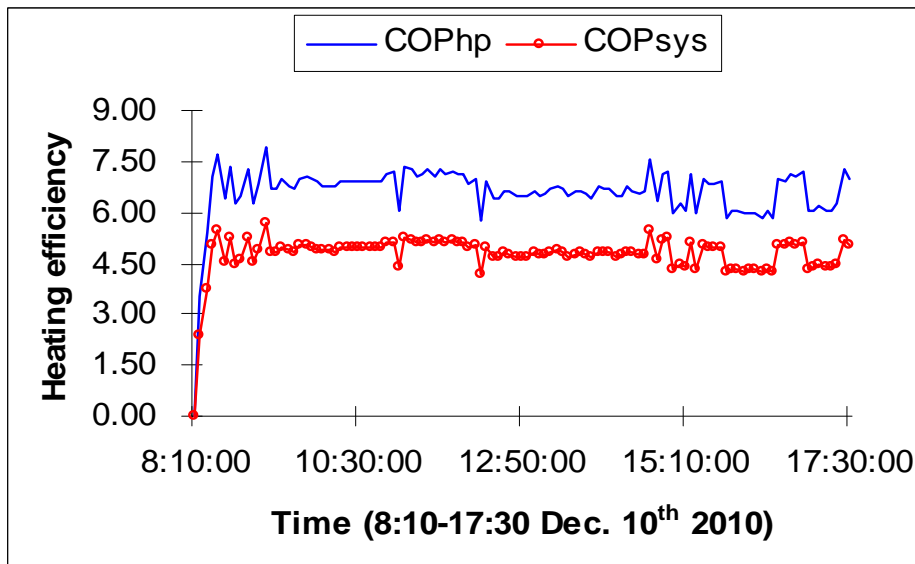
Mode 1

Figure 6.9 The COP_{hp} & COP_{sys} on a typical day in Mode 1

Table 6.2 Comparison of three heating periods in Mode 1

Item	Unit	Dec 9th	Dec 10th	Dec 11th
Average indoor temperature	℃	23.89	23.9	23.79
Average condenser outlet water temperature	℃	33.79	34.29	33.32
Average Evaporator inlet water temperature	℃	10.99	10.76	10.19
Average borehole 1 temperature	℃	9.83	9.36	9.15
Average heat supply from condenser	W	4017.13	4249.79	4206.52
Average heat absorption from evaporator	W	3377.68	3612.8	3574.15
Average power consumption	W	887.45	884.98	880.37
Average COP$_{sys}$		4.53	4.8	4.78

According to the manufacturer's manual, when the condenser outlet water temperature is kept constant, the COP$_{hp}$ should decrease with the evaporator inlet water temperature. However, the COP$_{hp}$ ranges between 5.77 and 7.95 instead of decreasing throughout the single heating operation, as shown in Figure 6.9. The COP$_{sys}$, including the constant power consumption of the circulating pumps, achieves an average of 4.80.

From the above results, the system is oversized. The designed inlet temperature supplied to the fan coils should be 45 ℃, while the daily average inlet temperature in the experiment is 10.71 ℃ lower. When the heat supply system is oversized, the required indoor air temperature could be satisfied with lower supply temperature, according to corresponding heat transfer theory. Comparison between the system performances of three heating periods in Mode 1 is concluded and listed in Table 6.2.

6.3.5 System performance of Mode 2

When the system operation is continuous, the borehole temperature drops quickly within the first 10 hours, which accounts for 85% temperature drop of the whole working

period. Then, the temperature descends gradually to 6.39 ℃ at the end as shown in Figure 6.10. When the system ceases to function, the borehole temperature rises together with the peripheral soil temperature and restores 82% of the aforementioned temperature drop after 16 hours. Although the system is oversized, the continuous operation mode decreases the evaporator inlet water temperature, the COP_{hp} and the COP_{sys} more rapidly than those in the intermittent operation mode. The COP_{sys} in the first 10 hours (4.57) decreased by 7.88 % compared with the COP_{sys} in the last 10 hours (4.21) during 48-hour uninterrupted operation, which is shown in Figure 6.11.
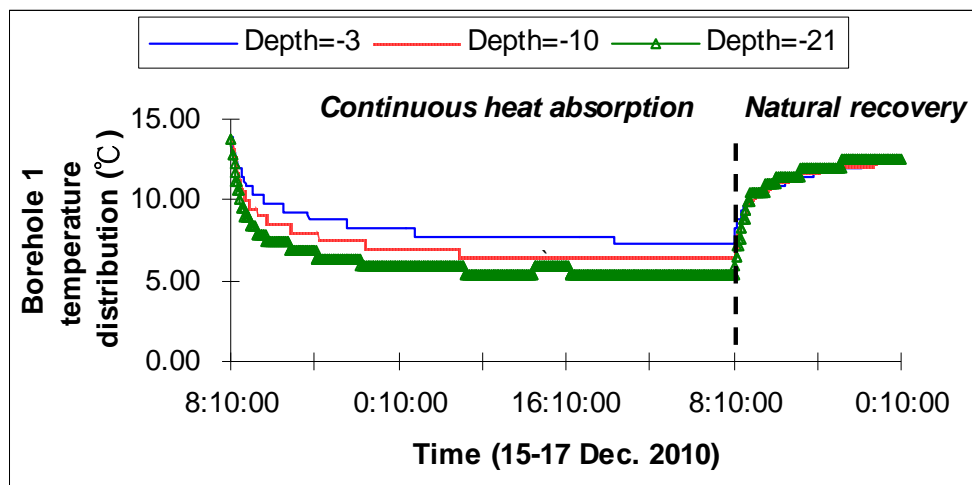
Figure 6.10 Temperature distribution of Borehole 1 in Mode 2

Furthermore, since the indoor air temperature is not controlled, it ascends throughout the whole heating session, which further proves that the system is oversized. As the heating load was over satisfied, the daily indoor air temperature increased from 25.4 to 29.3 and became too high to maintain a comfortable temperature. As displayed in Figure 6.12, the condenser outlet water temperature maintains the same growth rate in

response to the indoor air temperature.

Figure 6.11 Space heating efficiency & evaporator inlet water temperature in Mode 2
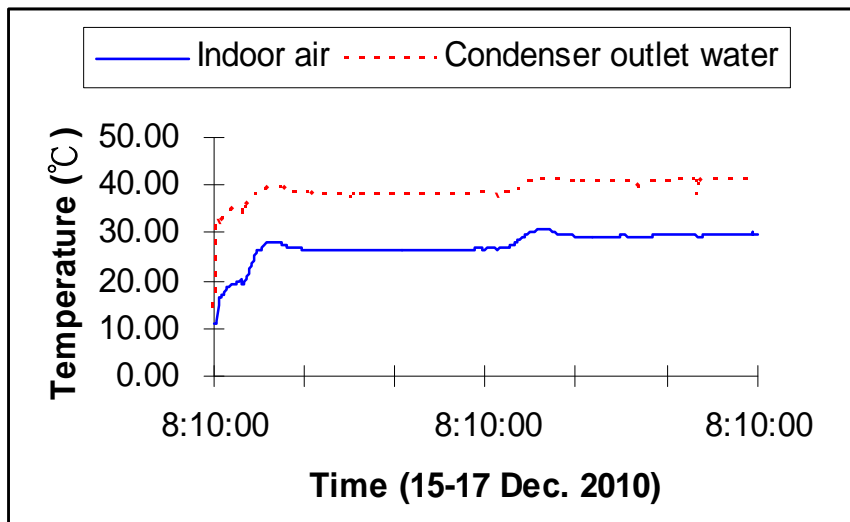
Figure 6.12 Indoor air & supply water temperature
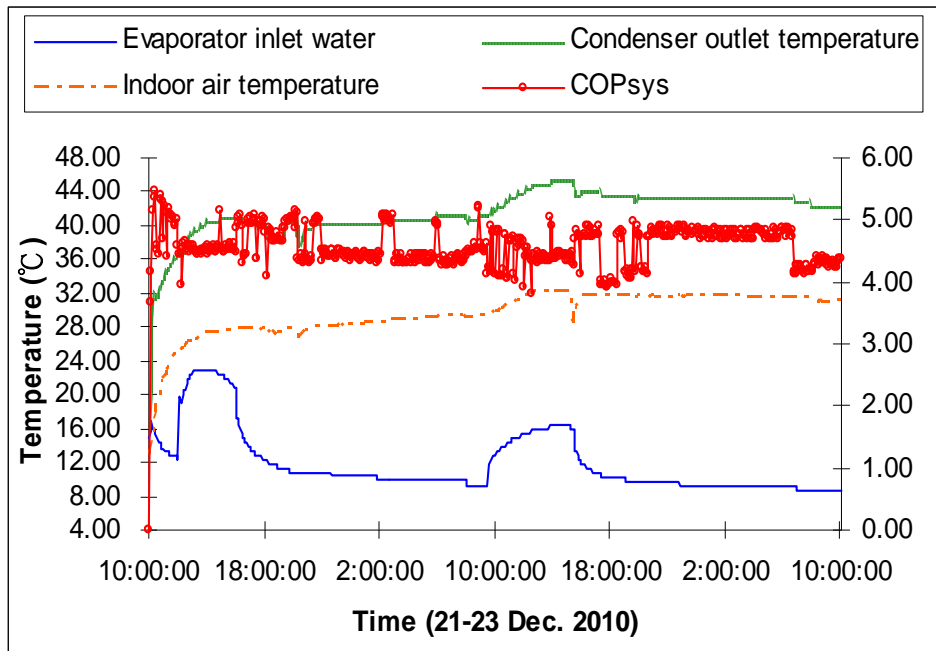
Figure 6.13 Operational characteristics of Mode 3

Table 6.3 Comparison between Mode 2 and Mode 3

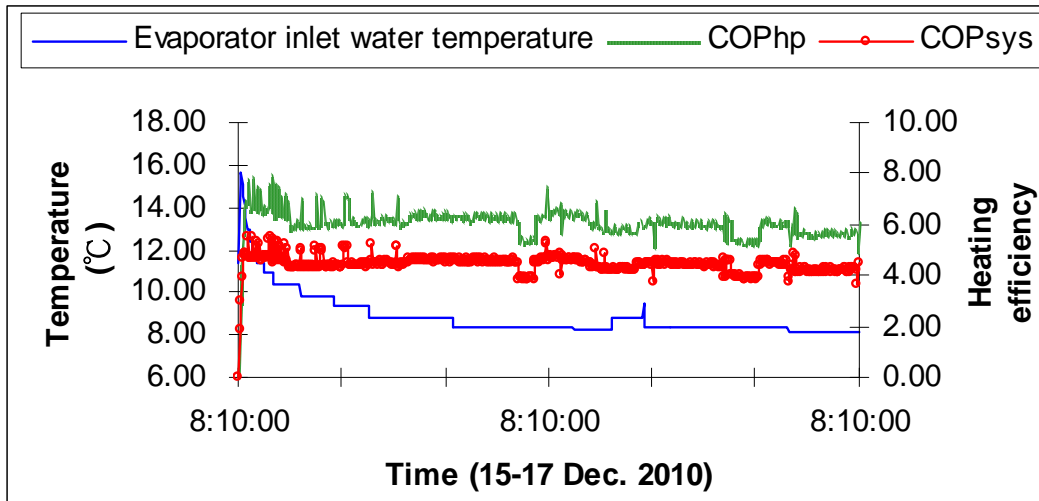| Time	Unit	Mode 2	Mode 3
Average indoor temperature	℃	27.34	29.49
Average condenser outlet water temperature	℃	38.93	41.59
Average evaporator inlet water temperature	℃	8.82	11.91
Average borehole 1 temperature	℃	7.13	8.55
Average heat supply from condenser	W	4165.01	4509.42
Average heat absorption from evaporator	W	3473.57	3788.70
Average system power consumption	W	939.44	985.67
Average COP_{sys}		4.43	4.57
Average COP_{hp}		6.02	6.26

6.3.6 System performance of Mode 3

In Mode 3 & Mode 4, solar collectors are manually controlled according to the available solar radiation on each day. The main operating features of Mode 3 are described in contrast to those of Mode 2 and displayed in Figure 6.13 and Table 6.3.

103

When the solar collectors are turned on, the outlet water temperature from the GHE could be further elevated. Therefore, unlike the consistent decreasing trend in Mode 2, the evaporator inlet temperature was increased to as high as 22.92 ℃ by the solar collector on Dec 21st. In contrast to the Mode 2, the average evaporator inlet temperature is improved by 35%. The condenser outlet water temperature increases with the indoor air temperature, which abides by the regulation in Mode 2. The average indoor air temperature and average condenser outlet temperature are 2.15 ℃ and 2.66 ℃, higher than those of Mode 2. The average COP$_{sys}$ of Mode 3 (4.57) is improved a little compared with that of Mode 2 (4.43), because of the extra power consumption of the circulating pump in the solar loop. Nevertheless, the average COP$_{sys}$ of 4.59 in the last 10-hour operation almost equals that in the initial 10 hours (4.56), which shows the influence of the solar assisted heating. In addition, heat supply and absorption of the heat pump ascends by 8 ~ 9 % accordingly, whereas the power consumption only shows a rise of no more than 5 %.
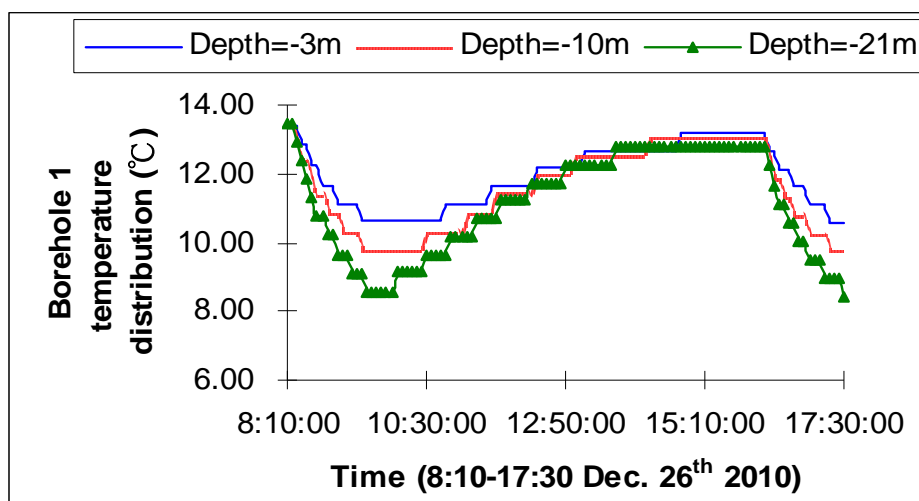
Figure 6.14 Borehole temperature distribution in a single heating period of Mode 4

6.3.7 System performances of Mode 4

In Mode 4, the average temperature of the Borehole 1 increases from 12.63 ℃ to 13.50 ℃ after three heating periods. Compared with the temperature drop in Mode 1, the solar heating effect is obvious. Figure 6.14 shows the borehole temperature variation in a single heating period. The borehole temperatures at different depths maintain a rising trend when the solar loop keeps running, but drop quickly once the solar heating is not available. At the end of the heating period, the average borehole temperature returns to the level before the solar assisted heating starts. The average borehole temperature decreases at 2.28℃ per hour, far greater than the increasing rate of 0.63℃ per hour. Therefore, high temperature soil thermal storage is not practical in the soil. For this experimental system, the borehole recharging by the solar system should be completed as soon as the soil temperature field is restored to the initial value.
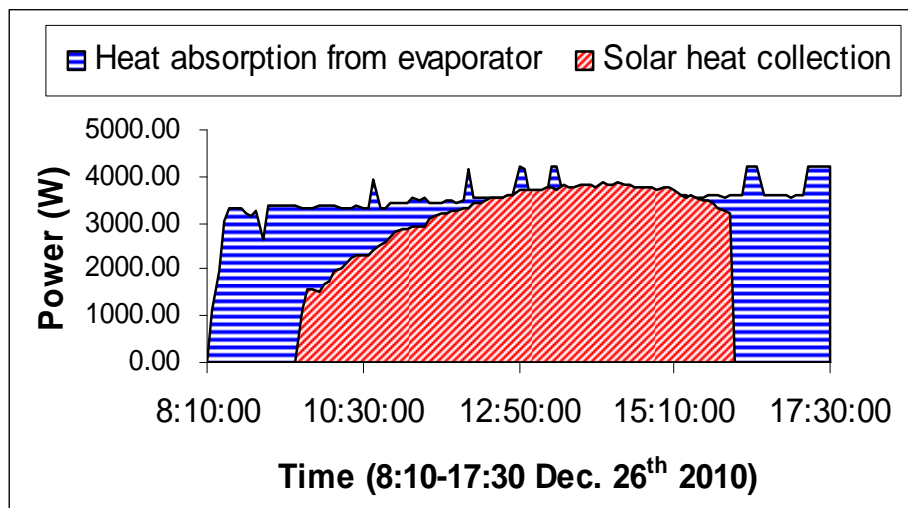
Figure 6.15 Solar heat collection in contrast to the heat absorption

In order to further investigate the solar collection process, the collected solar energy in relation to the heat absorption in one heating period is described in Figure 6.15. At the beginning, solar heat could only cover 34 % of the required heat extraction from the ground, while the solar collection at around 14:00 exceeds the total heat extraction by 9%. Solar collectors not only provide energy for space heating, but also recharge the soil for temperature recovery. The temperature recovery status of the soil should be observed by adding test boreholes at different distances away from the experimental GHE, which will be considered in future work. The average solar radiation of the sampled heating session is 692.52 W/m^2, and daily solar fraction of the system reaches as high as 0.53 with solar collectors' energy efficiency of 51%. The instant solar energy collection efficiency and solar fraction can be observed from Figure 6.16.

Figure 6.16 Solar collecting efficiency & solar fraction for a single heating period in

Mode 4

6.4 Summary

This chapter introduced the experimental investigations exploring the energy performance differences among four differen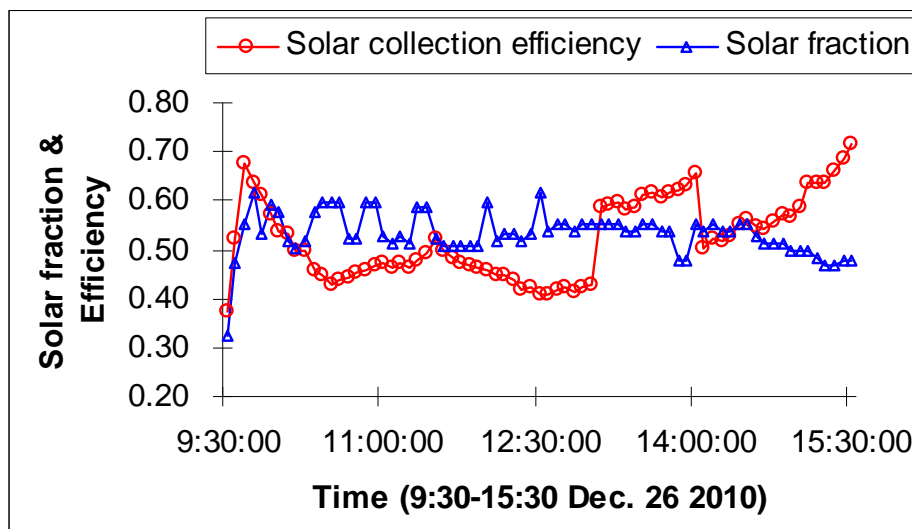t working modes of a solar assisted ground coupled heat pump (SAGCHP) system under the climatic conditions of Shijiazhuang. Conclusions can be drawn as follows:

(1) The heating performance is in direct relation with the borehole temperature. The average borehole temperature shows a little temperature drop within 0.68 ℃ under the intermittent working Mode 1 due to quick recovery of the borehole temperature in the resting hours of the system. On the contrary, a large borehole temperature decrease of 7.48 ℃ has been found for the continuous operating Mode 2. Correspondingly, the COP_{sys} of the Mode 2 at the end of the continuous operation decreased by 7.88 % compared to the initial state.

(2) The solar assisted heating process has significant effect on elevation of borehole temperature and system performance. The average evaporator inlet water temperature for the Mode 3 has increased by 35 % compared with the non-solar heating Mode 2. The COP_{sys} in Mode 3 showed constant performance in contrast with the decreasing tendency in Mode 2. The daily experimental COP_{sys} in the solar assisted heating modes reaches as high as 4.66 with a satisfactory solar fraction of 0.53, which shows its advantages in terms of energy efficiency over other conventional heating systems and great application potential in cold regions like Shijiazhuang near Beijing.

(3) The high temperature soil thermal storage method is not recommended due to the

enormous heat capacity of the earth. Soil recharging process should be ended once the initial ground temperature is recovered. The solar collectors of the system could be used as an alternative thermal source for the heat pump system or for low-temperature radiant floor heating, which means more flexible control strategies are required for operating the SAGCHP system.

CHAPTER 7 CONCLUSIONS

7.1 Summary of research results

The objective of this research is to study the performance of a designed multi-functional solar assisted ground coupled heat pump (SAGCHP) for its application in cold areas of China. The proposed SAGCHP system combines solar collector, ground heat exchanger (GHE) and heat pump together with water tanks, and performs flexible multi-functional space heating and domestic hot water (DHW) according to different control strategies. The advantage of the SAGCHP over traditional heating systems and its applicability in Beijing areas were proved through both simulative and experimental studies, which could be utilized to guide system design, optimization, and further experiments. Primary findings are summarized as:

Design and optimization of the system were performed in the TRNSYS environment. Different coupling methods of the solar collector and the GHE had great influence on the system performance, when environment situations and system components were given. From the comparison of several indicators of system performances, the indirect-coupled SAGCHP system (Model 5) was found to be the most appropriate combination strategy. Then, parametric studies on the solar collecting and storage subsystem demonstrated that the optimal mass flow rate and storage factor were about $50\text{kg}/(\text{hr}\cdot\text{m}^2)$ and 40 l/m^2, respectively for increasing the heating efficiency while achieving satisfactory solar fraction. The optimum design of the SAGCHP system, which is in relation to the collector area and corresponding GHE loop length, was finally determined by comparing

and analyzing the heating performance, solar collecting characteristics, energy saving rates and economic factors under the specified load conditions. From the simulation results, the GHE loop could be reduced by 3.9 m if 1 m^2 of solar collectors is added.

In addition, four control strategies were compared by examining their effects on the system performance. Solar collecting efficiency could be increased by 8% if wintertime DHW and soil recharging are allowed. However, the extra power consumed by circulation pumps could impair the system efficiency by 17.2%. If wintertime hot water is required, the total area of collectors should be enlarged to secure the stability of the SAGCHP system.

Long-term simulation for 20 years was performed after the accomplishment of the optimizing procedures. The SAGCHP system achieved an average COP$_{sys}$ of 3.89 for space heating and a 5.6 GJ reduction of electricity consumption each year. The solar fraction is 0.40 for space heating and 0.75 for DHW, based on an average solar collection efficiency of 55.7%. On the contrary, the inlet temperature, the heat pump coefficient as well as the average soil temperature of the conventional GCHP system decrease conspicuously under the same conditions. The system performance in a typical year during the simulation was selected for detailed analysis, and the operational characteristics of each working mode for space heating were studied. Among the five working modes, direct heating is most efficient with the only power input from circulating pumps. Solar assisted heating and solar coupled ground heat pump heating modes are also the energy saving modes that supply 22% of the total heating load together. The temperature of the HTF to load supplied by the SAGCHP exceeded that of a conventional GCHP system by about 3 ℃.

Furthermore, the calculated energy imbalance of the system was just within 0.75%, acceptable for a complicated compound system. The applicability of the designed system in severe cold areas like Harbin was discussed. Restricted by the local soil and weather conditions, the underground loop has to be charged with anti-freezing fluid to secure operating stability. The Harbin case showed higher seasonal storage efficiency and an enlarged heating load requirement due to prolonged heating period. The overall thermal balance is maintained at the cost of a much lower system efficiency of 2.84. As a result, the system was not recommended for the application in severe cold areas.

Finally, experimental investigation was carried out to explore practical differences among four different working modes of a SAGCHP system in Shijiazhuang near Beijing, whose climatic conditions were similar to Beijing. The heating performance was found to be in direct relation with the borehole temperature. The average borehole temperature showed minor temperature drop under the intermittent working due to quick recovery of the borehole temperature in the resting hours of the system, while a large borehole temperature decrease of 7.48 ℃ was observed in the continuous operating mode. Correspondingly, the COP_{sys} at the end of the continuous operation decreased by 7.88 % compared to the initial state. The solar assisted heating process practically elevated the borehole temperature and contributed to a daily COP_{sys} as high as 4.66 with a satisfactory solar fraction of 0.53, which exhibited the advantage in energy efficiency over other conventional heating systems and great application potential in cold regions like Shijiazhuang. It was also suggested that solar collectors should be used as an alternative thermal source for the heat pump system or for low-temperature radiant floor heating instead of high-temperature seasonal storage.

7.2 Limitations of the study and recommendations for future work

This thesis tried to present a method for design and optimization of the multi-functional SAGCHP system which could be applied for space heating and DHW production in Beijing areas of China. However, there are still aspects that are not covered or not analyzed profound enough in this study, which need to be carefully investigated before the industrialization of the technology.

From the theoretical basis, it is necessary that we create a user-friendly program that could be used for accurate design and optimization of the SAGCHP system. More detailed parametric studies should be performed to figure out possible dimensionless parameters consisting of multiple parameters that significantly affect the performance of the system, especially concerned with the coupling of solar collectors and the GHEs.

Due to the limitation of the research period and local conditions, the experiment had to be carried out on an existing test rig which is not strictly fit with the theoretical model of the proposed SAGCHP system. As a result, only part of the working functions was subject to practical verification, and the operational tests were restricted within a month. In future studies, experimental installations that could completely realize various functions of the system should be constructed and the test should last more than a year.

For future application of the technology in the specified areas, there should also be an exergy analysis and environment effects estimation of the compound system to examine its feasibility and ecological friendliness. In addition, detailed life-cycle analysis will be achieved to justify the economic advantage over traditional heating systems.

REFERENCES

AL-Juwayhel, F. I. (1981). Simulation of the dynamic performance of air-source, earth source, and solar assisted earth-source heat pump systems. Stillwater, Oklahoma, United States, Oklahoma State University. **Ph. D.**

Argiriou, A. A. (1997). CSHPSS systems in Greece: Test of simulation software and analysis of typical systems. Solar Energy **60**(3-4): 159-170.

Badescu, V. (2008). Optimal control of flow in solar collector systems with fully mixed water storage tanks. Energy Conversion and Management **49**(2): 169-184.

Bakker, M., H. A. Zondag, et al. (2005). Performance and costs of a roof-sized PV/thermal array combined with a ground coupled heat pump. Solar Energy **78**(2): 331-339.

Bi, Y. and L. Chen (2002). Ground heat exchanger temperature distribution analysis and experimental verification. Applied Thermal Engineering **22**(2): 183-189.

Bi, Y. and L. Chen (2004). Solar and ground source heat-pump system. Applied Energy **78**(2): 231-245.

Bi, Y. and L. Chen (2005). Heat source performance for solar-ground source heat pump. Journal of the Energy Institute **78**(4): 185-189.

Bose, J. E., J. D. Parker, et al. (1985). Design data/manual for closed-loop ground coupled heat pump systems. Atlanta, U.S., American Society of Heating, Refrigeration and Air-Conditioning Engineers, Inc.

Breger, D. S., J. E. Hubbell, et al. (1996). Thermal energy storage in the ground: Comparative analysis of heat transfer modeling using U-tubes and boreholes. Solar Energy **56**(6): 493-503.

Chiasson, A. (2007). Simulation and design of hybrid geothermal heat pumps. Department of Civil and Architectural Engineering. United states, University of Wyoming. **Ph. D.**

Cube, H. L. v. and F. Steimle (1981). Heat Pump Technology. London, U.K., Butterworth & Co Ltd.

Cui, P., H. Yang, et al. (2006). Heat transfer analysis of ground heat exchangers with inclined boreholes. Applied Thermal Engineering **26**(11-12): 1169-1175.

Cui, P., H. Yang, et al. (2008). Simulation of hybrid ground coupled heat pump with domestic hot water heating systems using HVACSIM+. Energy and Buildings **40**(9): 1731-1736.

Cullin, J. R. (2008). Improvements in design procedures for ground source and hybrid ground source heat pump systems. Stillwater, Oklahoma, United States, Oklahoma State University. **Master of Science**.

Duan, Z., J. Zhao, et al. (2006). Study on Testing System of Soil Thermal Conductivity. GAS & HEAT **26**(11): 45-47.

Esen, H., M. Inalli, et al. (2007). Energy and exergy analysis of a ground coupled heat pump system with two horizontal ground heat exchangers. Building and Environment **42**(10): 3606-3615.

Fujimitsu, Y., K. Fukuoka, et al. (2010). Evaluation of subsurface thermal environmental change caused by a ground coupled heat pump system. Current Applied Physics **10**(2, Supplement 1): S113-S116.

Gao, J., X. Zhang, et al. (2008). Thermal performance and ground temperature of vertical pile-foundation heat exchangers: A case study. Applied Thermal Engineering **28**(17-18): 2295-2304.

Han, Z., M. Zheng, et al. (2008). Numerical simulation of solar assisted ground-source heat pump heating system with latent heat energy storage in severely cold area. Applied Thermal Engineering **28**(11-12): 1427-1436.

Han, Z., M. Zheng, et al. (2006). Experimental research on solar assisted ground source heat pump heating system with a latent heat storage tank in severe cold area. ACTA ENERGIAE SOLARIS SINICA **27**(12): 1214-1218.

Han, Z. W. and M. Y. Zheng (2007). Modelling and transient simulation of solar-ground source heat pump heating system. Beijing, Tsinghua University Press.

Hellström, G. (1991). Ground heat storage: Thermal analyses of duct storage systems. Department of Mathematical Physics. Sweden, University of Lund. **Ph. D.:** 262.

Hern, S. A. (2004). Design of an experimental facility for hybrid ground source heat pump systems. Stillwater, Oklahoma, United States, Oklahoma State University. **Master of Science**.

Ji, J., K. Liu, et al. (2008). Performance analysis of a photovoltaic heat pump. Applied Energy **85**(8): 680-693.

Ji, J., G. Pei, et al. (2008). Experimental study of photovoltaic solar assisted heat pump system. Solar Energy **82**(1): 43-52.

Jordan, U. and K. Vajen (2000). Influence Of The DHW Load Profile On The Fractional Energy Savings: : A Case Study Of A Solar Combi-System With TRNSYS Simulations. Solar Energy **69**(Supplement 6): 197-208.

Jun, L., Z. Xu, et al. (2009). Heat Transfer Performance Test and Numerical Simulation of Pile-pipe Ground Source Heat Pump System. ACTA ENERGIAE SOLARIS SINICA **30**(6): 727-731.

Kjellsson, E., G. Hellström, et al. (2010). Optimization of systems with the combination of ground-source heat pump and solar collectors in dwellings. Energy **35**(6): 2667-2673.

Klein, S. A. (1976). A design procedure for solar heating systems. Wisconsin, United States, The University of Wisconsin - Madison. **Ph. D.**

Klein, S. A. e. a. (2007). TRNSYS manual, a transient simulation program. <u>Madison: Solar Engineering Laboratory</u>, University of Wisconsin-Madison.

Li, S., W. Yang, et al. (2009). Soil temperature distribution around a U-tube heat exchanger in a multi-function ground source heat pump system. Applied Thermal Engineering **29**(17-18): 3679-3686.

Lima, J. B. A., R. T. A. Prado, et al. (2006). Optimization of tank and flat-plate collector of solar water heating system for single-family households to assure economic efficiency through the TRNSYS program. Renewable Energy **31**(10): 1581-1595.

Lund, P. D. (1989). A GENERAL DESIGN METHODOLOGY FOR SEASONAL STORAGE SOLAR SYSTEMS. Solar Energy **42**(3): 235-251.

Lund, P. D. and M. B. Ostman (1985). A NUMERICAL-MODEL FOR SEASONAL STORAGE OF SOLAR HEAT IN THE GROUND BY VERTICAL PIPES. Solar Energy **34**(4-5): 351-366.

Lundh, M. and J. O. Dalenback (2008). Swedish solar heated residential area with seasonal storage in rock: Initial evaluation. Renewable Energy **33**(4): 703-711.

Man, Y., H. Yang, et al. (2010). A new model and analytical solutions for borehole and pile ground heat exchangers. International Journal of Heat and Mass Transfer **53**(13-14): 2593-2601.

Man, Y., H. Yang, et al. (2008). Study on hybrid ground coupled heat pump systems. Energy and Buildings **40**(11): 2028-2036.

Man, Y., H. Yang, et al. (2010). Study on hybrid ground coupled heat pump system for air-conditioning in hot-weather areas like Hong Kong. Applied Energy **87**(9): 2826-2833.

MICHAELIDES, I. M. (1993). Computer simulation and optimisation of solar heating systems for Cyprus. <u>Faculty of Engineering and Science</u>. London, U.K., University of Westminster. **Ph. D.**

Moffat, R. J. (1988). Describing the uncertainties in experimental results. Experimental Thermal and Fluid Science **1**(1): 3-17.

Nicolas, J. and J. P. Poncelet (1988). Solar assisted heat pump system and in-ground energy storage in a school building. Solar Energy **40**(2): 117-125.

Nordell, B. and G. Hellström (2000). High temperature solar heated seasonal storage system for low temperature heating of buildings. Solar Energy **69**(6): 511-523.

Novo, A. V., J. R. Bayon, et al. (2010). Review of seasonal heat storage in large basins: Water tanks and gravel-water pits. Applied Energy **87**(2): 390-397.

Olszewski, P. (2006). Optimization of working ground heat storage with seasonal regeneration. American Society of Mechanical Engineers, Advanced Energy Systems Division (Publication) AES, Chicago, IL.

Ozgener, O. and A. Hepbasli (2005). Experimental performance analysis of a solar assisted ground-source heat pump greenhouse heating system. Energy and Buildings **37**(1): 101-110.

Ozgener, O. and A. Hepbasli (2005). Performance analysis of a solar assisted ground-source heat pump system for greenhouse heating: an experimental study. Building and Environment **40**(8): 1040-1050.

Ozgener, O. and A. Hepbasli (2007). A parametrical study on the energetic and exergetic assessment of a solar assisted vertical ground-source heat pump system used for heating a greenhouse. Building and Environment **42**(1): 11-24.

P, S. K. (2005). Modeling, verification and optimization of hybrid ground source heat pump systems in EnergyPlus. Stillwater, Oklahoma, United States, Oklahoma State University. **Master of Science**.

Pahud, D. (2000). Central solar heating plants with seasonal duct storage and short-term water storage: design guidelines obtained by dynamic system simulations. Solar Energy **69**(6): 495-509.

Reuss, M., M. Beck, et al. (1997). Design of a seasonal thermal energy storage in the ground. Solar Energy **59**(4-6): 247-257.

Sanaye, S. and B. Niroomand (2010). Horizontal ground coupled heat pump: Thermal-economic modeling and optimization. Energy Conversion and Management **51**(12): 2600-2612.

Schlosser, K. and B. Teislev (1979). A mathematical simulation of a solar assisted heat pump system using the ground for energy storage. Energy and Buildings **2**(1): 37-43.

Schmidt, T., D. Mangold, et al. (2004). Central solar heating plants with seasonal storage in Germany. Solar Energy **76**(1-3): 165-174.

Trillat-Berdal, V., B. Souyri, et al. (2007). Coupling of geothermal heat pumps with thermal solar collectors. Applied Thermal Engineering **27**(10): 1750-1755.

Trillat-Berdal, V., B. Souyri, et al. (2006). Experimental study of a ground coupled heat pump combined with thermal solar collectors. Energy and Buildings **38**(12): 1477-1484.

Wan, K. K. W., D. H. W. Li, et al. (2011). Future trends of building heating and cooling loads and energy consumption in different climates. Building and Environment **46**(1): 223-234.

Wang, F., M. Zheng, et al. (2006). APPLICATION OF PHASE CHANGE MATERIAL IN SOLAR ASSISTED GROUND-SOURCE HEAT PUMP SYSTEM. ACTA ENERGIAE SOLARIS SINICA **27**(12): 1231-1234.

Wang, H. and C. Qi (2008). Performance study of underground thermal storage in a solar-ground coupled heat pump system for residential buildings. Energy and Buildings **40**(7): 1278-1286.

Wang, H., C. Qi, et al. (2009). A case study of underground thermal storage in a solar-ground coupled heat pump system for residential buildings. Renewable Energy **34**(1): 307-314.

Wang, K., Y. Li, et al. (2008). Heating experiment of solar-ground-source hybrid heat pumps. HV & AC **38**(2): 13-17.

Wang, X., M. Zheng, et al. (2010). Experimental study of a solar assisted ground coupled heat pump system with solar seasonal thermal storage in severe cold areas. Energy and Buildings **42**(11): 2104-2110.

Wu, X. (2008). Research and simulation analysis of combing solar collector and ground source heat pump heating system. Geology Engineering. P. R. China, Jilin University. **Ph. D.**

Xu, X. (2007). Simulation and optimal control of hybrid ground source heat pump systems. Stillwater, Oklahoma, United States, Oklahoma State University. **Ph. D.**

Yang, H., P. Cui, et al. (2010). Vertical-borehole ground coupled heat pumps: A review of models and systems. Applied Energy **87**(1): 16-27.

Yang, L., J. C. Lam, et al. (2008). Building energy simulation using multi-years and typical meteorological years in different climates. Energy Conversion and Management **49**(1): 113-124.

Yang, W. B., M. H. Shi, et al. (2006). Numerical simulation of the performance of a solar-earth source heat pump system. Applied Thermal Engineering **26**(17-18): 2367-2376.

Yu, Y. S., Z. L. Ma, et al. (2004). The simulative research on operation conditions of the solar ground coupled heat pump system.

Zeng, H., N. Diao, et al. (2003). Heat transfer analysis of boreholes in vertical ground heat exchangers. International Journal of Heat and Mass Transfer **46**(23): 4467-4481.

Zinko, H. and B. Perers (1985). MINSUN-simulation of a solar heated duct storage in comparison to measurements.